

Variational Sequential Optimal Experimental Design using Reinforcement Learning

Wanggang Shen^a, Jiayuan Dong^a, Xun Huan^a

^a*Department of Mechanical Engineering, University of Michigan, Ann Arbor, Michigan, United States*

Abstract

We present variational sequential optimal experimental design (vsOED), a novel method for optimally designing a finite sequence of experiments within a Bayesian framework with information-theoretic criteria. vsOED employs a one-point reward formulation with variational posterior approximations, providing a provable lower bound to the expected information gain. Numerical methods are developed following an actor-critic reinforcement learning approach, including derivation and estimation of variational and policy gradients to optimize the design policy, and posterior approximation using Gaussian mixture models and normalizing flows. vsOED accommodates nuisance parameters, implicit likelihoods, and multiple candidate models, while supporting flexible design criteria that can target designs for model discrimination, parameter inference, goal-oriented prediction, and their weighted combinations. We demonstrate vsOED across various engineering and science applications, illustrating its superior sample efficiency compared to existing sequential experimental design algorithms.

Keywords: Bayesian adaptive design, actor-critic, policy gradient, expected information gain, information lower bound, implicit likelihood

1. Introduction

Engineering and science revolve around the interplay between data and models: leveraging data to develop, calibrate, and improve models, and using models to predict outcomes, control processes, and guide decision-making. When data is expensive to acquire, carefully designing experiments becomes crucial. *Optimal experimental design (OED)* (see [1] for a recent review) is a field dedicated to systematically quantifying the value of experiments and identifying the best conditions to conduct them. Bayesian OED [2, 3, 4, 5, 6] further incorporates the effects of uncertainty, and optimizes experiments so that their data can maximize uncertainty reduction, often measured as the *expected information gain (EIG)* or mutual information [7].

Sequential experimental design involves planning multiple experiments conducted in sequence, where the results of earlier experiments can inform the design of subsequent ones—i.e., it involves ‘feedback’. A straightforward approach is to design one experiment (or a subset) at a time: plan the next experiment, perform it, use the resulting data to update the model and its uncertainty, and repeat. This approach is known as *greedy* or *myopic* design since it focuses on the immediate next experiment without considering future ones; i.e., it lacks ‘lookahead’. Greedy design is advantageous for its simplicity and flexibility in accommodating an unknown total number of experiments, and it has been studied extensively [8, 9, 10, 11, 12, 13, 14, 15, 16].

In this paper, we follow a sequential experimental design formulation (see, e.g., [17], [18, VII.G], [19, Chapter 3]) that incorporates both (i) lookahead, where each design is selected

while accounting for all remaining experiments, and (ii) feedback, where designs are given by adaptive policies that determine the next experiment based on the current state of information. This formulation, referred to as *sequential OED (sOED)* in [19, 20, 21], is general but computationally challenging. Previous approaches [22, 23, 24, 25, 26, 27, 28, 29, 30] have largely been limited to discrete settings or have not employed a Bayesian framework with information-theoretic design criteria. Only recently have more efficient computational techniques—often leveraging reinforcement learning—been developed to tackle sOED in more general settings [19, 20, 31, 32, 33, 34].

Huan and Marzouk [19, 20] presented sOED as a finite-horizon Markov decision process and proposed an approximate dynamic programming algorithm to solve it. However, their approach relies on an implicit policy representation, where each policy evaluation involves solving a stochastic optimization problem, making it computationally expensive for online applications. To address this, Shen and Huan [31, 21] introduced policy-gradient sOED (PG-sOED), an actor-critic method that trains an explicit parameterized policy network, significantly reducing computational costs. Around the same time, Foster *et al.* [32] proposed Deep Adaptive Design (DAD), which trains a policy network to maximize a lower bound estimator of the EIG, known as the sequential prior contrastive estimator (PCE), using its gradients. Unlike PG-sOED, DAD does not rely on an actor-critic framework but requires access to the derivatives of the observation model (i.e., parameter-to-observable map). Blau *et al.* [34] further proposed learning a stochastic policy to maximize the sequential PCE via randomized ensembled double Q-learning [35], which sidestepped the need for model derivatives. Building upon DAD, Ivanova *et al.* [33] developed implicit DAD (iDAD) to handle problems with implicit likelihood, where the likelihood is intractable but data samples can still be generated. iDAD constructs variational lower bounds of the EIG and tightens these bounds by simultaneously optimizing the policy and variational parameters, requiring only sample-based updates. However, similar to DAD, iDAD also requires model derivatives.

EIG bounds [36] have proven to be effective for OED, as demonstrated by iDAD and related works. For example, the tractable unnormalized Barber–Agakov (TUBA) lower bound [36] incorporates the tuning of a ‘critic’ function (different from the ‘critic’ in ‘actor-critic’). The Nguyen–Wainwright–Jordan (NWJ) bound [37], also known as the mutual information neural estimation f-divergence (MINE-f) bound [38], is a special case of TUBA and has been applied to OED by Kleinegesse and Gutmann [39]. The information noise-contrastive estimation (InfoNCE) bound [40] mirrors the PCE, but replaces the likelihood with an exponentiated critic function. Notably, all these bounds support implicit likelihoods. The Barber–Agakov (BA) lower bound [41], in particular, approximates the posterior density directly. Its advantage lies in enabling both density evaluation and posterior sampling. Foster *et al.* [42] first applied the BA bound to OED with simple variational distributions (e.g., Gaussian, Bernoulli, Gamma). Dong *et al.* [43] later proposed variational OED (vOED) to expand the capacity of the approximate posteriors by representing them with normalizing flows [44, 45].

The above OED efforts primarily focused on maximizing the EIG of unknown model parameters. However, the ultimate goals of the experiments often extend beyond parameter inference to predicting other *goal* quantities that depend on the model parameters but differ from the observation quantities. For example, while observations such as temperature and pressure facilitate the inference of a weather model’s parameters, the goal might not be to learn these parameters, but to forecast future precipitation using the resulting parameter distributions. A *goal-oriented* OED framework therefore directly targets the EIG for such

goal quantities. This concept builds on classical I-, V-, and G-optimal designs that seek to minimize predictive variance in linear regression models [46]. Attia *et al.* [47] demonstrated gradient-based optimization techniques to solve linear Bayesian D_A - and L-optimal design problems, while Wu *et al.* [48] developed scalable offline-online decompositions and low-rank approximations for high-dimensional linear settings. The theoretical formulation for *nonlinear* goal-oriented OED was presented in [49]. Computationally, Butler *et al.* [50] proposed OED for prediction (OED4P), a non-Bayesian approach based on matching push-forward distributions to observed data distributions [51, 52]. Later, Smith *et al.* [53] introduced expected predictive information gain (EPIG), a nested Monte Carlo estimator for predictive EIG under a greedy sequential (i.e., active learning) setting, but requiring the goal quantities to be the same as observation quantities except at new designs. More recently, Zhong *et al.* [54] combined Markov chain Monte Carlo with kernel density estimation to estimate the probability densities of goal quantities directly. These studies highlight the challenge of intractable predictive densities for the goal quantities, motivating the potential effectiveness of likelihood-free EIG bounds. Kleinegesse and Gutmann [55] explored such bounds for various goal-oriented OED settings. However, existing goal-oriented efforts all focused on batch (i.e., non-sequential) or greedy OED, and integrating goal-oriented objectives into sOED has yet to be developed.

Building on these advances, we propose *variational sequential optimal experimental design (vsOED)*, a method to solve the sOED problem under an actor-critic reinforcement learning framework powered by policy gradient and variational BA bound to the EIG. The key novelty and contributions of this work are summarized as follows.

- Comprehensive formulation: vsOED accommodates nuisance parameters, implicit likelihoods, and multiple candidate models, while offering flexible design criterion that can target designs for model discrimination, parameter inference, goal-oriented prediction, or weighted combinations thereof.
- Theoretical guarantees: We prove the lower bound property of vsOED, and the equivalence of various reward formulations for vsOED.
- Numerical methods: We develop techniques for solving vsOED, highlighted by estimating the actor-critic policy gradient and approximating posteriors using Gaussian mixture models and normalizing flows.
- Empirical demonstration: We illustrate the effectiveness of vsOED, particularly under limited sample budgets, through comparisons with existing algorithms across diverse numerical experiments.

The vsOED code is available at <https://github.com/wgshen/vsOED>.

The paper is structured as follows. Section 2 formulates the sOED and vsOED problem statements, including key theorems on their relationships. Section 3 details the numerical methods for solving vsOED, centering around deriving and computing the policy gradient under an actor-critic framework. Section 4 evaluates vsOED through numerical experiments and benchmarks against existing algorithms. Finally, Section 5 concludes with summarizing remarks and a discussion of future work.

2. Problem formulation

2.1. Preliminaries

We focus on the design of a finite sequence of N experiments indexed by $k \in \{0, \dots, N-1\}$. We assume N is known and fixed. Each experiment is associated with a real-valued design vector $\xi_k \in \mathcal{A}_k \subseteq \mathbb{R}^{N_\xi}$ and observation vector $Y_k \in \mathcal{Y}_k \subseteq \mathbb{R}^{N_y}$. We adopt the convention to use upper case for denoting a random variable or vector such as Y_k , and lower case for its realized value such as y_k . For simplicity, we assume N_ξ and N_y to be constant across k . At the k th experiment, the information sequence of all completed experiments' designs and observations is denoted by $I_k = \{\xi_0, Y_0, \dots, \xi_{k-1}, Y_{k-1}\}$, with $I_0 = \emptyset$. Furthermore, let \mathcal{M}_m be a countable set of models indexed by $m \in \{1, 2, \dots\}$ where each model has its own parameters of interest (PoIs) $\Theta_m \in \Theta_m \subseteq \mathbb{R}^{N_{\theta_m}}$, nuisance parameters $\Psi_m \in \Psi_m \subseteq \mathbb{R}^{N_{\psi_m}}$, and predictive quantities of interest (QoIs) $Z_m \in \mathcal{Z}_m \subseteq \mathbb{R}^{N_{z_m}}$. The experiment observation is related to the parameters via an observation model, for example often in the form

$$Y_k = G_k(\Theta_m, \Psi_m, \xi_k; m, I_k) + \mathcal{E}_k, \quad (1)$$

where G_k is a nonlinear observation forward operator and \mathcal{E}_k is the observation noise. The QoIs are related to the parameters via a predictive model

$$Z_m = H(\Theta_m, \Psi_m, \mathcal{E}_Z; m), \quad (2)$$

where H is a nonlinear predictive stochastic forward operator with \mathcal{E}_Z representing the predictive stochastic source. If the predictive model is deterministic, we can write $Z_m = H(\Theta_m, \Psi_m; m)$. G_k and H often involve the most expensive computations (e.g., solving various differential equations), hence the number of these forward solves is often used as the unit for computational cost.

Under a Bayesian approach, after the k th experiment, the joint probability density on M , Θ_m , and Ψ_m updates following Bayes' rule:

$$p(m, \theta_m, \psi_m | i_{k+1}) = p(m, \theta_m, \psi_m | \xi_k, y_k, i_k) = \frac{p(y_k | m, \theta_m, \psi_m, \xi_k, i_k) p(m, \theta_m, \psi_m | i_k)}{p(y_k | \xi_k, i_k)}, \quad (3)$$

where $p(m, \theta_m, \psi_m | \xi_k, y_k, i_k)$ is the posterior which can also be written as $p(m, \theta_m, \psi_m | i_{k+1})$, $p(m, \theta_m, \psi_m | i_k)$ is the prior, $p(y_k | m, \theta_m, \psi_m, \xi_k, i_k)$ is the likelihood, and $p(y_k | \xi_k, i_k)$ is the marginal likelihood. In order to simplify notation in the remainder of this paper, we adopt the convention where when m is not explicitly mentioned, conditioning on m is implied through other variables' subscripts, e.g., $p(\theta_m, \psi_m | i_k) = p(\theta_m, \psi_m | m, i_k)$. The posterior after the k th experiment $p(m, \theta_m, \psi_m | i_{k+1})$ then serves as the prior for the $(k+1)$ th experiment and is again applied to Eq. (3). Bayes' rule can be recursively applied for sequential experiments.

Upon propagating the parameter distributions through H , the prior- and posterior-predictive densities for Z_m can be respectively written as:

$$p(z_m) = \iint p(\theta_m, \psi_m) p(z_m | \theta_m, \psi_m) d\theta_m d\psi_m, \quad (4)$$

$$p(z_m | i_{k+1}) = \iint p(\theta_m, \psi_m | i_{k+1}) p(z_m | \theta_m, \psi_m) d\theta_m d\psi_m. \quad (5)$$

If H is deterministic, $p(z_m | \theta_m, \psi_m)$ collapses to a Dirac delta centered at $z_m = H(\theta_m, \psi_m; m)$.

2.2. Sequential optimal experimental design (sOED)

We present sOED following [21] and earlier works [19, 20] that modeled it through a Markov decision process (MDP). The MDP is defined by a tuple $(\mathcal{S}, \{\mathcal{A}_k\}_k, s_0, \{r_k(\cdot)\}_k, \{T_k(\cdot)\}_k)$ consisting of a state space \mathcal{S} for the state variable S_k that can take values $s_k \in \mathcal{S}$, action spaces \mathcal{A}_k comprising possible actions (which here are designs) $\xi_k \in \mathcal{A}_k$, an initial state s_0 , scalar-valued reward functions $r_k(s_k, \xi_k, y_k)$ that evaluate the instantaneous reward when taking action ξ_k and observing y_k at state s_k , and state transition kernels $T_k(\mathcal{S}_{k+1}|s_k, \xi_k)$ that evaluate the probability of transitioning to any set of states $\mathcal{S}_{k+1} \subseteq \mathcal{S}$ at stage $k+1$ having taken action ξ_k at state s_k . In the context of experimental design, the action being taken is the selection of a design; thus we use the terms ‘action’ and ‘design’ interchangeably.

State. The state before the k th experiment is described by $S_k = \{S_k^b, S_k^p\}$, a quantity that summarizes all information deemed relevant to future design decisions. We split S_k into a ‘belief state’ S_k^b representing the state of knowledge/uncertainty in M , Θ_m , Ψ_m , and Z_m , and a ‘physical state’ S_k^p comprising any other deterministic variables that may be relevant to the design process. A realization of the belief state, s_k^b , is simply the joint posterior distribution of M , Θ_m , Ψ_m , and Z_m given all past experimental designs and realized observations, \mathbf{i}_k . Numerically, it can be represented by, for example, a density or distribution function approximation, or an ensemble of particles, or by tracking \mathbf{i}_k directly. Tracking \mathbf{i}_k is easiest to implement since it does not require additional calculations translating $(\xi_i)_{i < k}$ and $(y_i)_{i < k}$ to another representation, but the dimension of \mathbf{i}_k grows with k albeit bounded for finite N .

Maintaining only a belief state, in the form of the posterior, does not suffice to preserve the Markov property of the system if the likelihood depends on the history of past experiments \mathbf{i}_k , as in Eq. (3). This can be fixed by introducing a physical state. With regard to the \mathbf{i}_k -dependence in $p(y_k|m, \theta, \psi_k, \xi_k, \mathbf{i}_k)$, the physical state essentially extracts and tracks relevant features from \mathbf{i}_k that allow the likelihood to be evaluated or the observations Y_k simulated. If I_k is adopted as the belief state, then information about the physical state is already contained in I_k , even if only implicitly. We adopt $S_k = I_k$ in this work and will use them interchangeably.

Action (design) and policy. Sequential experimental design is adaptive in nature, and looks for a strategy, called a *policy* (or *actor*), describing *how to choose* the design depending on the current state. The policy is a collection of functions $\pi = \{\mu_k : \mathcal{S} \rightarrow \mathcal{A}_k, k = 0, \dots, N-1\}$, where the policy function μ_k returns the design for the k th experiment given the current state, $\xi_k = \mu_k(s_k)$.

State transition dynamics. When an experiment is performed, the state changes according to a transition kernel $T_k(\mathcal{S}_{k+1}|s_k, \xi_k)$ describing the probability of transitioning from the current state s_k , having chosen design ξ_k and observed the outcome of resulting experiment, to any set of states at stage $k+1$, $\mathcal{S}_{k+1} \subseteq \mathcal{S}$. This kernel is generally intractable to evaluate, but can be simulated by first sampling Y_k given the design ξ_k , and then applying Bayes’ rule Eq. (3). We denote the latter transition dynamics by $s_{k+1} = \mathcal{F}_k(s_k, \xi_k, y_k)$; the function \mathcal{F}_k encapsulates the transition from prior to posterior, given values of ξ_k and the realized data y_k , following Eq. (3). If adopting I_k as the state, then the transition is a simple concatenation $\mathbf{i}_{k+1} = \{\mathbf{i}_k, \xi_k, y_k\}$.

Reward (utility). Here $r_k(s_k, \xi_k, y_k) \in \mathbb{R}$ denotes the reward immediately obtained from the k th experiment, and $r_N(s_N) \in \mathbb{R}$ is the terminal reward that can be computed only after all

experiments are completed. Examples of information-theoretic rewards will be provided in Sections 2.3 and 2.4.

sOED problem statement. The sOED problem seeks a design policy that maximizes the expected utility $U(\pi)$:

$$\begin{aligned} \pi^* \in \arg \max_{\pi=\{\mu_0, \dots, \mu_{N-1}\}} & \left\{ U(\pi) := \mathbb{E}_{Y_{0:N-1}|\pi, s_0} \left[\sum_{k=0}^{N-1} r_k(S_k, \xi_k, Y_k) + r_N(S_N) \right] \right\} \\ \text{subject to} & \quad \xi_k = \mu_k(S_k) \in \mathcal{A}_k, \\ & \quad S_{k+1} = \mathcal{F}_k(S_k, \xi_k, Y_k), \quad \text{for } k = 0, \dots, N-1. \end{aligned} \quad (6)$$

Here $Y_{0:N-1} = Y_0, Y_1, \dots, Y_{N-1}$. The initial state s_0 is assumed known; if it is not known, another expectation can be taken over S_0 . While we strive to explicitly write out the conditioning on s_0 , it should be interpreted that all terms in this paper are implicitly conditioning on s_0 even if not written. When adopting $S_k = I_k$, the constraints can be written as $\xi_k = \mu_k(I_k) \in \mathcal{A}_k$ and $I_{k+1} = \{I_k, \xi_k, Y_k\}$. This sOED formulation generalizes both the batch and greedy designs [21, Section 2.3].

2.3. Experimental design rewards

We propose two information gain (IG)-based [7, 56] reward formulations incorporating multiple design objectives. Non-IG-based reward terms (i.e., those that do not depend on the posteriors, such as a cost term of the experiment that depends only on ξ_k) may also be added without affecting the results below, but we omit them for simplicity of presentation. We will largely use I_k in place of S_k from hereon.

(1) *Terminal-information-gain (TIG).* TIG targets the overall IG (i.e., the Kullback–Leibler [KL] divergence from prior to posterior) from all N experiments via the terminal reward:

$$r_k(i_k, \xi_k, y_k) = 0, \quad k = 0, \dots, N-1, \quad (7)$$

$$\begin{aligned} r_N(i_N) = \alpha_M D_{\text{KL}}(P_{M|i_N} \parallel P_M) \\ + \mathbb{E}_{M|i_N} [\alpha_\Theta D_{\text{KL}}(p_{\Theta_m|i_N} \parallel p_{\Theta_m}) + \alpha_Z D_{\text{KL}}(p_{Z_m|i_N} \parallel p_{Z_m})], \end{aligned} \quad (8)$$

where in the KL divergence the upper case P denotes probability mass (for discrete random variables), subscript indicates the random variable that corresponds to the probability mass or density, and $\alpha_M, \alpha_\Theta, \alpha_Z \in [0, 1]$ are the weights for IG respectively coming from the model indicator, PoIs, and QoIs. For example, setting $\alpha_M = 1$ and $\alpha_\Theta = \alpha_Z = 0$ reduces to ‘OED for model indicator’ (i.e., design for model discrimination); $\alpha_\Theta = 1$ and $\alpha_M = \alpha_Z = 0$ reduces to ‘OED for PoIs’ (i.e., design for parameter inference); $\alpha_Z = 1$ and $\alpha_\Theta = \alpha_M = 0$ reduces to ‘OED for QoIs’ (i.e., design for goal-oriented prediction). In the special case when $\alpha_M = \alpha_\Theta = 1$ and $\alpha_Z = 0$, the terminal reward r_N becomes $D_{\text{KL}}(p_{M, \Theta_m|i_N} \parallel p_{M, \Theta_m})$ (Appendix A.1); when $\alpha_M = \alpha_Z = 1$ and $\alpha_\Theta = 0$, it similarly becomes $D_{\text{KL}}(p_{M, Z_m|i_N} \parallel p_{M, Z_m})$ (Appendix A.1). When nuisance parameters Ψ_m are absent, one should not set both α_Θ and α_Z to 1 since the IG in Z_m is already absorbed into the IG in Θ_m (Appendix A.2).

(2) *Incremental-information-gain (IIG)*. IIG adopts incremental IG as the immediate rewards:

$$r_k(\mathbf{i}_k, \xi_k, y_k) = \alpha_M D_{\text{KL}}(P_{M|\mathbf{i}_{k+1}} \| P_{M|\mathbf{i}_k}) + \mathbb{E}_{M|\mathbf{i}_{k+1}} \left[\alpha_\Theta D_{\text{KL}}(p_{\Theta_m|\mathbf{i}_{k+1}} \| p_{\Theta_m|\mathbf{i}_k}) + \alpha_Z D_{\text{KL}}(p_{Z_m|\mathbf{i}_{k+1}} \| p_{Z_m|\mathbf{i}_k}) \right], \quad k = 0, \dots, N-1, \quad (9)$$

$$r_N(\mathbf{i}_N) = 0. \quad (10)$$

Note that \mathbf{i}_{k+1} can be evaluated in Eq. (9) since $\mathbf{i}_{k+1} = \{\mathbf{i}_k, \xi_k, y_k\}$.

Let $U_T(\pi)$ denote the resulting sOED expected utility in Eq. (6) when adopting the TIG rewards in Eqs. (7) and (8), and $U_I(\pi)$ denote that when adopting the IIG rewards in Eqs. (9) and (10).

Theorem 1 (Terminal-incremental equivalence). $U_T(\pi) = U_I(\pi)$ for any policy π .

A proof is provided in [Appendix A.3](#). Hence, both formulations induce the same sOED problem.

2.4. One-point formulation of rewards

To compute the sOED objective in Eq. (6) with the TIG or IIG rewards, an expectation needs to be taken over $Y_{0:N-1}|\pi, s_0$. This requires sampling trajectories. For each trajectory, a model indicator and corresponding PoIs and nuisance parameters are drawn from the priors, $m_0^{(i)} \sim P_M$, $\theta_{m,0}^{(i)} \sim p(\theta_{m,0}|m_0^{(i)})$, $\psi_{m,0}^{(i)} \sim p(\psi_{m,0}|m_0^{(i)})$, and a corresponding QoI sample is also drawn, $z_{m,0}^{(i)} \sim p(z_{m,0}|\theta_{m,0}^{(i)}, \psi_{m,0}^{(i)}, m_0^{(i)})$ (if Z_m has a deterministic H , then simply $z_{m,0}^{(i)} = H(\theta_{m,0}^{(i)}, \psi_{m,0}^{(i)}; m_0^{(i)})$). Then, $m_0^{(i)}$, $\theta_{m,0}^{(i)}$, and $\psi_{m,0}^{(i)}$ generate a trajectory \mathbf{i}_N . For any such trajectory, we substitute these ‘oracle’ values of the model indicator and model parameters that generated \mathbf{i}_N into the integrands of the KL divergence terms to produce a ‘one-point’ approximation \check{r}_k for each r_k .

(1) *One-point-TIG*. One-point-TIG entails the following new reward terms:

$$\check{r}_k(\mathbf{i}_k, \xi_k, y_k) = 0, \quad k = 0, \dots, N-1, \quad (11)$$

$$\check{r}_N(\mathbf{i}_N) = \alpha_M \log \frac{P(m_0|\mathbf{i}_N)}{P(m_0)} + \alpha_\Theta \log \frac{p(\theta_{m,0}|\mathbf{i}_N)}{p(\theta_{m,0})} + \alpha_Z \log \frac{p(z_{m,0}|\mathbf{i}_N)}{p(z_{m,0})}. \quad (12)$$

(2) *One-point-IIG*. One-point-IIG entails the following new reward terms:

$$\check{r}_k(\mathbf{i}_k, \xi_k, y_k) = \alpha_M \log \frac{P(m_0|\mathbf{i}_{k+1})}{P(m_0|\mathbf{i}_k)} + \alpha_\Theta \log \frac{p(\theta_{m,0}|\mathbf{i}_{k+1})}{p(\theta_{m,0}|\mathbf{i}_k)} + \alpha_Z \log \frac{p(z_{m,0}|\mathbf{i}_{k+1})}{p(z_{m,0}|\mathbf{i}_k)}, \quad k = 0, \dots, N-1, \quad (13)$$

$$\check{r}_N(\mathbf{i}_N) = 0. \quad (14)$$

More precisely, the one-point reward terms are now functions of the trajectory-generating oracle model and parameter values, i.e., $\check{r}_k(\mathbf{i}_k, \xi_k, y_k, m_0, \theta_{m,0}, z_{m,0})$ and $\check{r}_N(\mathbf{i}_N, m_0, \theta_{m,0}, z_{m,0})$, but with the constraint that the $m_0, \theta_{m,0}, z_{m,0}$ arguments are those that generated the \mathbf{i}_N

argument; we omitted the oracle arguments in the \check{r}_k expressions above for simplicity. Thus, we need to take expectation jointly over these inputs, to arrive at the *one-point expected utility*:

$$\check{U}(\pi) = \mathbb{E}_{M_0, \Theta_{m,0}, \Psi_{m,0}, Z_{m,0}} \left[\mathbb{E}_{I_N | \pi, s_0, M_0, \Theta_{m,0}, \Psi_{m,0}} \left[\sum_{k=0}^{N-1} \check{r}_k(I_k, \xi_k, Y_k) + \check{r}_N(I_N) \right] \right], \quad (15)$$

where we switch to the notation with $S_k = I_k$ to correspond to the I_k -based reward definitions, use the equivalence of $\mathbb{E}_{Y_{0:N-1} | \pi, s_0, \dots}$ and $\mathbb{E}_{I_N | \pi, s_0, \dots}$, and follow the policy $\xi_k = \mu_k(I_k)$. Moreover, the inner expectation's conditioning on $Z_{m,0}$ is dropped since the I_N sequence (and the Y_k 's within I_N) does not depend on Z_m when π is given. Furthermore, the expectation over $Z_{m,0}$ can be ignored altogether for Z_m 's with deterministic H .

Let $\check{U}_T(\pi)$ denote the resulting sOED expected utility from Eq. (15) when adopting the one-point-TIG rewards in Eqs. (11) and (12), and $\check{U}_I(\pi)$ denote that when adopting the one-point-IIG rewards in Eqs. (13) and (14).

Theorem 2 (One-point equivalence). $U_T(\pi) = \check{U}_T(\pi) = \check{U}_I(\pi) = U_I(\pi)$ for any policy π .

A proof is provided in [Appendix A.4](#). Hence, both the original sOED and one-point formulations, using either TIG or IIG, induce the same sOED problem.

Remark 1. For $\check{U}_I(\pi)$, under the summation, all intermediate posteriors cancel out and only the prior terms $p(\cdot)$ and the final posterior terms $p(\cdot | I_N)$ survive. However, working with intermediate posteriors in the incremental rewards can lead to denser rewards that improves numerical performance [34].

Remark 2. For any expected utility form, the prior terms $p(\cdot)$ may be omitted since they are independent of π and would only shift the expected utility without affecting the maximizer ([Appendix A.5](#)). Therefore, when the prior is difficult to compute (e.g., the prior-predictive $p(z_m)$ in Eq. (4) that needs to marginalize out Θ_m and Ψ_m), we will drop that prior term when optimizing the policy.

2.5. Variational sequential optimal experimental design (vsOED)

Evaluating the probability terms of the one-point formulations in Section 2.4 remains highly challenging. To make the computation tractable, we replace all posterior terms $p(\cdot | i_k)$ with variational posterior approximations $q(\cdot | i_k; \phi_{(\cdot)})$ parameterized by $\phi_{(\cdot)}$.

(1) *Variational-one-point-TIG.* Variational-one-point-TIG reward terms update to:

$$\tilde{r}_k(i_k, \xi_k, y_k; \phi) = 0, \quad k = 0, \dots, N-1, \quad (16)$$

$$\tilde{r}_N(i_N; \phi) = \alpha_M \log \frac{q(m_0 | i_N; \phi_M)}{P(m_0)} + \alpha_\Theta \log \frac{q(\theta_{m,0} | i_N; \phi_{\Theta_m})}{p(\theta_{m,0})} + \alpha_Z \log \frac{q(z_{m,0} | i_N; \phi_{Z_m})}{p(z_{m,0})}, \quad (17)$$

where $\phi = \{\phi_M, \phi_{\Theta_m}, \phi_{Z_m}\}$ is the full set of variational parameters.

(2) *Variational-one-point-IIG*. Variational-one-point-IIG reward terms update to:

$$\begin{aligned} \tilde{r}_k(i_k, \xi_k, y_k; \phi) &= \alpha_M \log \frac{q(m_{0,0}|i_{k+1}; \phi_M)}{q(m_{0,0}|i_k; \phi_M)} + \alpha_\Theta \log \frac{q(\theta_{m,0}|i_{k+1}; \phi_{\Theta_m})}{q(\theta_{m,0}|i_k; \phi_{\Theta_m})} \\ &\quad + \alpha_Z \log \frac{q(z_{m,0}|i_{k+1}; \phi_{Z_m})}{q(z_{m,0}|i_k; \phi_{Z_m})}, \quad k = 0, \dots, N-1, \end{aligned} \quad (18)$$

$$\tilde{r}_N(i_N; \phi) = 0, \quad (19)$$

with the understanding that here $q(\cdot|i_0; \phi_{(\cdot)})$ is simply the prior $p(\cdot)$ without any approximation. Similar to \tilde{r}_k , the new \tilde{r}_k expressions are also functions of the oracle variables, but we omitted them in the expressions above for simplicity. Upon taking expectation over all random variables, the corresponding *variational one-point expected utility* becomes:

$$\tilde{U}(\pi, \phi) = \mathbb{E}_{M_0, \Theta_{m,0}, \Psi_{m,0}, Z_{m,0}} \left[\mathbb{E}_{I_N | \pi, s_0, M_0, \Theta_{m,0}, \Psi_{m,0}} \left[\sum_{k=0}^{N-1} \tilde{r}_k(I_k, \xi_k, Y_k; \phi) + \tilde{r}_N(I_N; \phi) \right] \right], \quad (20)$$

where $\xi_k = \mu_k(I_k)$, and again the outer expectation over $Z_{m,0}$ can be ignored for Z_m 's with deterministic H .

Let $\tilde{U}_T(\pi)$ denote the resulting sOED expected utility from Eq. (20) when adopting the variational-one-point-TIG rewards in Eqs. (16) and (17), and $\tilde{U}_I(\pi)$ denote that when adopting the variational-one-point-IIG rewards in Eqs. (18) and (19).

Theorem 3 (Variational lower bound). $\tilde{U}_I(\pi; \phi) = \tilde{U}_T(\pi; \phi) \leq \check{U}_T(\pi) = \check{U}_I(\pi) = U_T(\pi) = U_I(\pi)$ for any policy π and variational parameters ϕ . The bound is tight if and only if all final posteriors are perfectly approximated, i.e., $q(\cdot|i_N; \phi_{(\cdot)}) = p(\cdot|i_N)$ (except the trivial case when $\alpha_M = \alpha_\Theta = \alpha_Z = 0$).

A proof is provided in [Appendix A.6](#).

Remark 3. In batch OED and when $\alpha_M = \alpha_Z = 0$ and $\alpha_\Theta = 1$, Eq. (20) becomes the BA lower bound for mutual information between Θ and Y [41, 36, 42].

Remark 4. The results in all aforementioned theorems also hold when incorporating non-IG-based reward terms (i.e., those that do not depend on the posteriors, such as a cost term of the experiment that depends only on ξ_k).

Remark 5. The tightness of the bound does not depend on the quality of the intermediate variational posteriors (i.e., $q(\cdot|i_k; \phi_{(\cdot)})$ for $k = 1, \dots, N-1$) due to their cancellations, similar to Remark 1. Thus, low-quality intermediate posterior approximations may be used without affecting the theoretical value of the bound (see the first part of [Appendix A.6](#)). In the special case where all intermediate posteriors are approximated by the prior, variational-one-point-IIG collapses to variational-one-point-TIG. As we will show through numerical examples, however, good intermediate posterior approximations can lead to better computational performance.

Variational sOED problem statement. The **vsOED** problem seeks a design policy that maximizes the lower bound $\tilde{U}(\pi; \phi)$:

$$\begin{aligned} \{\pi^*, \phi^*\} &\in \arg \max_{\pi = \{\mu_0, \dots, \mu_{N-1}\}, \phi} \tilde{U}(\pi; \phi) \\ &\text{subject to} \quad \xi_k = \mu_k(I_k) \in \mathcal{A}_k, \\ &\quad I_{k+1} = \{I_k, \xi_k, Y_k\}, \quad \text{for } k = 0, \dots, N-1, \end{aligned} \quad (21)$$

where we used the notation adopting $S_k = I_k$.

3. Numerical methods for vsOED

Taking a similar approach as [21], we propose an actor-critic policy gradient method to solve the vsOED problem in Eq. (21). The key to this method is to derive and compute gradients of the expected utility lower bound \tilde{U} defined in Eq. (20) with respect to the variational parameters and the policy, and use the gradients to improve the policy via, for example, gradient ascent.

To bring the policy (which entails functions) to a finite-dimensional space, we parameterize the policy π by $w \in \mathbb{R}^{N_w}$ and denote the parameterized policy as π_w . Forming the policy (i.e., the *actor*) explicitly in such a manner offers significantly faster online evaluation speeds [31, 32, 33, 34] compared to dynamic programming [20] and greedy design that require solving optimization problems on the fly. Upon replacing π with π_w , the vsOED problem from Eq. (21) becomes:

$$\begin{aligned} \{w^*, \phi^*\} \in \arg \max_{w, \phi} \quad & \tilde{U}(w; \phi) \\ \text{subject to} \quad & \xi_k = \mu_{k,w}(I_k) \in \mathcal{A}_k, \\ & I_{k+1} = \{I_k, \xi_k, Y_k\}, \quad \text{for } k = 0, \dots, N-1. \end{aligned} \quad (22)$$

The gradient of \tilde{U} with respect to ϕ can be obtained trivially by applying the Leibniz rule:

$$\nabla_{\phi} \tilde{U}(w; \phi) = \mathbb{E}_{M_0, \Theta_{m,0}, \Psi_{m,0}, Z_{m,0}} \left[\mathbb{E}_{I_N | w, s_0, M_0, \Theta_{m,0}, \Psi_{m,0}} \left[\sum_{k=0}^{N-1} \nabla_{\phi} \tilde{r}_k(I_k, \xi_k, Y_k; \phi) + \nabla_{\phi} \tilde{r}_N(I_N; \phi) \right] \right], \quad (23)$$

where $\xi_k = \mu_{k,w}(I_k)$. The actor-critic policy gradient can be derived near-identically as the proof in Appendix B of [21] except that the expressions for vsOED now involve an additional outer expectation jointly over $M_0, \Theta_{m,0}, \Psi_{m,0}, Z_{m,0}$; therefore we do not repeat the derivation in this paper. The final vsOED policy gradient expression is:

$$\nabla_w \tilde{U}(w; \phi) = \mathbb{E}_{M_0, \Theta_{m,0}, \Psi_{m,0}, Z_{m,0}} \left[\sum_{k=0}^{N-1} \mathbb{E}_{I_k | w, s_0, M_0, \Theta_{m,0}, \Psi_{m,0}} \left[\nabla_w \mu_{k,w}(I_k) \nabla_{\xi_k} \tilde{Q}_k^{\pi_w}(I_k, \xi_k; \phi) \right] \right], \quad (24)$$

where $\xi_k = \mu_{k,w}(I_k)$, and $\tilde{Q}_k^{\pi_w}$ is the *action-value function* (i.e., the *critic*) induced by the variational one-point reward terms \tilde{r}_k and \tilde{r}_N and defined as:

$$\begin{aligned} \tilde{Q}_k^{\pi_w}(i_k, \xi_k; \phi) &= \mathbb{E}_{M_0, \Theta_{m,0}, \Psi_{m,0}, Z_{m,0} | i_k} \left[\mathbb{E}_{Y_{k:N-1} | w, s_0, i_k, \xi_k, M_0, \Theta_{m,0}, \Psi_{m,0}} \left[\tilde{r}_k(i_k, \xi_k, Y_k; \phi) \right. \right. \\ &\quad \left. \left. + \sum_{t=k+1}^{N-1} \tilde{r}_t(I_t, \mu_{t,w}(I_t), Y_t; \phi) + \tilde{r}_N(I_N; \phi) \right] \right] \quad (25) \end{aligned}$$

$$\begin{aligned} &= \mathbb{E}_{M_0, \Theta_{m,0}, \Psi_{m,0}, Z_{m,0} | i_k} \left[\mathbb{E}_{Y_k | w, s_0, i_k, \xi_k, M_0, \Theta_{m,0}, \Psi_{m,0}} \left[\tilde{r}_k(i_k, \xi_k, Y_k; \phi) \right. \right. \\ &\quad \left. \left. + \tilde{Q}_{k+1}^{\pi_w}(I_{k+1}, \mu_{k+1,w}(I_{k+1}); \phi) \right] \right], \quad (26) \end{aligned}$$

$$\tilde{Q}_N^{\pi_w}(i_N, \cdot; \phi) = \mathbb{E}_{M_0, \Theta_{m,0}, \Psi_{m,0}, Z_{m,0} | i_N} \left[\tilde{r}_N(i_N; \phi) \right], \quad (27)$$

for $k = 0, \dots, N - 1$ and subject to $I_{k+1} = \{I_k, \xi_k, Y_k\}$. The value of the critic $\tilde{Q}_k^{\pi_w}(i_k, \xi_k; \phi)$ is the expected remaining cumulative reward (i.e., the expected sum of all remaining rewards) under variational parameters ϕ , for performing the k th experiment at design ξ_k from state i_k (i.e., from the latest posterior that is conditioned on i_k , as indicated by the outer conditional expectation) and thereafter following policy π_w . The critic can also be written in a recursive manner in Eq. (26). To facilitate computing the $\nabla_{\xi_k} \tilde{Q}_k^{\pi_w}$ term in Eq. (24), we also parameterize the critic functions by $\nu \in \mathbb{R}^{N_\nu}$ and denote the parameterized form as $\tilde{Q}_{k,\nu}^{\pi_w}$.

In summary, the two main steps involve: (a) forming variational posterior approximations q and estimating $\nabla_\phi \tilde{U}$ in Eq. (23), and (b) forming approximate critic $\tilde{Q}_{k,\nu}^{\pi_w}$ and estimating $\nabla_w \tilde{U}$ in Eq. (24). We detail these two steps below.

3.1. Variational gradient

Adopting the variational-one-point-TIG rewards into Eq. (23), it is easy to verify that

$$\begin{aligned} \nabla_\phi \tilde{U}(w; \phi) = \mathbb{E}_{M_0, \Theta_{m,0}, \Psi_{m,0}, Z_{m,0}} \left[\mathbb{E}_{I_N | w, s_0, M_0, \Theta_{m,0}, \Psi_{m,0}} \left[\alpha_M \nabla_{\phi_M} \log q(M_0 | I_N; \phi_M) \right. \right. \\ \left. \left. + \alpha_\Theta \nabla_{\phi_{\Theta_m}} \log q(\Theta_{m,0} | I_N; \phi_{\Theta_m}) \right. \right. \\ \left. \left. + \alpha_Z \nabla_{\phi_{Z_m}} \log q(Z_{m,0} | I_N; \phi_{Z_m}) \right] \right], \quad (28) \end{aligned}$$

where the log-prior terms disappear under the gradient operation since they do not depend on ϕ . The variational gradient for the variational-one-point IIG case is exactly the same, since the intermediate variational posteriors all cancel per Appendix A.6 and the gradient to those terms' ϕ 's will always be zero. In order to obtain good intermediate posterior approximations in the variational-one-point-IIG case, we first note that the variational 'partial-length' expected utility up to stage k remains a lower bound to its non-variational counterpart for all k —that is, the result in Appendix A.6 remains true if we replace I_N with I_k , $\forall k$. Then, we can optimize the intermediate posteriors' ϕ 's by successively maximizing these partial-length lower bounds.

We can then form a Monte Carlo (MC) estimator for the variational gradient in Eq. (28):

$$\begin{aligned} \nabla_\phi \tilde{U}(w; \phi) \approx \frac{1}{n} \sum_{i=1}^n \left[\alpha_M \nabla_{\phi_M} \log q(m_0^{(i)} | i_N^{(i)}; \phi_M) \right. \\ \left. + \alpha_\Theta \nabla_{\phi_{\Theta_m}} \log q(\theta_{m,0}^{(i)} | i_N^{(i)}; \phi_{\Theta_m}) \right. \\ \left. + \alpha_Z \nabla_{\phi_{Z_m}} \log q(z_{m,0}^{(i)} | i_N^{(i)}; \phi_{Z_m}) \right], \quad (29) \end{aligned}$$

where the samples $m_0^{(i)}, \theta_{m,0}^{(i)}, \psi_{m,0}^{(i)}, z_{m,0}^{(i)}$ and corresponding trajectories $i_N^{(i)}$ are generated following the same procedure described at the beginning of Section 2.4. In practice, multiple steps of gradient update can be applied to ϕ at a given w to more efficiently make use of the trajectory samples.

3.2. Policy gradient

In order to compute the policy gradient $\nabla_w \tilde{U}(w; \phi)$ in Eq. (24), we need to first form the approximate critic $\tilde{Q}_{k,\nu}^{\pi_w}$. This can be achieved by training $\tilde{Q}_{k,\nu}^{\pi_w}$, for any given ϕ , in a supervised

learning manner to optimize ν towards the true $\tilde{Q}_k^{\pi_w}$ by minimizing a loss function based on the recursive definition in Eq. (26). Since the true $\tilde{Q}_{k+1}^{\pi_w}$ values would not be available, they are replaced with the current approximations $\tilde{Q}_{k+1,\nu}^{\pi_w}$:

$$\nu^* \in \operatorname{argmin}_{\nu} \left\{ \mathcal{L}_{\phi}(\nu) := \frac{1}{n} \sum_{i=1}^n \sum_{k=0}^{N-1} \left[\tilde{Q}_{k,\nu}^{\pi_w}(\mathbf{i}_k^{(i)}, \xi_k^{(i)}; \phi) - \left(\tilde{r}_k(\mathbf{i}_k^{(i)}, \xi_k^{(i)}, y_k^{(i)}; \phi) + \gamma \tilde{Q}_{k+1,\nu}^{\pi_w}(\mathbf{i}_{k+1}^{(i)}, \xi_{k+1}^{(i)}; \phi) \right) \right]^2 \right\}, \quad (30)$$

where $\gamma \in [0, 1]$ is a weighing factor inserted for regularization. In practice, we first sample entire trajectories of $\mathbf{i}_N^{(i)}$ following the procedure described at the beginning of Section 2.4. Then, we extract the partial sequences $\mathbf{i}_k^{(i)}$ and designs $\xi_k^{(i)}$ resulting from the same sample trajectory $\mathbf{i}_N^{(i)}$ to use for all k , instead of generating new $\mathbf{i}_{k+1}^{(i)}$ from their latest posteriors which would be much more expensive. The gradient $\nabla_{\nu} \mathcal{L}_{\phi}(\nu)$ can be obtained readily by differentiating $\tilde{Q}_{k,\nu}^{\pi_w}$ with respect to ν , while the contribution from $\tilde{Q}_{k+1,\nu}^{\pi_w}$ is typically omitted as it is a stand-in of the true $\tilde{Q}_{k+1}^{\pi_w}$ that does not depend on ν . The optimal value of ν^* needs not be precisely found, and often just a few steps of gradient update at this π_w can already lead to good performance.

The loss \mathcal{L}_{ϕ} from Eq. (30) can be used for both variational-one-point-TIG and -IIG. However, the TIG case has $\tilde{r}_k = 0$ for $k = 0, \dots, N-1$ (except for possible non-IG reward terms) and as a result it would take many ν updates from Eq. (30)—especially when N is large—for the non-zero \tilde{r}_N to propagate to the $\tilde{Q}_{k,\nu}^{\pi_w}$'s at early k 's. This can lead to slow or even divergent policy gradient updates. To mitigate this effect, we follow the REINFORCE algorithm [57] and propose a modified loss as a more stable option for the TIG case:

$$\mathcal{L}_{\phi,T}(\nu) = \frac{1}{n} \sum_{i=1}^n \sum_{k=0}^{N-1} \left[\tilde{Q}_{k,\nu}^{\pi_w}(\mathbf{i}_k^{(i)}, \xi_k^{(i)}; \phi) - \eta \left(\tilde{r}_k(\mathbf{i}_k^{(i)}, \xi_k^{(i)}, y_k^{(i)}; \phi) + \gamma \tilde{Q}_{k+1,\nu}^{\pi_w}(\mathbf{i}_{k+1}^{(i)}, \xi_{k+1}^{(i)}; \phi) \right) - (1 - \eta) \left(\sum_{t=k}^{N-1} \gamma^{t-k} \tilde{r}_t(\mathbf{i}_t^{(i)}, \xi_t^{(i)}, y_t^{(i)}; \phi) + \gamma^{N-k} \tilde{r}_N(\mathbf{i}_N^{(i)}; \phi) \right) \right]^2, \quad (31)$$

where η linearly increases from 0 to 1 during the training process.

Once $\tilde{Q}_{k,\nu}^{\pi_w}$ is obtained, we finally form the MC estimator for the policy gradient in Eq. (24):

$$\nabla_w \tilde{U}(w; \phi) \approx \frac{1}{n} \sum_{i=1}^n \sum_{k=0}^{N-1} \nabla_w \mu_{k,w}(\mathbf{i}_k^{(i)}) \nabla_{\xi_k} \tilde{Q}_{k,\nu}^{\pi_w}(\mathbf{i}_k^{(i)}, \xi_k^{(i)}; \phi), \quad (32)$$

where $\mathbf{i}_N^{(i)}$ is generated following the same procedure described at the beginning of Section 2.4 using policy π_w , and $\mathbf{i}_k^{(i)}$ and $\xi_k^{(i)}$ are the partial sequences and designs, respectively, of the full sample sequence $\mathbf{i}_N^{(i)}$.

3.3. Implementation techniques and the overall algorithm

Variational posteriors. We use a neural network (NN) to represent the approximate posterior of model indicator, $q(m_0 | \mathbf{i}_k; \phi_M)$; the NN takes \mathbf{i}_k as input and uses a softmax output

activation to output model probability. For the approximate posteriors of PoIs and QoIs, respectively $q(\theta_{m,0}|i_k; \phi_{\Theta_m})$ and $q(z_{m,0}|i_k; \phi_{Z_m})$, we adopt independent Gaussian mixture models (GMMs) with NNs predicting the GMM weights, means, and standard deviations. Truncated normal is used for variables with compact support. We also explore the use of normalizing flows (NFs) [43] for posterior approximations. More details can be found in [Appendix B.1](#) and [Appendix B.2](#).

Policy and critic networks. We employ NNs to represent both π_w and $\tilde{Q}_{k,\nu}^{\pi_w}$, therefore we also refer to these NNs as the policy network and critic network, respectively. The optimizations of the policy and critic networks are both carried out using Adam [58] with mini-batching. More details about these networks can be found in [Appendix B.3](#) and [Appendix B.4](#).

Target networks. We adopt target networks for the actor and critic—i.e., secondary networks updated less frequently and with a damping factor—in order to promote stability in the training process by smoothing the learning target and mitigating drastic changes of Q-values and designs across training iterations. Target networks have been shown to greatly improve robustness and effectiveness of policy-gradient-based methods [59].

Replay buffer. We use a replay buffer to store past trajectory samples from previously encountered policies, and resample these stored samples for use during the policy optimization process. Replay buffer permits off-policy learning, which entails optimizing the policy using data generated from policies that differ from the current one [60]. This can help stabilize the optimization and improve sample efficiency by allowing multiple uses of the simulation data, for example those generated from policies in previous iterations and from exploration policies [61].

Exploration policy. A balance of exploration and exploitation is important for the numerical optimizer to identify a good policy. Insufficient exploration limits understanding of the objective function’s global landscape, while too much exploration can delay convergence. To inject exploration, we make use of an exploration policy during the policy optimization (i.e., training) phase by adding perturbation to the deterministic base policy: $\xi_k = \mu_{k,w}(I_k) + \mathcal{E}_{k,\text{explore}}$, where $\mathcal{E}_{k,\text{explore}} \sim \mathcal{N}(0, \Sigma_{k,\text{explore}})$ and $\Sigma_{k,\text{explore}} = \mathbb{I}\sigma_{k,\text{explore}}^2$ is a diagonal covariance whose entries reflect the exploration length scale for each dimension of \mathcal{A}_k . A reasonable strategy is to set larger exploration in the early training iterations and reduce it gradually; details will be specified for each numerical case in [Section 4](#). Once the final policy is obtained, its evaluation (i.e., testing phase) will use the deterministic policy only.

Overall algorithm. Pseudocode for the overall vsOED algorithm is presented in [Algorithm 1](#). While we write the simple gradient ascent update formulas in the pseudocode for illustration, it can be replaced by any other gradient-based updates.

4. Numerical experiments

We demonstrate vsOED and compare it against other state-of-the-art sequential experimental design methods across a number of problems with varying complexity and that illuminate different challenges. We first describe the demonstration setup in [Section 4.1](#), and then present results for four cases: Case 1—source location finding in [Section 4.2](#); Case 2—constant elasticity of substitution (CES) in [Section 4.3](#); Case 3—SIR model for disease spread in [Section 4.4](#); and Case 4—convection-diffusion-reaction in [Section 4.5](#).

Algorithm 1: The vsOED algorithm.

- 1: Initialize variational parameters ϕ , actor (policy) parameters w , critic (action-value function) parameters ν ;
 - 2: **for** $l = 1, \dots, n_{\text{updates}}$ **do**
 - 3: Simulate n_{traj} trajectories: for the i th trajectory, sample $m_0^{(i)} \sim P_M$, $\theta_{m,0}^{(i)} \sim p(\theta_{m,0} | m_0^{(i)})$, $\psi_{m,0}^{(i)} \sim p(\psi_{m,0} | m_0^{(i)})$, $z_{m,0}^{(i)} \sim p(z_{m,0} | \theta_{m,0}^{(i)}, \psi_{m,0}^{(i)}, m_0^{(i)})$, and then for $k = 0, \dots, N - 1$ generate $\xi_k^{(i)} = \mu_{k,w_i}(\mathbf{i}_k^{(i)}) + \epsilon_{k,\text{explore}}^{(i)}$ and $y_k^{(i)} \sim p(y_k | m_0^{(i)}, \theta_{m,0}^{(i)}, \psi_{m,0}^{(i)}, \xi_k^{(i)}, \mathbf{i}_k^{(i)})$;
 - 4: Update newly generated information sequences $\{\mathbf{i}_N^{(i)}\}_{i=1}^{n_{\text{traj}}}$ into replay buffer;
 - 5: Sample n_{batch} trajectories from the replay buffer;
 - 6: Use batch trajectories to estimate $\nabla_{\phi} \tilde{U}$ following Eq. (29), update $\phi_{l+1} = \phi_l + a_{\phi,l} \nabla_{\phi} \tilde{U}$ with learning rate $a_{\phi,l}$ (can be done multiple times per l -iteration), and calculate $\{\tilde{r}_k^{(i)}\}_{i=1}^{n_{\text{batch}}}$ with the new ϕ_{l+1} ;
 - 7: Update ν towards the ν^* in Eq. (30) (or Eq. (31)), e.g., through multiple steps of gradient ascent;
 - 8: Estimate $\nabla_w \tilde{U}$ following Eq. (32), and then update $w_{l+1} = w_l + a_{w,l} \nabla_w \tilde{U}$ with learning rate $a_{w,l}$;
 - 9: **end for**
 - 10: Return final policy π_w ;
-

4.1. Demonstration setup

For **vsOED**, we employ GMMs and NFs for posterior approximation, and variational one-point-TIG and -IIG for reward formulation: we adopt the naming convention where, for example, **vsOED-G-I** stands for **GMM** with **IIG**, and **vsOED-N-T** for **NFs** with **TIG**. Other sequential experimental design algorithms being compared include **Random** design, **DAD** [32], **iDAD** [33], and a stochastic policy based **RL** method [34]. **RL** can also be combined with TIG and IIG, denoted by **RL-T** and **RL-I** respectively. DAD and iDAD require the derivative of the forward model, vsOED and iDAD can accommodate implicit likelihood, and vsOED can handle multiple models through the model indicator. Table 1 summarizes which of these aspects have been considered or studied with these algorithms. For DAD, iDAD, and RL, we directly use code from their original publications’ Github repositories.

Table 1: Properties of different sequential experimental design methods.

	Adaptive	Implicit likelihood	No model derivative	Multiple models
Random	✗	✓	✓	✓
DAD [32]	✓	✗	✗	✗
iDAD [33]	✓	✓	✗	✗
RL [34]	✓	✗	✓	✗
vsOED	✓	✓	✓	✓

In this work, we pay special attention to study algorithm efficiency in terms of trajectory samples since they entail the majority of forward model runs (i.e., evaluating G_k and H). We

make comparisons under two computational settings: (i) ‘fully trained’ where the policies are trained using algorithms’ default (usually a conservatively large) number of trajectory samples from their respective publications—8 trillion, 100 billion, and 200 million for RL, DAD, and iDAD, respectively—and we will use 10 million for vsOED; and (ii) ‘limited budget’ where we restrict to a significantly smaller total budget of 10 million training trajectories for all algorithms and cases (except for Case 3—SIR model where the budget is set to 1 million).

To ensure fair comparisons, it is important to evaluate the final policies resulting from different algorithms in a common manner. To this end, we adopt PCE [62, 32], specifically its sequential version, to evaluate the final expected utilities for policies resulting from ‘OED for model indicator’ and ‘OED for PoIs’ when likelihood is explicit and when there are no nuisance parameters (see Appendix C.1 for details on PCE, including a new variant we derive to handle ‘OED for model indicator’). PCE itself is intractable to compute due to its outer expectation operator, and must be estimated numerically, for example by MC integration of the expectation. The final MC estimation of PCE results in a nested loop structure; in our numerical cases, we use 2000 trajectory samples for the outer loop and 10^6 samples for the inner loop to achieve a high-quality estimation; when multiple models are involved, we split the inner samples to $10^6/|\mathcal{M}|$ for each model so that the total number of inner loop samples remains the same overall. In the remainder of the paper, we will refer to ‘the MC estimate of PCE’ simply as ‘PCE’ for brevity. PCE cannot be used for other OED scenarios involving QoIs and nuisance parameters because the prior predictive densities and likelihood in those scenarios are intractable; similarly, PCE cannot be used for cases where likelihood is implicit. For those situations, we instead evaluate the policies by calculating a high-quality MC estimate of \tilde{U} using 10^6 trajectory samples (except for Case 3—SIR model where 3×10^5 samples are used). In the remainder of the paper, we similarly refer to ‘the MC estimate of \tilde{U} ’ simply as ‘ \tilde{U} ’ for brevity.

All numerical experiments are conducted on the University of Michigan Great Lakes Slurm High Performance Computing Cluster nodes, where each node is equipped with a single Nvidia Tesla A40 or V100 GPU. All experiments are implemented in Python using PyTorch.

4.2. Case 1: source location finding

We adapt the source location finding problem from [32]. We enlist three candidate models with uniform model prior $P(m) = 1/3$ for $m = 1, 2, 3$. The m th model contains m sources randomly located in a two-dimensional (2D) domain, each emitting a signal that decays inversely with the square of the distance. The PoIs are the source locations $\Theta_m = \{\Theta_{m,i}\}_{i=1}^m$ where $\Theta_{m,i} = [\Theta_{m,i,x}, \Theta_{m,i,y}] \in \mathbb{R}^2$ denotes the location of the i th source and is endowed with independent priors $\Theta_{m,i,x}, \Theta_{m,i,y} \sim \mathcal{N}(0, 1^2)$. The total intensity at location $[x, y] \in \mathbb{R}^2$, aggregated from all sources, is

$$G(\Theta_m, x, y; m) = a_{\text{bg}} + \sum_{i=1}^m \frac{1}{a_{\text{max}} + \|\Theta_{m,i} - [x, y]\|_2^2},$$

where $a_{\text{bg}} = 10^{-1}$ is the background signal and $a_{\text{max}} = 10^{-4}$ is the maximum signal. The design variables $\xi_k = [\xi_{k,x}, \xi_{k,y}] \in [-4, 4]^2$ entail selecting the location of measurement within the allowable design space. The observation model is then $Y_k = G(\Theta_m, \xi_{k,x}, \xi_{k,y}; m) + \mathcal{E}_k$, where $\mathcal{E}_k \sim \mathcal{N}(0, \sigma_\epsilon^2)$ with $\sigma_\epsilon = 0.5$.

Additionally, we are also interested in a QoI that is the log of the total flux magnitude over an infinite vertical wall located at $x = 6$. The flux vector J at a spatial location $[x, y]$ is

given by Fick’s law:

$$J(\Theta_m, x, y; m) = -D\nabla_{(x,y)}G(\Theta_m, x, y; m),$$

where $D = 1$ is the scalar diffusivity. The total flux across the vertical wall at $x = 6$ is then

$$\varphi(\Theta_m; m) = \int_{-\infty}^{+\infty} J(\Theta_m, x = 6, y; m) dy = \sum_{i=1}^m \frac{\pi(\Theta_{m,i,x} - 6)}{(a_{\max} + (\Theta_{m,i,x} - 6)^2)^{\frac{3}{2}}}. \quad (33)$$

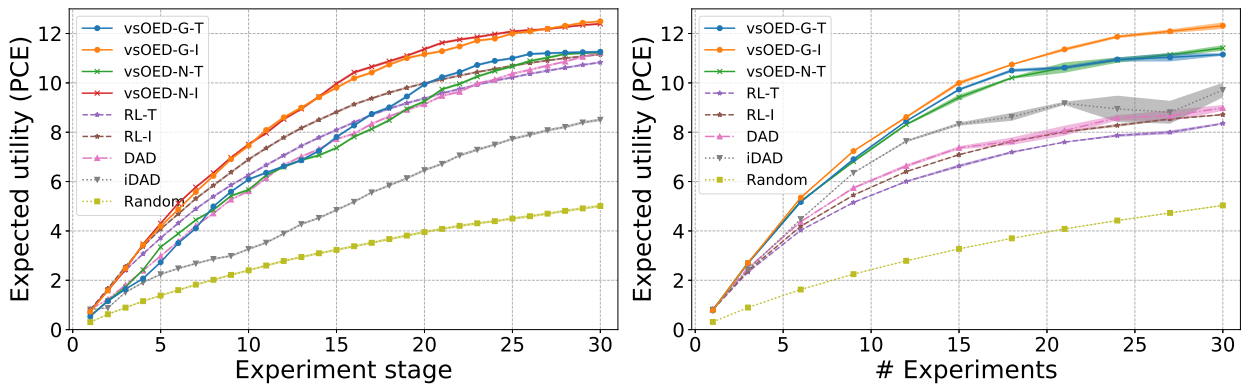
At last, the final QoI is $Z_m = \log |\varphi(\Theta_m; m)|$.

4.2.1. Case 1a: single-model

Let us first consider the single-model case where m is fixed at 2.

OED for PoIs (design for inference). The first example entails design for inferring the source location PoIs Θ , with $\alpha_\Theta = 1$ and $\alpha_Z = 0$; this setup is identical to those from previous literature [32, 33, 34]. Figure 1a presents the expected cumulative utility, evaluated using PCE, at different experiment stages k for policies optimized for a horizon of $N = 30$ experiments under the fully trained setting. The plot suggests vsOED with IIG to achieve noticeably higher expected utilities throughout, while vsOED with TIG is lower in comparison but maintains a similar level as other algorithms at later stage numbers while lower in earlier stages.

Figure 1b presents the average expected utility, averaged over four training replicates with different random seeds where each replicate is again evaluated using PCE, for policies trained under different design horizons N under the limited budget setting—that is, each point corresponds to policies optimized specifically for that horizon. Here with limited budget, vsOED outperforms other algorithms throughout. IIG again performs better than TIG, especially for $N > 15$. The standard errors are plotted as shaded regions and illustrate general training robustness with iDAD exhibiting some instability at longer horizons. Lastly, Fig. 2 provides examples showing that GMMs and NFs can effectively approximate posteriors even when they are highly non-Gaussian.



(a) Expected cumulative utility at different experiment stage k for policies optimized for $N = 30$

(b) Average expected utility over four training replicates versus design horizon N

Figure 1: Case 1a. Expected utility comparisons using policies resulting from different algorithms. The shaded regions represent the standard error.

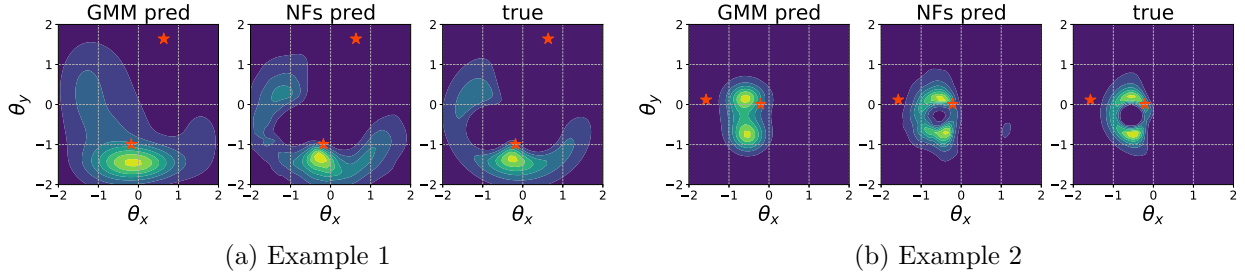


Figure 2: Case 1a. Examples of GMM and NFs approximate posterior and true posterior for PoIs. The red stars indicate the true data-generating parameter values for these trajectory samples.

OED for QoIs (design for prediction). The second example involves goal-oriented design for predicting the flux-based QoI Z introduced earlier, with $\alpha_\theta = 0$ and $\alpha_Z = 1$. Only vsOED is used here since the other algorithms cannot accommodate ‘OED for QoIs’; furthermore, only GMM version of vsOED is presented since the QoI Z is a scalar and unsuitable for the particular architecture of NFs we adopt that requires at least two dimensions for decomposition (see [Appendix B.2.2](#)). Figure 3 plots the average \tilde{U} , averaged over four training replicates, versus N . The standard errors are plotted as shaded regions illustrating training robustness for vsOED. As observed in ‘OED for PoIs’, we again see higher expected utility estimates reached by IIG over TIG. Figure 4 presents examples of trajectory using policies resulting from ‘OED for PoIs’ and ‘OED for QoIs’ for $N = 15$: the former tends to move toward the estimated source locations while the latter forms a roughly vertical design pattern. We can explain this behavior through physics. In Eq. (33), since the integration is over the entire y , the flux is solely dependent on the x -position of the source (i.e., $\Theta_{m,i,x}$). Due to the isotropic nature of source emission, spreading measurements along a vertical line is thus more sensitive at detecting changes in θ_x . We see this effect in Fig. 5a, where a greater QoI posterior shrinkage takes place under a vertical sensor design than a horizontal sensor design. Figure 5b supports that GMMs can also capture well the QoI posteriors.

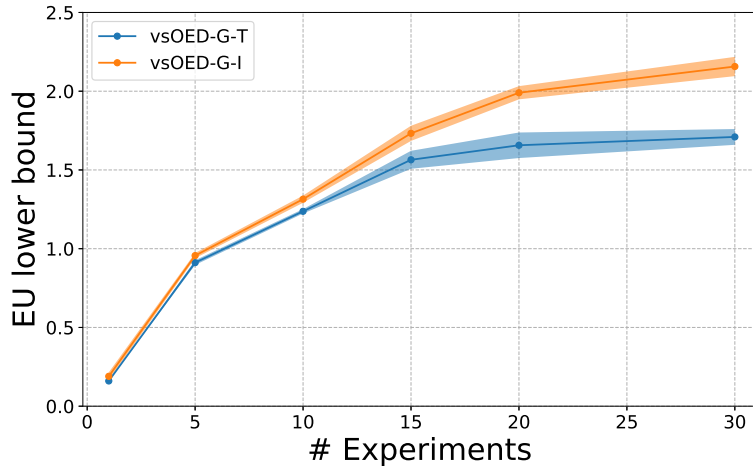


Figure 3: Case 1a. Average \tilde{U} over four training replicates for ‘OED for QoIs’. The shaded regions represent the standard error.

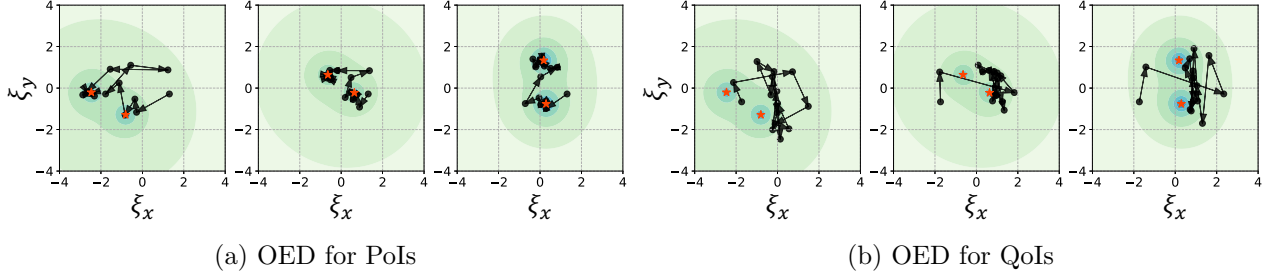


Figure 4: Case 1a. Examples of policy trajectory for $N = 15$. The contour background plots the true signal strength, and the red stars indicate the true source locations.

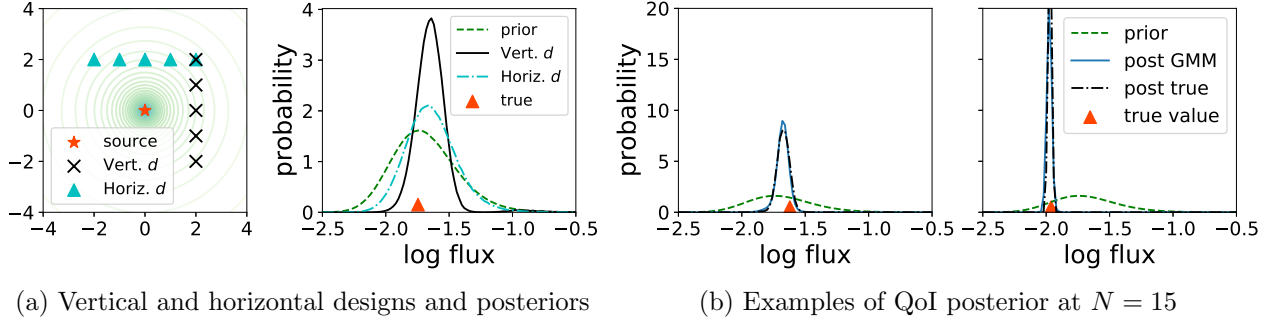


Figure 5: Case 1a. Design and posterior comparisons for ‘OED for QoIs’.

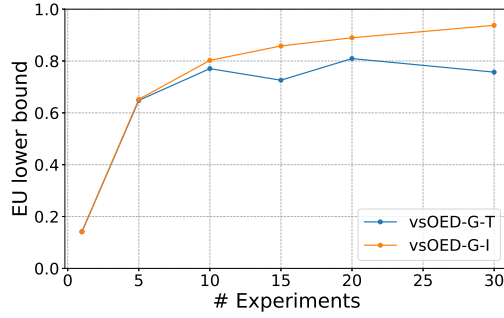
Hyperparameters and training stability. Hyperparameter settings and training stability results can be found in [Appendix C.2](#).

4.2.2. Case 1b: multi-model

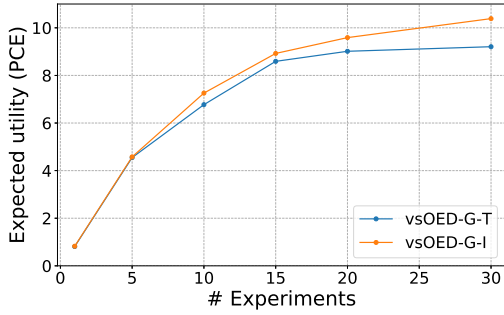
We now consider a multi-model case for the source location finding problem, with three candidate models. Five scenarios are considered: OED for model indicator (i.e., design for model discrimination, $\alpha_M = 1$, $\alpha_\Theta = \alpha_Z = 0$), OED for PoIs (i.e., design for parameter inference, $\alpha_\Theta = 1$, $\alpha_M = \alpha_Z = 0$), OED for QoIs (i.e., design for goal-oriented prediction, $\alpha_Z = 1$, $\alpha_M = \alpha_\Theta = 0$), OED for both model indicator and PoIs (‘model-PoIs’, $\alpha_M = \alpha_\Theta = 1$, $\alpha_Z = 0$), and OED for both model indicator and QoIs (‘model-QoIs’, $\alpha_M = \alpha_Z = 1$, $\alpha_\Theta = 0$).

Results. Only vsOED is used in this case since the other algorithms cannot handle multiple models. Only the GMM version of vsOED is presented for brevity as this example focuses on vsOED capabilities across the five OED scenarios. Figure 6 presents the average expected utilities or \tilde{U} over two training replicates for the five OED scenarios. IIG again demonstrates greater performance over TIG, especially for $N \geq 15$. Figure 7 presents examples of trajectory using policies resulting from the five OED scenarios for $N = 30$. Generally, trajectories from ‘OED for model indicator’ tend to explore more and appear more diffuse, while those from ‘OED for PoIs’ tend to be more exploitative and remain closer to the estimated source location. Similar to the single-model case, ‘OED for QoIs’ promotes more vertically aligned design locations. The model-PoIs and model-QoIs scenarios appear more diffuse than ‘OED for PoIs’ and ‘OED for QoIs’, respectively, due to the addition of exploratory property from ‘OED for model indicator’.

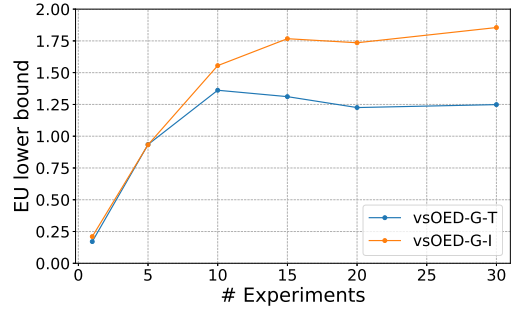
Figure 8 shows examples of approximate posterior and true posterior for model indicator



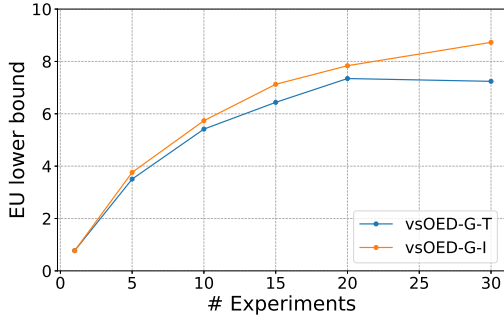
(a) OED for model indicator



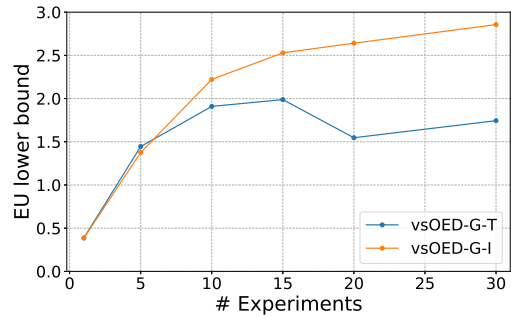
(b) OED for PoIs



(c) OED for for QoIs

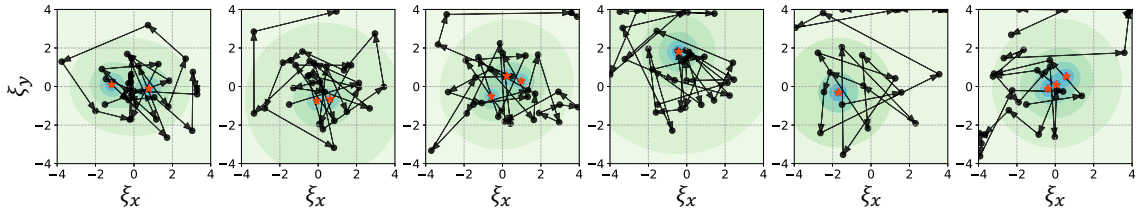


(d) Model-PoIs OED

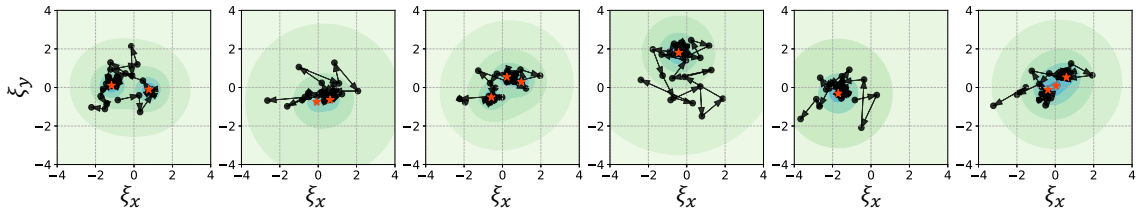


(e) Model-QoIs OED

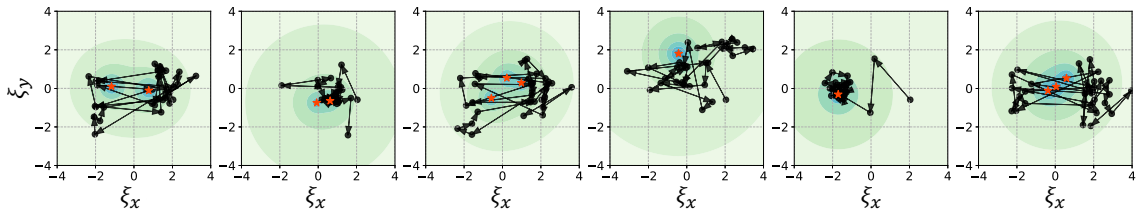
Figure 6: Case 1b. Average expected utility or \tilde{U} over two training replicates versus design horizon N using policies resulting from the five OED scenarios.



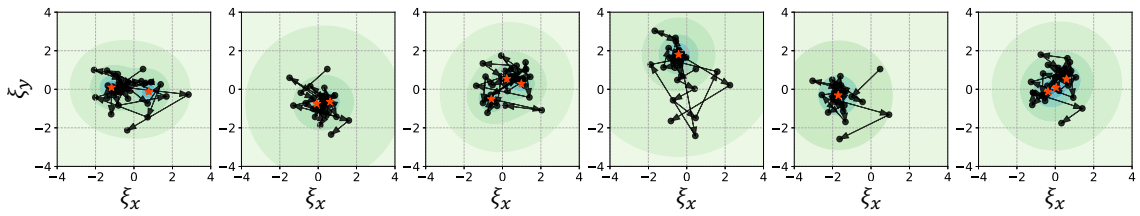
(a) OED for model indicator



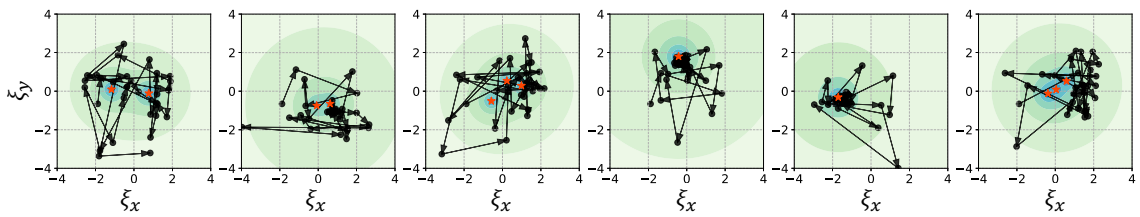
(b) OED for PoIs



(c) OED for QoIs



(d) Model-PoIs OED



(e) Model-QoIs OED

Figure 7: Case 1b. Examples of policy trajectory for $N = 30$. The contour background plots the true signal strength, and the red stars indicate the true source locations.

using policy resulting from ‘OED for model indicator’ with vsOED-G-I for $N = 30$. The policy appears effective in discriminating the candidate models with highly concentrated posteriors, and the approximate model posteriors match well with the true model posteriors. Table 2 presents the PCE estimates of the EIG for model indicator and PoIs using policies resulting from the five OED scenarios, all using vsOED-G-I. The model discrimination OED finds the optimal policy in terms of maximizing the expected utility on model probability. Indeed, the ‘OED for model indicator’ policy achieves the highest EIG estimate for model indicator, while model-PoIs and model-QoIs achieve higher values compared to their counterparts of ‘OED for PoIs’ and ‘OED for QoIs’. Similarly, the policy from ‘OED for PoIs’ achieves the highest EIG estimate on PoIs, with model-PoIs slightly lower.

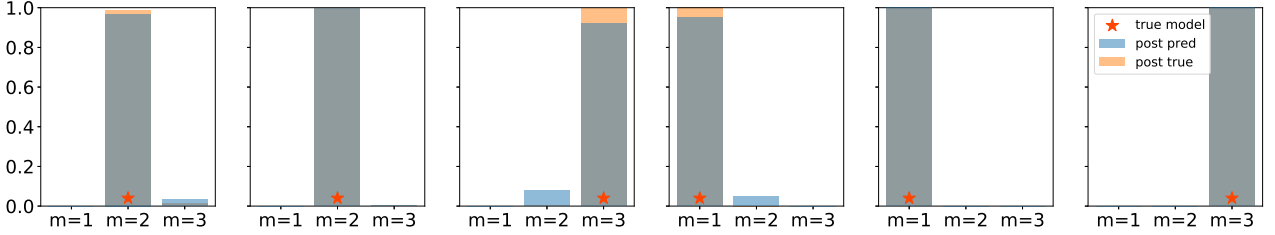


Figure 8: Case 1b. Examples of approximate posterior and true posterior for model indicator using policy resulting from ‘OED for model indicator’, for $N = 30$.

Table 2: Case 1b. PCE estimate of the EIG on model indicator and PoIs using policies resulting from the five OED scenarios. \pm represents standard error.

	EIG on model indicator	EIG on PoIs
OED for model indicator	1.020 \pm 0.003	5.956 \pm 0.065
OED for PoIs	0.896 \pm 0.005	10.567 \pm 0.048
OED for QoIs	0.815 \pm 0.005	6.999 \pm 0.053
Model-PoIs OED	0.950 \pm 0.005	10.330 \pm 0.049
Model-QoIs OED	0.967 \pm 0.004	7.830 \pm 0.052

Hyperparameters and training stability. Hyperparameter settings and training stability results can be found in [Appendix C.2](#).

4.3. Case 2: constant elasticity of substitution

The CES case involves a single model and ‘OED for PoIs’ only, and has been previously studied in [42, 62, 34]. CES originates from behavioral economics, where participants are presented with two baskets of goods and asked to assess the subjective difference in utility between the two baskets. The CES model [63] represents the underlying utility function with latent PoIs $\Theta = \{\rho, \beta, \log u\}$, where $\beta \in \mathbb{R}^3$ while ρ and u are scalars. We adopt independent priors $\rho \sim \text{Beta}(1, 1)$, $\beta \sim \text{Dirichlet}([1, 1, 1])$, $\log u \sim \mathcal{N}(1, 3^2)$. Note that the degree of freedom for β is 2 since the sum of its components is constraint to $\beta_1 + \beta_2 + \beta_3 = 1$; hence, only β_1 and β_2 are included in Θ . The design variables are $\xi_k = [\xi_{k,x}, \xi_{k,x'}]$ and constrained to the design space $\xi_{k,x} \in [0, 100]^3$ and $\xi_{k,x'} \in [0, 100]^3$. The observation model is

$$Y_k = \text{clip}\left(\text{sigmoid}(\varphi_k), \epsilon, 1 - \epsilon\right), \quad (34)$$

where the clipping threshold parameter is set to $\epsilon = 2^{-22}$, and $\varphi_k \sim \mathcal{N}(\mu_\varphi, \sigma_\varphi^2)$ with

$$\mu_\varphi = u \left[\left(\sum_{i=1}^3 (\xi_{k,x,i})^\rho \beta_i \right)^{\frac{1}{\rho}} - \left(\sum_{j=1}^3 (\xi_{k,x',j})^\rho \beta_j \right)^{\frac{1}{\rho}} \right], \quad \sigma_\varphi = \tau u \left(1 + \|\xi_{k,x} - \xi_{k,x'}\|_2 \right),$$

and $\tau = 0.005$. While the observation model in Eq. (34) differs from the form in Eq. (1), the likelihood remains explicit and can be evaluated by applying a change of variable to the sigmoid function and integrating the tail probabilities beyond the clipped thresholds; we do not write the likelihood formula here for brevity, and refer interested readers to the associated vsOED code implementation on Github.

Results. We use vsOED only with TIG since the horizons of this problem are relatively short, at most $N = 10$, and Fig. 1b indicates that TIG and IIG perform similarly under those horizons. Figure 9a presents the expected cumulative utility, evaluated using PCE, at different experiment stages k for policies optimized for a horizon of $N = 10$ experiments under the fully trained setting. The plot suggests that vsOED with GMM and TIG is slightly inferior to fully-trained RL but significantly better than fully-trained DAD and iDAD. The lower values for vsOED with GMM and TIG in the earlier stages suggest that the policy prioritizes long-term expected utility accumulation over short-term rewards.

Figure 9b presents the average expected utility, averaged over four training replicates where each replicate is again evaluated using PCE, for policies trained under different design horizons N under the limited budget setting. Here vsOED with GMM and TIG outperforms other approaches for all values of N . The standard errors are plotted as shaded regions and illustrate a greater robustness of vsOED-G-T and RL over vsOED-N-T and DAD.

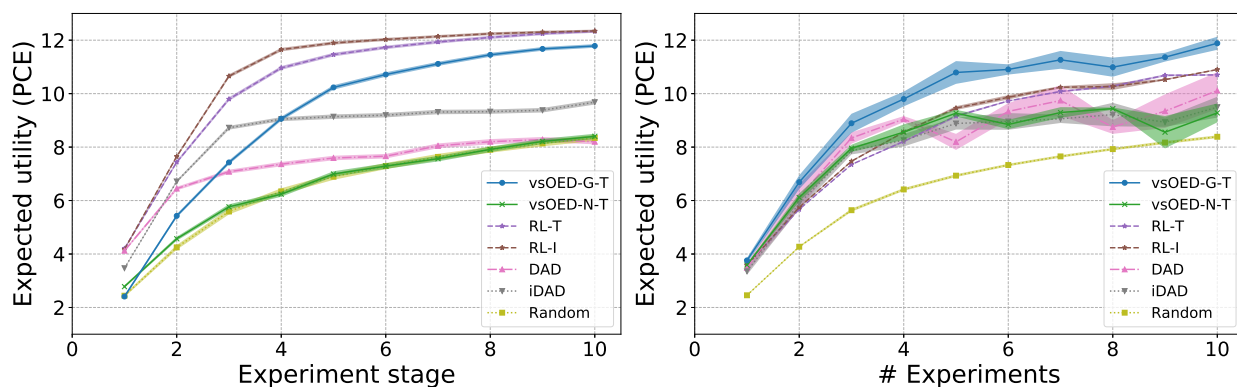
For this case, vsOED with NFs appears significantly worse compared to vsOED with GMM. This is likely due to NFs having more difficulty in representing distributions of random variables with compact support, ρ and β in this case.

Figure 10 provides examples comparing the GMM approximate posterior and the true posterior. GMM performs well for $\log u$, but tends to produce wider posteriors for ρ and β . This is likely due to that many observations are clipped at the two ends per Eq. (34) which leads to numerous observations with identical values, and the non-uniqueness makes it difficult for GMM to learn the mapping from designs and observations to the posterior. Despite this challenge, vsOED with GMM is still able to find good policies.

Hyperparameters and training stability. Hyperparameter settings and training stability results can be found in Appendix C.3.

4.4. Case 3: SIR model for disease spread

The SIR case involves a single model and ‘OED for PoIs’ only, and has been previously studied in [33]. As the model involves solving a stochastic differential equation (SDE), the case tests the ability of vsOED to handle an expensive forward model and implicit likelihood. SIR is a stochastic model [55, 64] describing the spread of infectious diseases in a population. Individuals in the population are divided into three categories: susceptible, infected, and recovered. The number of individuals in these categories at any given time t are respectively represented by $S(t)$, $I(t)$, and $R(t)$, which always sum to a fixed population size $S(t) + I(t) + R(t) = N_p, \forall t$. Thus, the population state vector is defined to be $X(t) = [S(t), I(t)]$, where $R(t)$ is implied by the population constraint and can be ignored.



(a) Expected cumulative utility at different experiment stage k for policies optimized for $N = 10$ (b) Average expected utility over four training replicates versus design horizon N

Figure 9: Case 2. Expected utility comparisons using policies resulting from different algorithms. The shaded regions represent the standard error.

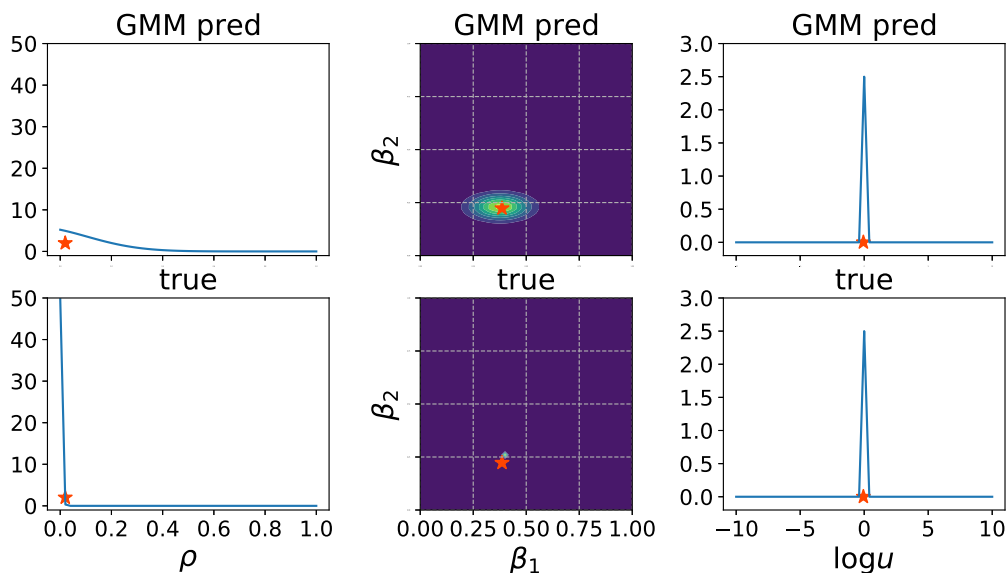


Figure 10: Case 2. Examples of GMM approximate posterior and true posterior at $N = 10$. The red stars indicate the true data-generating parameter values for these trajectory samples.

An individual at time t in the susceptible category has a probability to become infected controlled by rate parameter β , an individual who is infected has a probability to recover controlled by rate parameter ρ , and an individual who is already recovered remains recovered. The PoIs $\Theta = \{\log \beta, \log \rho\}$ entail the logarithm of the rates to ensure their non-negativity. We adopt independent priors $\log \beta \sim \mathcal{N}(\log 0.5, 0.5^2)$, $\log \rho \sim \mathcal{N}(\log 0.1, 0.5^2)$. The design variable for the k th experiment is $\xi_k \in [0, 100]$, which is the time chosen for observing the number of infected $I(t = \xi_k)$. The designs are also constrained by $\xi_k \leq \xi_{k+1}$. The overall SIR model is often defined by a continuous-time Markov chain and can be sampled via the Gillespie algorithm [65], but it generally yields discrete population states that have undefined gradients. To circumvent these limitations, we follow [33] and adopt a continuous-state alternative (i.e., where $X(t)$ can be real-valued) form based on an SDE formulation.

In this SIR model formulation, the state dynamics follows the Itô SDE:

$$dX(t) = f(X(t)) dt + D(X(t)) dW(t), \quad (35)$$

where $W(t)$ is a vector of independent Wiener processes (i.e., Brownian motion), and f and D are the state-dependent drift vector and diffusion matrix, respectively, defined as [55]

$$f(X(t)) = \begin{bmatrix} -\beta \frac{S(t)I(t)}{N_p} \\ \beta \frac{S(t)I(t)}{N_p} - \rho I(t) \end{bmatrix}, \quad D(X(t)) = \begin{bmatrix} -\sqrt{\beta \frac{S(t)I(t)}{N_p}} & 0 \\ \sqrt{\beta \frac{S(t)I(t)}{N_p}} & -\sqrt{\rho I(t)} \end{bmatrix}. \quad (36)$$

Given Eqs. (35) and (36), we can simulate state $X(t)$ by solving the SDE via finite-differencing, such as the Euler–Maruyama method; here we directly adopt the solver from [33]. For a fair comparison, we follow [33] and use the solutions of Eq. (35) as data and do not consider an additional Poisson observational model that increases the noise in simulated data as suggested in [55]—that is, $Y_k = I(\xi_k)$. The likelihood is implicit for this case, since computing the probability of all stochastic transitions leading to the observed value would be intractable. Hence, we can sample from the observation model, but not evaluate its probability density.

Solving the SDE is quite computationally expensive, we thus limit the computational budget to 1 million trajectory samples for both vsOED and iDAD. To accelerate the training process, we pre-generate and store 1 million simulations and then access the stored simulations during the training. A new set of 3×10^5 simulations are used as evaluation data.

Results. Only vsOED and iDAD are used in this case since the other algorithms cannot handle implicit likelihood. We use vsOED only with TIG since the horizons of this problem are relatively short, at most $N = 10$, and Fig. 1b indicates that TIG and IIG perform similarly under those horizons. Figure 11 presents the average \tilde{U} , averaged over four training replicates, for policies trained under different design horizons N . vsOED and iDAD appear to perform similarly, with vsOED slightly better at some spots. However, we note that the comparison is not entirely commensurable since iDAD is trained based on a different EIG lower bound estimator than \tilde{U} (which vsOED uses and is also used here for evaluation), and that iDAD additionally uses the forward model derivatives. The absence of requiring model derivatives in vsOED can be potentially valuable in situations where model derivatives are inaccessible.

Figure 12 presents examples of infected state trajectory $I(t)$ and corresponding designs (observation times) ξ_k for $N = 10$ with three realizations of (β, ρ) and different ratios $r = \beta/\rho$. We observe that smaller r corresponds to a more spread out design of observation times, which aligns with the results in [33].

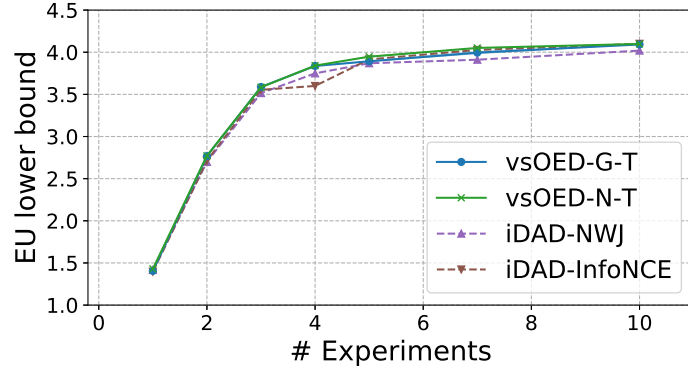


Figure 11: Case 3. Average \tilde{U} over four training replicates versus design horizon N . The shaded regions represent the standard error.

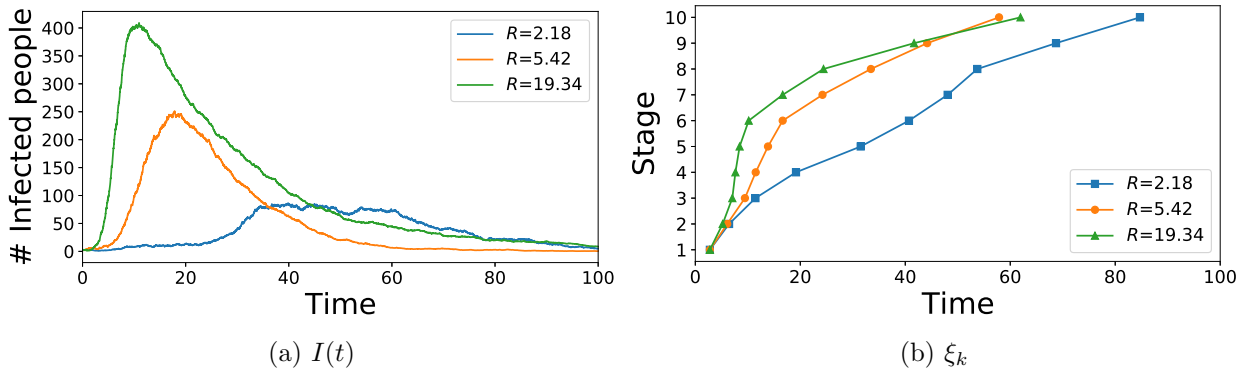


Figure 12: Case 3. Examples of infected state trajectory $I(t)$ and corresponding designs (observation times) ξ_k for $N = 10$ with three realizations of (β, ρ) and different ratios $r = \beta/\rho$.

Hyperparameters and training stability. Hyperparameter settings and training stability results can be found in [Appendix C.4](#).

4.5. Case 4: convection-diffusion-reaction

The convection-diffusion-reaction case involves nuisance parameters and physical state, and has been previously studied in [31] under the single-model setting. The case entails designing mobile sensor movements within a contaminant plume whose dynamics are governed by a 2D convection-diffusion-reaction partial differential equation (PDE). In this paper, we consider three candidate models with uniform model prior $P(m) = 1/3$ for $m = 1, 2, 3$. The m th model contains m Gaussian-profiled contaminant sources randomly located in a 2D domain. The PoIs are the source locations $\Theta_m = \{\Theta_{m,i}\}_{i=1}^m$ where $\Theta_{m,i} = [\Theta_{m,i,x}, \Theta_{m,i,y}] \in \mathbb{R}^2$ denotes the location of the i th source and is endowed with independent priors $\Theta_{m,i,x}, \Theta_{m,i,y} \sim \mathcal{U}(0, 1^2)$. For the m th model, the contaminant concentration G at location $[x, y]$ and time t is governed by

$$\frac{\partial G(\Theta_m, \Psi_m, x, y, t; m)}{\partial t} = \nabla_{(x,y)}^2 G - u(\Psi_m) \cdot \nabla_{(x,y)} G + S(\Theta_m, x, y, t; m),$$

for $[x, y] \in [-1, 2]^2$ and $0 < t \leq 0.2$. Here $u = [v \cos \beta, v \sin \beta]^\top \in \mathbb{R}^2$ is a time-invariant convection velocity that is described by nuisance parameters $\Psi_m = \{v, \beta\}$ with independent priors on the convection speed (magnitude) $v \sim \mathcal{U}(0, 20)$ and convection angle $\beta \sim \mathcal{U}(0, 2\pi)$. The source function is

$$S(\Theta_m, x, y, t; m) = \sum_{i=1}^m \frac{s}{2\pi h^2} \exp\left(-\frac{\|\Theta_{m,i} - [x, y]\|_2^2}{2h^2}\right),$$

where $s = 2$ is the known source strength and $h = 0.05$ is the known source width. The initial condition is $G(\Theta_m, \Psi_m, x, y, 0; m) = 0$ and homogeneous Neumann boundary conditions are applied to all sides of the computational domain. The design variables $\xi_k = [\xi_{k,x}, \xi_{k,y}] \in [0, 1]^2$ entail selecting the location of concentration measurement within the allowable design space at prescribed time intervals $t_k = 0.01(k + 1)$. The observation model is then $Y_k = G(\Theta_m, \Psi_m, \xi_{k,x}, \xi_{k,y}, t_k; m) + \mathcal{E}_k$ where $\mathcal{E}_k \sim \mathcal{N}(0, \sigma_\epsilon^2)$ with $\sigma_\epsilon = 0.05$. Moreover, the measurement sensor is initially located at $[x_0, y_0] = [0.5, 0.5]$, and a sensor movement penalty of $-0.1 \|\xi_k - \xi_{k-1}\|_2$ for $k = 1, \dots, N - 1$ (and $-0.1 \|\xi_k - [x_0, y_0]\|_2$ for $k = 0$) is incurred in the immediate rewards to reflect the cost of moving the sensor.

Similar to Section 4.2, we are interested in a QoI that is the log of the integrated flux magnitude crossing the right boundary $x = 1$ of the design space (i.e., spanning from $y = 0$ to $y = 1$) at a future time $t = 0.2$. The QoI is $Z_m = \log(|\varphi(\Theta_m, \Psi_m; m)|)$, where

$$\varphi(\Theta_m, \Psi_m; m) = \int_0^1 -\frac{\partial G(\Theta_m, \Psi_m, x = 1, y, t = 0.2; m)}{\partial x} dy.$$

We apply a second-order finite volume method to solve the PDE numerically. The computational domain $[-1, 2]^2$ is discretized into a uniform grid with cell size $\Delta x = \Delta y = 0.01$. Second-order fractional step method is used for time integration, with a step size $\Delta t = 5.0 \times 10^{-4}$. The integrated flux φ is computed by first estimating the derivative term using finite difference on the grid values at the target boundary, and then numerically integrated using midpoint rule.

While we can directly use the finite volume solver as the forward model, it can be expensive and inefficient since each solve calculates the concentrations for all $[x, y]$ and all t , while in

the OED problem only a small subset of these values are needed for each forward model evaluation. Therefore, to accelerate computations, we pre-build NN surrogate models to replace $G(\Theta_m, \Psi_m, \xi, t_k; m)$ and $\varphi(\Theta_m, \Psi_m; m)$, one for each m and t_k . The architectures of these NN surrogates can be found in [Appendix C.5](#).

A separate G surrogate is built for each m and t_k , and a separate φ surrogate is built for each m . For each m , 20,000 simulations are generated with random samples of Θ_m and Ψ_m , with 18,000 used for training and 2,000 for testing. The testing mean squared errors (MSE) are shown in [Table 3](#) for G surrogates at the end time $t = 0.2$ and the three φ surrogates, illustrating excellent accuracy. [Figure 13](#) presents examples of the true and surrogate concentration fields G at the end time $t = 0.2$; they demonstrate excellent agreement.

Table 3: Case 4. Testing MSE of the surrogate models.

Model	Surrogate G at $t = 0.2$	Surrogate φ
$m = 1$	3.094×10^{-5}	4.141×10^{-5}
$m = 2$	3.284×10^{-4}	4.986×10^{-4}
$m = 3$	1.650×10^{-3}	2.080×10^{-3}

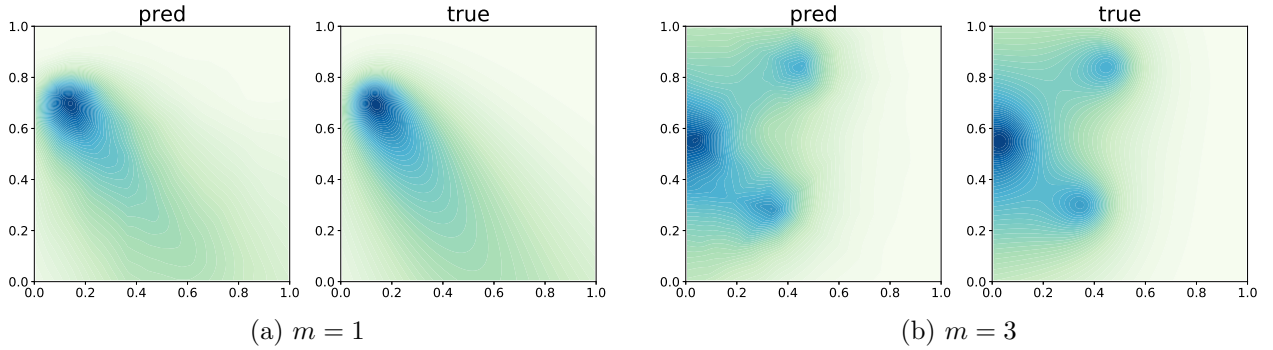
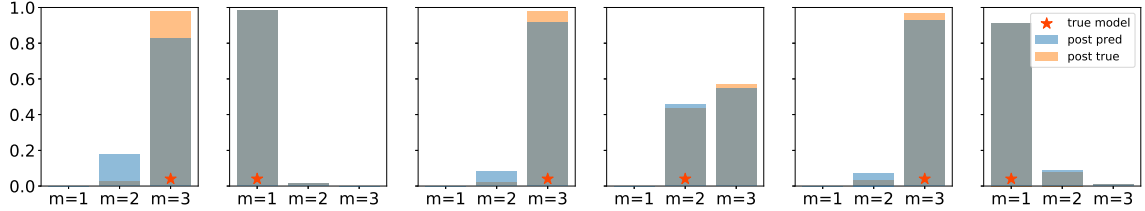


Figure 13: Case 4. Examples of the true and surrogate concentration fields G at $t = 0.2$.

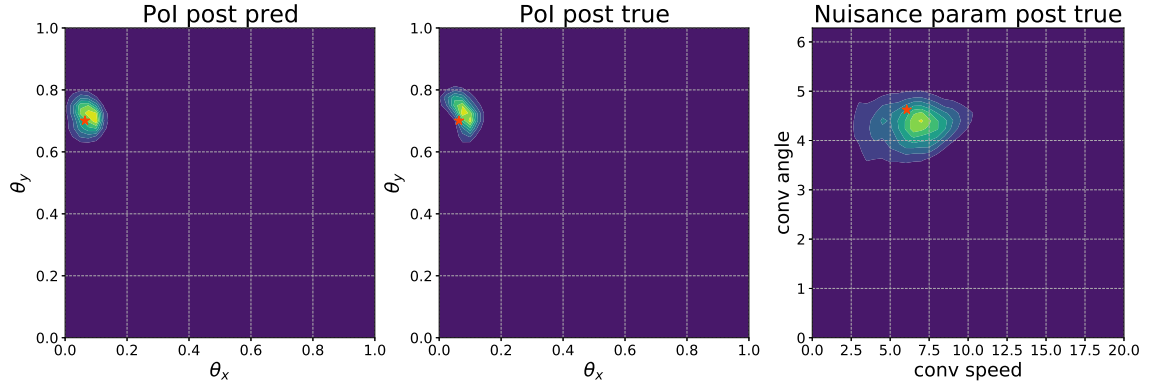
Results. Only vsOED is used in this case since the other algorithms cannot handle nuisance parameters and multiple models. We use vsOED only with TIG since the horizons of this problem are relatively short, at most $N = 15$, and [Fig. 1b](#) indicates that TIG and IIG perform similarly under those horizons. Only the GMM version of vsOED is presented for brevity. Similar to Case 1b, we consider five OED scenarios: OED for model indicator (i.e., design for model discrimination, $\alpha_M = 1, \alpha_\Theta = \alpha_Z = 0$), OED for PoIs (i.e., design for parameter inference, $\alpha_\Theta = 1, \alpha_M = \alpha_Z = 0$), OED for QoIs (i.e., design for goal-oriented prediction, $\alpha_Z = 1, \alpha_M = \alpha_\Theta = 0$), OED for both model indicator and PoIs (‘model-PoIs’, $\alpha_M = \alpha_\Theta = 1, \alpha_Z = 0$), and OED for both model indicator and QoIs (‘model-QoIs’, $\alpha_M = \alpha_Z = 1, \alpha_\Theta = 0$).

[Figure 14](#) presents examples comparing the GMM approximate posterior and true posterior for model indicator and PoIs (from $m = 1$) using policies respectively resulting from ‘OED for model indicator’ and ‘OED for PoIs’ for $N = 10$; the GMMs again approximate the posteriors well for this case. Notably, an example PoI posterior and the corresponding nuisance parameter posterior are shown in [Fig. 14b](#), both plotted over the full support of their respective uniform priors. We see that the PoI posterior has shrunk more substantially than that for the nuisance

parameter, which is consistent with the expected behavior of ‘OED for PoIs’ that targets to reduce the PoI uncertainty. Figure 15 presents examples of trajectory using policies from the five OED scenarios for $N = 10$. The overall policy behavior is similar to the multi-model source location finding problem of Case 1b. Trajectories from ‘OED for model indicator’ tend to explore more and appear more diffuse compared to the other scenarios, often extending to the boundaries of the design space and leading to narrow posteriors of model indicator as shown in Fig. 14a. Trajectories from ‘OED for PoIs’ tend to be more exploitative, remaining closer to the estimated sources while leveraging the background convection. Trajectories from ‘OED for QoIs’ exhibit a vertical design tendency, due to the same effects as explained in Case 1b.



(a) Posteriors for model indicator from ‘OED for model indicator’.



(b) Posteriors for PoIs from ‘OED for PoIs’ for $m = 1$, along with the true posterior for the nuisance parameters.

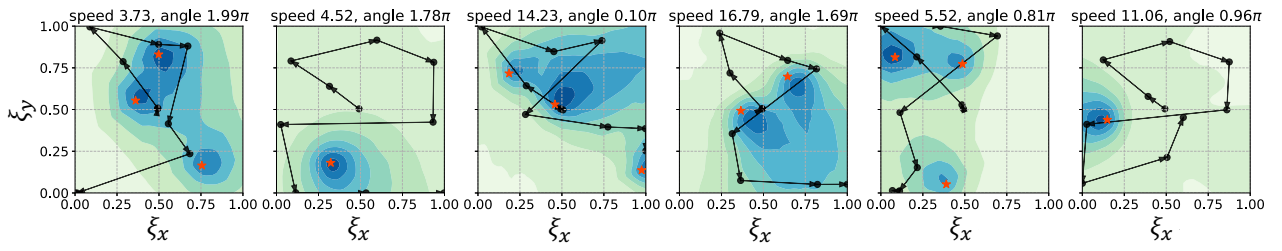
Figure 14: Case 4. Examples of approximate posterior and true posterior for model indicator and PoIs using policy resulting from ‘OED for model indicator’ and ‘OED for PoIs’, respectively, for $N = 10$.

Hyperparameters, training stability, and surrogate architectures. Hyperparameter settings, training stability, and surrogate architectures can be found in [Appendix C.5](#).

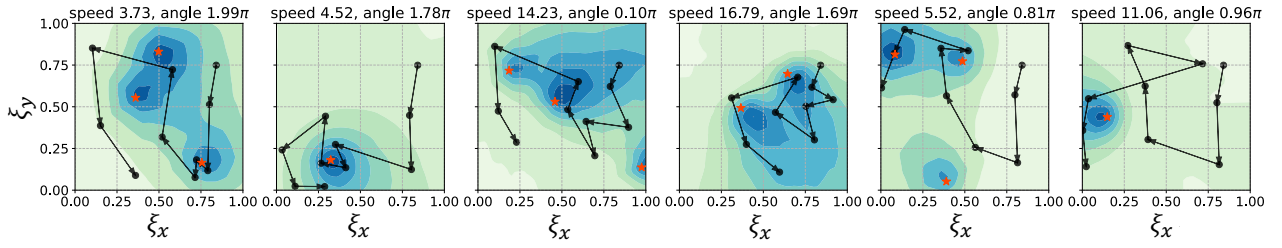
5. Conclusions

We introduced vsOED, a novel method for solving Bayesian sequential OED problem using an actor-critic reinforcement learning framework powered by policy gradient techniques and the variational Barber–Agakov bound to the EIG. vsOED is capable of accommodating nuisance parameters, implicit likelihoods, and multiple candidate models, while supporting a flexible design criterion that can target designs for model discrimination, parameter inference, goal-oriented prediction, or their weighted combinations.

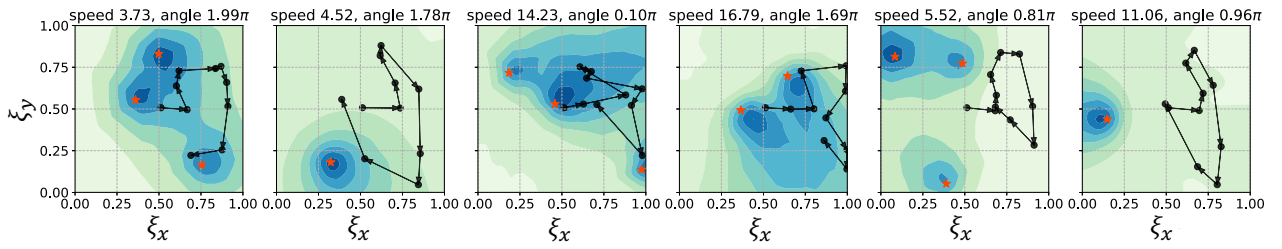
We provided key theoretical results including theorems proving the equivalence between incremental and terminal information gain rewards, equivalence between EIG and its one-point



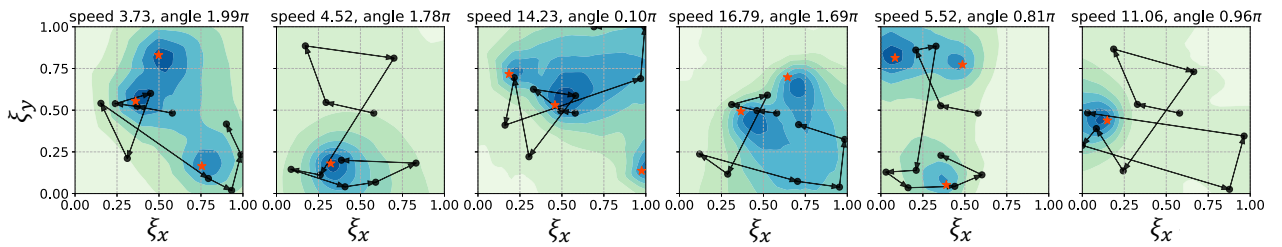
(a) OED for model indicator



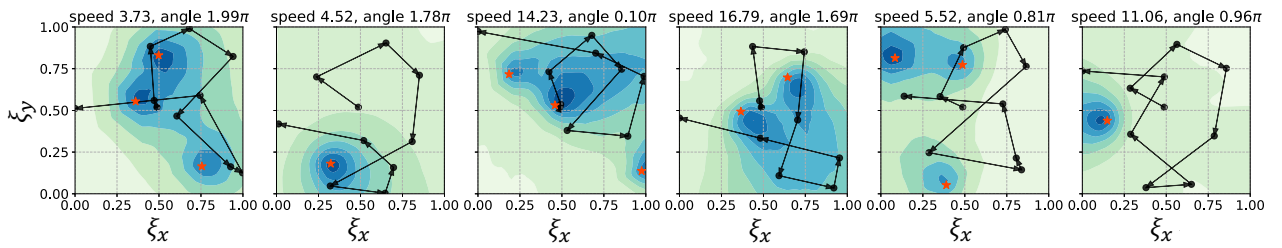
(b) OED for PoIs



(c) OED for QoIs



(d) Model-PoIs OED



(e) Model-QoIs OED

Figure 15: Case 4. Examples of policy trajectory for $N = 10$. The background contour plots the true contaminant concentration at the end time $t = 0.2$, and the red stars indicate the true source locations.

reward formulations, and the lower bound property of vsOED when posteriors are approximated. We then developed numerical methods under an actor-critic framework, deriving and estimating the policy gradient and utilizing Gaussian mixture models and normalizing flows to approximate the posteriors.

Finally, we demonstrated vsOED across four numerical cases—source location finding, constant elasticity of substitution, SIR model for disease spread, and convection-diffusion-reaction. These scenarios involved challenges of multiple models, implicit likelihoods, and nuisance parameters. Comparisons with existing algorithms (DAD, iDAD, and RL) showed that vsOED achieves superior sample efficiency under limited budgets and avoids reliance on model derivatives.

Despite its strengths, vsOED has limitations. Its performance is sensitivity to inaccurate posterior approximations, especially for posteriors with compact support, multiple modes, and highly non-Gaussian features. Developing more accurate and adaptive posterior representations, particularly in high-dimensional spaces, will be highly valuable. Additionally, vsOED currently does not handle discrete designs or stochastic policies, which could expand its applicability, as demonstrated by [34]. Further enhancements could also stem from advanced reinforcement learning techniques, such as proximal policy optimization, trust region policy optimization, and soft actor-critic [66, 67, 68, 69].

Acknowledgments

This research is based upon work supported in part by the U.S. Department of Energy, Office of Science, Office of Advanced Scientific Computing Research, under Award Numbers DE-SC0021397 and DE-SC0021398. This work relates to Department of Navy award N00014-23-1-2735 issued by the Office of Naval Research. This research is supported in part through computational resources and services provided by Advanced Research Computing at the University of Michigan, Ann Arbor.

References

- [1] X. Huan, J. Jagalur, Y. Marzouk, Optimal experimental design: Formulations and computations, *Acta Numerica* 33 (2024) 715–840. doi:10.1017/S0962492924000023.
- [2] K. Chaloner, I. Verdinelli, Bayesian experimental design: A review, *Statistical Science* 10 (3) (1995) 273–304. doi:10.1214/ss/1177009939.
- [3] E. G. Ryan, C. C. Drovandi, J. M. McGree, A. N. Pettitt, A review of modern computational algorithms for Bayesian optimal design, *International Statistical Review* 84 (1) (2016) 128–154. doi:10.1111/insr.12107.
- [4] A. Alexanderian, Optimal experimental design for infinite-dimensional Bayesian inverse problems governed by PDEs: A review, *Inverse Problems* 37 (4) (2021) 043001. doi:10.1088/1361-6420/abe10c.
- [5] T. Rainforth, A. Foster, D. R. Ivanova, F. B. Smith, Modern Bayesian experimental design, *Statistical Science* 39 (1) (2024) 100–114. doi:10.1214/23-ST5915.

- [6] D. Strutz, A. Curtis, Variational Bayesian experimental design for geophysical applications: Seismic source location, amplitude versus offset inversion, and estimating CO₂ saturations in a subsurface reservoir, *Geophysical Journal International* 236 (3) (2024) 1309–1331. doi:10.1093/gji/ggad492.
- [7] D. V. Lindley, On a measure of the information provided by an experiment, *The Annals of Mathematical Statistics* 27 (4) (1956) 986–1005. doi:10.1214/aoms/1177728069.
- [8] G. E. P. Box, Sequential experimentation and sequential assembly of designs, *Quality Engineering* 5 (2) (1992) 321–330. doi:10.1080/08982119208918971.
- [9] H. A. Dror, D. M. Steinberg, Sequential experimental designs for generalized linear models, *Journal of the American Statistical Association* 103 (481) (2008) 288–298. doi:10.1198/016214507000001346.
- [10] D. R. Cavagnaro, J. I. Myung, M. A. Pitt, J. V. Kujala, Adaptive design optimization: A mutual information-based approach to model discrimination in cognitive science, *Neural Computation* 22 (4) (2010) 887–905. doi:10.1162/neco.2009.02-09-959.
- [11] A. Solonen, H. Haario, M. Laine, Simulation-based optimal design using a response variance criterion, *Journal of Computational and Graphical Statistics* 21 (1) (2012) 234–252. doi:10.1198/jcgs.2011.10070.
- [12] C. C. Drovandi, J. M. McGree, A. N. Pettitt, Sequential Monte Carlo for Bayesian sequentially designed experiments for discrete data, *Computational Statistics & Data Analysis* 57 (1) (2013) 320–335. doi:10.1016/j.csda.2012.05.014.
- [13] C. C. Drovandi, J. M. McGree, A. N. Pettitt, A sequential Monte Carlo algorithm to incorporate model uncertainty in Bayesian sequential design, *Journal of Computational and Graphical Statistics* 23 (1) (2014) 3–24. doi:10.1080/10618600.2012.730083.
- [14] W. Kim, M. A. Pitt, Z.-L. Lu, M. Steyvers, J. I. Myung, A hierarchical adaptive approach to optimal experimental design, *Neural Computation* 26 (2014) 2565–2492. doi:10.1162/NECO_a_00654.
- [15] M. Hainy, C. C. Drovandi, J. M. McGree, Likelihood-free extensions for Bayesian sequentially designed experiments, in: J. Kunert, C. Müller, A. Atkinson (Eds.), *mODa 11: Advances in Model-Oriented Design and Analysis, Contributions to Statistics*, Springer, 2016, pp. 153–161.
- [16] S. Kleinegesse, C. Drovandi, M. U. Gutmann, Sequential Bayesian experimental design for implicit models via mutual information, *Bayesian Analysis* 16 (3) (2021) 773–802. doi:10.1214/20-BA1225.
- [17] P. Müller, D. A. Berry, A. P. Grieve, M. Smith, M. Krams, Simulation-based sequential Bayesian design, *Journal of Statistical Planning and Inference* 137 (10) (2007) 3140–3150. doi:10.1016/j.jspi.2006.05.021.
- [18] U. Von Toussaint, Bayesian inference in physics, *Reviews of Modern Physics* 83 (2011) 943–999. doi:10.1103/RevModPhys.83.943.

- [19] X. Huan, Numerical approaches for sequential Bayesian optimal experimental design, Ph.D. thesis, Massachusetts Institute of Technology (2015).
- [20] X. Huan, Y. M. Marzouk, Sequential Bayesian optimal experimental design via approximate dynamic programming (2016). [arXiv:1604.08320](https://arxiv.org/abs/1604.08320).
- [21] W. Shen, X. Huan, Bayesian sequential optimal experimental design for nonlinear models using policy gradient reinforcement learning, *Computer Methods in Applied Mechanics and Engineering* 416 (2023) 116304. [doi:10.1016/j.cma.2023.116304](https://doi.org/10.1016/j.cma.2023.116304).
- [22] B. P. Carlin, J. B. Kadane, A. E. Gelfand, Approaches for optimal sequential decision analysis in clinical trials, *Biometrics* 54 (3) (1998) 964–975. [doi:10.2307/2533849](https://doi.org/10.2307/2533849).
- [23] R. Gautier, L. Pronzato, Adaptive control for sequential design, *Discussiones Mathematicae Probability and Statistics* 20 (1) (2000) 97–113. [doi:10.7151/dmps.1006](https://doi.org/10.7151/dmps.1006).
- [24] L. Pronzato, É. Thierry, Sequential experimental design and response optimisation, *Statistical Methods and Applications* 11 (3) (2002) 277–292. [doi:10.1007/BF02509828](https://doi.org/10.1007/BF02509828).
- [25] A. E. Brockwell, J. B. Kadane, A gridding method for Bayesian sequential decision problems, *Journal of Computational and Graphical Statistics* 12 (3) (2003) 566–584. [doi:10.1198/1061860032274](https://doi.org/10.1198/1061860032274).
- [26] J. A. Christen, M. Nakamura, Sequential stopping rules for species accumulation, *Journal of Agricultural, Biological & Environmental Statistics* 8 (2) (2003) 184–195. [doi:10.1198/108571103322161540](https://doi.org/10.1198/108571103322161540).
- [27] S. A. Murphy, Optimal dynamic treatment regimes, *Journal of the Royal Statistical Society: Series B (Statistical Methodology)* 65 (2) (2003) 331–355. [doi:10.1111/1467-9868.00389](https://doi.org/10.1111/1467-9868.00389).
- [28] J. K. Wathen, J. A. Christen, Implementation of backward induction for sequentially adaptive clinical trials, *Journal of Computational and Graphical Statistics* 15 (2) (2006) 398–413. [doi:10.1198/016214506X113406](https://doi.org/10.1198/016214506X113406).
- [29] P. Müller, Y. Duan, M. Garcia Tec, Simulation-based sequential design, *Pharmaceutical Statistics* 21 (4) (2022) 729–739. [doi:10.1002/pst.2216](https://doi.org/10.1002/pst.2216).
- [30] M. Tec, Y. Duan, P. Müller, A comparative tutorial of Bayesian sequential design and reinforcement learning, *The American Statistician* 77 (2) (2023) 223–233. [doi:10.1080/00031305.2022.2129787](https://doi.org/10.1080/00031305.2022.2129787).
- [31] W. Shen, X. Huan, Bayesian sequential optimal experimental design for nonlinear models using policy gradient reinforcement learning (2021). [arXiv:2110.15335](https://arxiv.org/abs/2110.15335).
- [32] A. Foster, D. R. Ivanova, I. Malik, T. Rainforth, Deep adaptive design: Amortizing sequential Bayesian experimental design, in: M. Meila, T. Zhang (Eds.), *Proceedings of the 38th International Conference on Machine Learning (ICML 2021)*, Vol. 139 of *Proceedings of Machine Learning Research*, PMLR, 2021, pp. 3384–3395.

- [33] D. R. Ivanova, A. Foster, S. Kleinegese, M. U. Gutmann, T. Rainforth, Implicit deep adaptive design: Policy-based experimental design without likelihoods, in: M. Ranzato, A. Beygelzimer, Y. Dauphin, P. Liang, J. W. Vaughan (Eds.), *Advances in Neural Information Processing Systems 34*, Curran Associates, 2021, pp. 25785–25798.
- [34] T. Blau, E. V. Bonilla, I. Chades, A. Dezfouli, Optimizing sequential experimental design with deep reinforcement learning, in: K. Chaudhuri, S. Jegelka, L. Song, C. Szepesvari, G. Niu, S. Sabato (Eds.), *Proceedings of the 39th International Conference on Machine Learning (ICML 2022)*, Vol. 162 of *Proceedings of Machine Learning Research*, PMLR, 2022, pp. 2107–2128.
- [35] X. Chen, C. Wang, Z. Zhou, K. Ross, Randomized ensembled double Q-learning: Learning fast without a model, in: *9th International Conference on Learning Representations (ICLR 2021)*, 2021, available at <https://openreview.net/forum?id=AY8zfZm0tDd>.
- [36] B. Poole, S. Ozair, A. Van Den Oord, A. Alemi, G. Tucker, On variational bounds of mutual information, in: *Proceedings of the 36th International Conference on Machine Learning (ICML 2019)*, Vol. 97 of *Proceedings of Machine Learning Research*, PMLR, 2019, pp. 5171–5180.
- [37] X. Nguyen, M. J. Wainwright, M. I. Jordan, Estimating divergence functionals and the likelihood ratio by convex risk minimization, *IEEE Transactions on Information Theory* 56 (11) (2010) 5847–5861. doi:10.1109/TIT.2010.2068870.
- [38] M. I. Belghazi, A. Baratin, S. Rajeswar, S. Ozair, Y. Bengio, A. Courville, R. D. Hjelm, Mutual information neural estimation, in: *Proceedings of the 35th International Conference on Machine Learning (ICML 2018)*, Vol. 80 of *Proceedings of Machine Learning Research*, PMLR, 2018, pp. 531–540.
- [39] S. Kleinegese, M. U. Gutmann, Bayesian Experimental Design for Implicit Models by Mutual Information Neural Estimation (2020). arXiv:2002.08129.
- [40] A. van den Oord, Y. Li, O. Vinyals, Representation learning with contrastive predictive coding (2018). arXiv:1807.03748.
- [41] D. Barber, F. Agakov, The IM algorithm: A variational approach to information maximization, in: *Advances in Neural Information Processing Systems 16*, MIT Press, 2003, pp. 201–208.
- [42] A. Foster, M. Jankowiak, E. Bingham, P. Horsfall, Y. W. Teh, T. Rainforth, N. Goodman, Variational Bayesian optimal experimental design, in: H. Wallach, H. Larochelle, A. Beygelzimer, F. d’Alché Buc, E. Fox, R. Garnett (Eds.), *Advances in Neural Information Processing Systems 32*, Curran Associates, 2019, pp. 14036–14047.
- [43] J. Dong, C. Jacobsen, M. Khalloufi, M. Akram, W. Liu, K. Duraisamy, X. Huan, Variational Bayesian optimal experimental design with normalizing flows, *Computer Methods in Applied Mechanics and Engineering* 433 (2025) 117457. doi:10.1016/j.cma.2024.117457.

- [44] G. Papamakarios, E. Nalisnick, D. J. Rezende, S. Mohamed, B. Lakshminarayanan, Normalizing flows for probabilistic modeling and inference, *Journal of Machine Learning Research* 22 (1) (2021) 2617–2680.
- [45] I. Kobyzev, S. J. Prince, M. A. Brubaker, Normalizing flows: An introduction and review of current methods, *IEEE Transactions on Pattern Analysis and Machine Intelligence* 43 (11) (2020) 3964–3979. doi:[10.1109/TPAMI.2020.2992934](https://doi.org/10.1109/TPAMI.2020.2992934).
- [46] A. C. Atkinson, A. N. Donev, R. D. Tobias, *Optimum Experimental Designs, with SAS*, Oxford University Press, 2007.
- [47] A. Attia, A. Alexanderian, A. K. Saibaba, Goal-oriented optimal design of experiments for large-scale Bayesian linear inverse problems, *Inverse Problems* 34 (9) (2018) 095009. doi:[10.1088/1361-6420/aad210](https://doi.org/10.1088/1361-6420/aad210).
- [48] K. Wu, P. Chen, O. Ghattas, An offline-online decomposition method for efficient linear Bayesian goal-oriented optimal experimental design: Application to optimal sensor placement, *SIAM Journal on Scientific Computing* 45 (1) (2023) B57–B77. doi:[10.1137/21M1466542](https://doi.org/10.1137/21M1466542).
- [49] J. M. Bernardo, Expected information as expected utility, *The Annals of Statistics* 7 (3) (1979) 686–690. doi:[10.1214/aos/1176344689](https://doi.org/10.1214/aos/1176344689).
- [50] T. Butler, J. D. Jakeman, T. Wildey, Optimal experimental design for prediction based on push-forward probability measures, *Journal of Computational Physics* 416 (2020) 109518. doi:[10.1016/j.jcp.2020.109518](https://doi.org/10.1016/j.jcp.2020.109518).
- [51] T. Butler, J. Jakeman, T. Wildey, Combining push-forward measures and Bayes’ rule to construct consistent solutions to stochastic inverse problems, *SIAM Journal on Scientific Computing* 40 (2) (2018) A984–A1011. doi:[10.1137/16M1087229](https://doi.org/10.1137/16M1087229).
- [52] T. Butler, J. Jakeman, T. Wildey, Convergence of probability densities using approximate models for forward and inverse problems in uncertainty quantification, *SIAM Journal on Scientific Computing* 40 (5) (2018) A3523–A3548. doi:[10.1137/18M1181675](https://doi.org/10.1137/18M1181675).
- [53] F. Bickford Smith, A. Kirsch, S. Farquhar, Y. Gal, A. Foster, T. Rainforth, Prediction-oriented bayesian active learning, in: F. Ruiz, J. Dy, J.-W. van de Meent (Eds.), *Proceedings of the 26th International Conference on Artificial Intelligence and Statistics*, Vol. 206 of *Proceedings of Machine Learning Research*, PMLR, 2023, pp. 7331–7348.
- [54] S. Zhong, W. Shen, T. Catanach, X. Huan, Goal-oriented Bayesian optimal experimental design for nonlinear models using Markov chain Monte Carlo (2024). [arXiv:2403.18072](https://arxiv.org/abs/2403.18072).
- [55] S. Kleinegesse, M. U. Gutmann, Gradient-based Bayesian experimental design for implicit models using mutual information lower bounds (2021). [arXiv:2105.04379](https://arxiv.org/abs/2105.04379).
- [56] J. Ginebra, On the measure of the information in a statistical experiment, *Bayesian Analysis* 2 (1) (2007) 167–212. doi:[10.1214/07-BA207](https://doi.org/10.1214/07-BA207).
- [57] R. J. Williams, Simple statistical gradient-following algorithms for connectionist reinforcement learning, *Machine learning* 8 (3) (1992) 229–256. doi:[10.1007/BF00992696](https://doi.org/10.1007/BF00992696).

- [58] D. P. Kingma, J. Ba, Adam: A method for stochastic optimization (2014). [arXiv:1412.6980](https://arxiv.org/abs/1412.6980).
- [59] T. P. Lillicrap, J. J. Hunt, A. Pritzel, N. Heess, T. Erez, Y. Tassa, D. Silver, D. Wierstra, Continuous control with deep reinforcement learning (2015). [arXiv:1509.02971](https://arxiv.org/abs/1509.02971).
- [60] C. J. Watkins, P. Dayan, Q-learning, *Machine learning* 8 (3-4) (1992) 279–292. [doi:10.1007/BF00992698](https://doi.org/10.1007/BF00992698).
- [61] V. Mnih, K. Kavukcuoglu, D. Silver, A. A. Rusu, J. Veness, M. G. Bellemare, A. Graves, M. Riedmiller, A. K. Fidjeland, G. Ostrovski, S. Petersen, C. Beattie, A. Sadik, I. Antonoglou, H. King, D. Kumaran, D. Wierstra, S. Legg, D. Hassabis, Human-level control through deep reinforcement learning, *Nature* 518 (2015) 529–533. [doi:10.1038/nature14236](https://doi.org/10.1038/nature14236).
- [62] A. Foster, M. Jankowiak, M. O’Meara, Y. W. Teh, T. Rainforth, A unified stochastic gradient approach to designing Bayesian-optimal experiments, in: *Proceedings of the 23rd International Conference on Artificial Intelligence and Statistics*, Vol. 108 of *Proceedings of Machine Learning Research*, PMLR, 2020, pp. 2959–2969.
- [63] K. J. Arrow, H. B. Chenery, B. S. Minhas, R. M. Solow, Capital-labor substitution and economic efficiency, *The Review of Economics and Statistics* 43 (3) (1961) 225–250. [doi:10.2307/1927286](https://doi.org/10.2307/1927286).
- [64] A. R. Cook, G. J. Gibson, C. A. Gilligan, Optimal observation times in experimental epidemic processes, *Biometrics* 64 (3) (2008) 860–868. [doi:10.1111/j.1541-0420.2007.00931.x](https://doi.org/10.1111/j.1541-0420.2007.00931.x).
- [65] L. J. Allen, A primer on stochastic epidemic models: Formulation, numerical simulation, and analysis, *Infectious Disease Modelling* 2 (2) (2017) 128–142. [doi:10.1016/j.idm.2017.03.001](https://doi.org/10.1016/j.idm.2017.03.001).
- [66] J. Schulman, F. Wolski, P. Dhariwal, A. Radford, O. Klimov, Proximal policy optimization algorithms (2017). [arXiv:1707.06347](https://arxiv.org/abs/1707.06347).
- [67] J. Schulman, S. Levine, P. Abbeel, M. Jordan, P. Moritz, Trust region policy optimization, in: F. Bach, D. Blei (Eds.), *Proceedings of the 32nd International Conference on Machine Learning*, Vol. 37 of *Proceedings of Machine Learning Research*, PMLR, 2015, pp. 1889–1897.
- [68] T. Haarnoja, A. Zhou, P. Abbeel, S. Levine, Soft actor-critic: Off-policy maximum entropy deep reinforcement learning with a stochastic actor, in: J. Dy, A. Krause (Eds.), *Proceedings of the 35th International Conference on Machine Learning*, Vol. 80 of *Proceedings of Machine Learning Research*, PMLR, 2018, pp. 1861–1870.
- [69] S. Fujimoto, H. van Hoof, D. Meger, Addressing function approximation error in actor-critic methods, in: J. Dy, A. Krause (Eds.), *Proceedings of the 35th International Conference on Machine Learning*, Vol. 80 of *Proceedings of Machine Learning Research*, PMLR, 2018, pp. 1587–1596.

- [70] D. M. Borth, A total entropy criterion for the dual problem of model discrimination and parameter estimation, *Journal of the Royal Statistical Society: Series B (Methodological)* 37 (1) (1975) 77–87. doi:10.1111/j.2517-6161.1975.tb01032.x.
- [71] J. Burkardt, The truncated normal distribution, Tech. rep., Florida State University, available at https://people.sc.fsu.edu/~jburkardt/presentations/truncated_normal.pdf (2023).
- [72] D. Rezende, S. Mohamed, Variational inference with normalizing flows, in: F. Bach, D. Blei (Eds.), *Proceedings of the 32nd International Conference on Machine Learning*, Vol. 37 of *Proceedings of Machine Learning Research*, PMLR, 2015, pp. 1530–1538.
- [73] E. G. Tabak, E. Vanden-Eijnden, Density estimation by dual ascent of the log-likelihood, *Communications in Mathematical Sciences* 8 (1) (2010) 217–233.
- [74] L. Dinh, J. Sohl-Dickstein, S. Bengio, Density estimation using Real NVP (2016). arXiv:1605.08803.
- [75] J. Kruse, G. Detommaso, U. Köthe, R. Scheichl, HINT: Hierarchical invertible neural transport for density estimation and Bayesian inference, in: *Proceedings of the AAAI Conference on Artificial Intelligence*, Vol. 35, 2021, pp. 8191–8199. doi:10.1609/aaai.v35i9.16997.
- [76] S. T. Radev, U. K. Mertens, A. Voss, L. Ardizzone, U. Köthe, BayesFlow: Learning complex stochastic models with invertible neural networks, *IEEE Transactions on Neural Networks and Learning Systems* 33 (4) (2020) 1452–1466. doi:10.1109/TNNLS.2020.3042395.
- [77] D. P. Kingma, P. Dhariwal, Glow: Generative flow with invertible 1x1 convolutions, in: S. Bengio, H. Wallach, H. Larochelle, K. Grauman, N. Cesa-Bianchi, R. Garnett (Eds.), *Advances in Neural Information Processing Systems*, Vol. 31, Curran Associates, Inc., 2018.
- [78] L. Ardizzone, J. Kruse, C. Rother, U. Köthe, Analyzing inverse problems with invertible neural networks, in: *7th International Conference on Learning Representations (ICLR 2019)*, 2019, available at <https://openreview.net/forum?id=rJed6j0cKX>.
- [79] F. Draxler, S. Wahl, C. Schnörr, U. Köthe, On the universality of coupling-based normalizing flows (2024). arXiv:2402.06578.
- [80] G. A. Padmanabha, N. Zabaras, Solving inverse problems using conditional invertible neural networks, *Journal of Computational Physics* 433 (2021) 110194. doi:10.1016/j.jcp.2021.110194.
- [81] H. Hasselt, Double Q-learning, in: J. Lafferty, C. Williams, J. Shawe-Taylor, R. Zemel, A. Culotta (Eds.), *Advances in Neural Information Processing Systems*, Vol. 23, Curran Associates, Inc., 2010.

Appendix A. Proofs

Appendix A.1. Information gain jointly with model indicator

Akin to the total entropy in [70], the IG jointly on the model indicator and PoIs is:

$$\begin{aligned}
& D_{\text{KL}} \left(P_{M, \Theta_m | i_{k_2}} \parallel P_{M, \Theta_m | i_{k_1}} \right) \\
&= \sum_{m=1}^{|\mathcal{M}_m|} \int p(m, \theta_m | i_{k_2}) \log \frac{p(m, \theta_m | i_{k_2})}{p(m, \theta_m | i_{k_1})} d\theta_m \\
&= \sum_{m=1}^{|\mathcal{M}_m|} P(m | i_{k_2}) \int p(\theta_m | m, i_{k_2}) \log \frac{P(m | i_{k_2}) p(\theta_m | m, i_{k_2})}{P(m | i_{k_1}) p(\theta_m | m, i_{k_1})} d\theta_m \\
&= \sum_{m=1}^{|\mathcal{M}_m|} P(m | i_{k_2}) \log \frac{P(m | i_{k_2})}{P(m | i_{k_1})} + \sum_{m=1}^{|\mathcal{M}_m|} P(m | i_{k_2}) \int p(\theta_m | m, i_{k_2}) \log \frac{p(\theta_m | m, i_{k_2})}{p(\theta_m | m, i_{k_1})} d\theta_m \\
&= D_{\text{KL}} \left(P_{M | i_{k_2}} \parallel P_{M | i_{k_1}} \right) + \mathbb{E}_{M | i_{k_2}} \left[D_{\text{KL}} \left(p_{\Theta_m | i_{k_2}} \parallel p_{\Theta_m | i_{k_1}} \right) \right],
\end{aligned}$$

where $0 \leq k_1 \leq k_2 \leq N$, and $p(\theta_m | m, i_k) = p(\theta_m | i_k)$ per our notation convention. When setting $k_1 = 0$ and $k_2 = N$, we recover the terminal reward in Eq. (8) under the special case of $\alpha_M = \alpha_\Theta = 1$ and $\alpha_Z = 0$. Similarly, the IG jointly on the model indicator and QoIs is:

$$\begin{aligned}
& D_{\text{KL}} \left(p_{M, Z_m | i_{k_2}} \parallel p_{M, Z_m | i_{k_1}} \right) \\
&= \sum_{m=1}^{|\mathcal{M}_m|} \int p(m, z_m | i_{k_2}) \log \frac{p(m, z_m | i_{k_2})}{p(m, z_m | i_{k_1})} dz_m \\
&= \sum_{m=1}^{|\mathcal{M}_m|} P(m | i_{k_2}) \int p(z_m | m, i_{k_2}) \log \frac{P(m | i_{k_2}) p(z_m | m, i_{k_2})}{P(m | i_{k_1}) p(z_m | m, i_{k_1})} dz_m \\
&= \sum_{m=1}^{|\mathcal{M}_m|} P(m | i_{k_2}) \frac{P(m | i_{k_2})}{P(m | i_{k_1})} + \sum_{m=1}^{|\mathcal{M}_m|} P(m | i_{k_2}) \int p(z_m | m, i_{k_2}) \log \frac{p(z_m | m, i_{k_2})}{p(z_m | m, i_{k_1})} dz_m \\
&= D_{\text{KL}} \left(P_{M | i_{k_2}} \parallel P_{M | i_{k_1}} \right) + \mathbb{E}_{M | i_{k_2}} \left[D_{\text{KL}} \left(p_{Z_m | i_{k_2}} \parallel p_{Z_m | i_{k_1}} \right) \right],
\end{aligned}$$

where $0 \leq k_1 \leq k_2 \leq N$, and $p(z_m | m, i_k) = p(z_m | i_k)$ per our notation convention. When setting $k_1 = 0$ and $k_2 = N$, we recover the terminal reward in Eq. (8) under the special case of $\alpha_M = \alpha_Z = 1$ and $\alpha_\Theta = 0$.

Appendix A.2. Information gain jointly on PoIs and QoIs

When nuisance parameters Ψ_m are absent, the IG jointly on the PoIs and QoIs given model m is:

$$\begin{aligned}
& D_{\text{KL}} \left(p_{\Theta_m, Z_m | i_{k_2}} \parallel p_{\Theta_m, Z_m | i_{k_1}} \right) \\
&= \iint p(\theta_m, z_m | i_{k_2}) \log \frac{p(\theta_m, z_m | i_{k_2})}{p(\theta_m, z_m | i_{k_1})} dz_m d\theta_m \\
&= \iint p(\theta_m, z_m | i_{k_2}) \log \frac{p(\theta_m | i_{k_2}) p(z_m | \theta_m, i_{k_2})}{p(\theta_m | i_{k_1}) p(z_m | \theta_m, i_{k_1})} dz_m d\theta_m \\
&= \iint p(\theta_m, z_m | i_{k_2}) \log \frac{p(\theta_m | i_{k_2}) p(z_m | \theta_m)}{p(\theta_m | i_{k_1}) p(z_m | \theta_m)} dz_m d\theta_m \\
&= \iint p(\theta_m, z_m | i_{k_2}) \log \frac{p(\theta_m | i_{k_2})}{p(\theta_m | i_{k_1})} dz_m d\theta_m \\
&= \int p(\theta_m | i_{k_2}) \log \frac{p(\theta_m | i_{k_2})}{p(\theta_m | i_{k_1})} d\theta_m \\
&= D_{\text{KL}} \left(p_{\Theta_m | i_{k_2}} \parallel p_{\Theta_m | i_{k_1}} \right),
\end{aligned}$$

where $0 \leq k_1 \leq k_2 \leq N$, and the third equality is due to Z_m only depending on Θ_m when Ψ_m is absent (see Eq. (2)). Hence, the IG on the QoIs is fully absorbed into the IG on the PoIs when nuisance parameters are absent.

Appendix A.3. Proof of Theorem 1 (Terminal-incremental equivalence)

Proof. We first decompose $U_T(\pi)$ into four summing parts:

$$U_T(\pi) = U_{T, \text{NIG}}(\pi) + U_{T, M}(\pi) + U_{T, \Theta}(\pi) + U_{T, Z}(\pi),$$

where $U_{T, \text{NIG}}(\pi)$ captures any non-IG reward contributions, and the other three parts are (with the conditioning on I_0 written out explicitly for the prior terms)

$$\begin{aligned}
U_{T, M}(\pi) &= \alpha_M \mathbb{E}_{Y_{0:N-1} | \pi, s_0} \left[D_{\text{KL}} \left(P_{M | I_N} \parallel P_{M | I_0} \right) \right], \\
U_{T, \Theta}(\pi) &= \alpha_{\Theta} \mathbb{E}_{Y_{0:N-1} | \pi, s_0} \mathbb{E}_{M | I_N} \left[D_{\text{KL}} \left(p_{\Theta_m | I_N} \parallel p_{\Theta_m | I_0} \right) \right], \\
U_{T, Z}(\pi) &= \alpha_Z \mathbb{E}_{Y_{0:N-1} | \pi, s_0} \mathbb{E}_{M | I_N} \left[D_{\text{KL}} \left(p_{Z_m | I_N} \parallel p_{Z_m | I_0} \right) \right].
\end{aligned}$$

Similarly, $U_I(\pi)$ is also decomposed into four summing parts:

$$U_I(\pi) = U_{I, \text{NIG}}(\pi) + U_{I, M}(\pi) + U_{I, \Theta}(\pi) + U_{I, Z}(\pi),$$

where $U_{I, \text{NIG}}(\pi)$ captures any non-IG reward contributions, and the other three parts are

$$\begin{aligned}
U_{I, M}(\pi) &= \alpha_M \mathbb{E}_{Y_{0:N-1} | \pi, s_0} \left[\sum_{k=0}^{N-1} D_{\text{KL}} \left(P_{M | I_{k+1}} \parallel P_{M | I_k} \right) \right] \\
U_{I, \Theta}(\pi) &= \alpha_{\Theta} \mathbb{E}_{Y_{0:N-1} | \pi, s_0} \left[\sum_{k=0}^{N-1} \mathbb{E}_{M | I_{k+1}} \left[D_{\text{KL}} \left(p_{\Theta_m | I_{k+1}} \parallel p_{\Theta_m | I_k} \right) \right] \right] \\
U_{I, Z}(\pi) &= \alpha_Z \mathbb{E}_{Y_{0:N-1} | \pi, s_0} \left[\sum_{k=0}^{N-1} \mathbb{E}_{M | I_{k+1}} \left[D_{\text{KL}} \left(p_{Z_m | I_{k+1}} \parallel p_{Z_m | I_k} \right) \right] \right].
\end{aligned}$$

Since TIG and IIG formulations only entail the IG contributions, the non-IG reward contributions are not affected by this choice, and hence

$$U_{T,\text{NIG}}(\pi) = U_{I,\text{NIG}}(\pi).$$

For the part corresponding to the IG contribution from model indicator:

$$\begin{aligned}
& U_{I,M}(\pi) - U_{T,M}(\pi) \\
&= \alpha_M \mathbb{E}_{Y_{0:N-1}|\pi, s_0} \left[\sum_{k=0}^{N-1} D_{\text{KL}}(P_{M|I_{k+1}} || P_{M|I_k}) - D_{\text{KL}}(P_{M|I_N} || P_{M|I_0}) \right] \\
&= \alpha_M \mathbb{E}_{Y_{0:N-1}|\pi, s_0} \left[\sum_{k=0}^{N-1} \sum_{m=1}^{|\mathcal{M}_m|} P(m|I_{k+1}) \log \frac{P(m|I_{k+1})}{P(m|I_k)} - \sum_{m=1}^{|\mathcal{M}_m|} P(m|I_N) \log \frac{P(m|I_N)}{P(m|I_0)} \right] \\
&= \alpha_M \sum_{m=1}^{|\mathcal{M}_m|} \mathbb{E}_{Y_{0:N-1}|\pi, s_0} \left[\sum_{k=0}^{N-1} P(m|I_{k+1}) \log \frac{P(m|I_{k+1})}{P(m|I_k)} - P(m|I_N) \log \frac{P(m|I_N)}{P(m|I_0)} \right] \\
&= \alpha_M \sum_{m=1}^{|\mathcal{M}_m|} \mathbb{E}_{Y_{0:N-1}|\pi, s_0} \left[\sum_{k=0}^{N-2} P(m|I_{k+1}) \log \frac{P(m|I_{k+1})}{P(m|I_k)} + P(m|I_N) \log \frac{P(m|I_N)}{P(m|I_{N-1})} \right. \\
&\quad \left. - P(m|I_N) \log \frac{P(m|I_N)}{P(m|I_0)} \right] \\
&= \alpha_M \sum_{m=1}^{|\mathcal{M}_m|} \mathbb{E}_{Y_{0:N-1}|\pi, s_0} \left[\sum_{k=0}^{N-2} P(m|I_{k+1}) \log \frac{P(m|I_{k+1})}{P(m|I_k)} - P(m|I_N) \log \frac{P(m|I_{N-1})}{P(m|I_0)} \right] \\
&= \alpha_M \sum_{m=1}^{|\mathcal{M}_m|} \mathbb{E}_{Y_{0:N-2}|\pi, s_0} \left[\sum_{k=0}^{N-2} P(m|I_{k+1}) \log \frac{P(m|I_{k+1})}{P(m|I_k)} \right. \\
&\quad \left. - \mathbb{E}_{Y_{N-1}|Y_{0:N-2}, \pi, s_0} \left[P(m|I_N) \log \frac{P(m|I_{N-1})}{P(m|I_0)} \right] \right] \\
&= \alpha_M \sum_{m=1}^{|\mathcal{M}_m|} \mathbb{E}_{Y_{0:N-2}|\pi, s_0} \left[\sum_{k=0}^{N-2} P(m|I_{k+1}) \log \frac{P(m|I_{k+1})}{P(m|I_k)} - P(m|I_{N-1}) \log \frac{P(m|I_{N-1})}{P(m|I_0)} \right] \\
&\quad \vdots \\
&= \alpha_M \sum_{m=1}^{|\mathcal{M}_m|} \mathbb{E}_{Y_0|\pi, s_0} \left[\sum_{k=0}^0 P(m|I_{k+1}) \log \frac{P(m|I_{k+1})}{P(m|I_k)} - P(m|I_1) \log \frac{P(m|I_1)}{P(m|I_0)} \right] \\
&= 0,
\end{aligned}$$

where the seventh equality is due to

$$\begin{aligned}
& \mathbb{E}_{Y_{N-1}|Y_{0:N-2}, \pi, s_0} \left[P(m|I_N) \log \frac{P(m|I_{N-1})}{P(m|I_0)} \right] \\
&= \int p(y_{N-1}|Y_{0:N-2}, \pi, s_0) P(m|I_N) \log \frac{P(m|I_{N-1})}{P(m|I_0)} dy_{N-1} \\
&= \int p(y_{N-1}|\pi, I_{N-1}) P(m|y_{N-1}, \pi, I_{N-1}) \log \frac{P(m|I_{N-1})}{P(m|I_0)} dy_{N-1} \\
&= \int p(y_{N-1}, m|\pi, I_{N-1}) \log \frac{P(m|I_{N-1})}{P(m|I_0)} dy_{N-1} \\
&= P(m|I_{N-1}) \log \frac{P(m|I_{N-1})}{P(m|I_0)},
\end{aligned}$$

and the eighth equality results from repeatedly applying the steps between the third and seventh equalities $N - 1$ times.

For the part corresponding to the IG contribution from PoIs:

$$\begin{aligned}
& U_{I,\Theta}(\pi) - U_{T,\Theta}(\pi) \\
&= \alpha_{\Theta} \mathbb{E}_{Y_{0:N-1}|\pi, s_0} \left[\sum_{k=0}^{N-1} \mathbb{E}_{M|I_{k+1}} D_{\text{KL}}(p_{\Theta_m|I_{k+1}} \| p_{\Theta_m|I_k}) - \mathbb{E}_{M|I_N} D_{\text{KL}}(p_{\Theta_m|I_N} \| p_{\Theta_m|I_0}) \right] \\
&= \alpha_{\Theta} \sum_{m=1}^{|\mathcal{M}_m|} \mathbb{E}_{Y_{0:N-1}|\pi, s_0} \left[\sum_{k=0}^{N-1} P(m|I_{k+1}) D_{\text{KL}}(p_{\Theta_m|I_{k+1}} \| p_{\Theta_m|I_k}) \right. \\
&\quad \left. - P(m|I_N) D_{\text{KL}}(p_{\Theta_m|I_N} \| p_{\Theta_m|I_0}) \right] \\
&= \alpha_{\Theta} \sum_{m=1}^{|\mathcal{M}_m|} \mathbb{E}_{Y_{0:N-1}|\pi, s_0} \left[\sum_{k=0}^{N-2} P(m|I_{k+1}) D_{\text{KL}}(p_{\Theta_m|I_{k+1}} \| p_{\Theta_m|I_k}) \right. \\
&\quad + P(m|I_N) D_{\text{KL}}(p_{\Theta_m|I_N} \| p_{\Theta_m|I_{N-1}}) \\
&\quad \left. - P(m|I_N) D_{\text{KL}}(p_{\Theta_m|I_N} \| p_{\Theta_m|I_0}) \right] \\
&= \alpha_{\Theta} \sum_{m=1}^{|\mathcal{M}_m|} \mathbb{E}_{Y_{0:N-1}|\pi, s_0} \left[\sum_{k=0}^{N-2} P(m|I_{k+1}) D_{\text{KL}}(p_{\Theta_m|I_{k+1}} \| p_{\Theta_m|I_k}) \right. \\
&\quad \left. + P(m|I_N) \int p(\theta_m|I_N) \log \frac{p(\theta_m|I_0)}{p(\theta_m|I_{N-1})} d\theta_m \right] \\
&= \alpha_{\Theta} \sum_{m=1}^{|\mathcal{M}_m|} \mathbb{E}_{Y_{0:N-2}|\pi, s_0} \left[\sum_{k=0}^{N-2} P(m|I_{k+1}) D_{\text{KL}}(p_{\Theta_m|I_{k+1}} \| p_{\Theta_m|I_k}) \right. \\
&\quad \left. + \mathbb{E}_{Y_{N-1}|Y_{0:N-2}, \pi, s_0} \left[P(m|I_N) \int p(\theta_m|I_N) \log \frac{p(\theta_m|I_0)}{p(\theta_m|I_{N-1})} d\theta_m \right] \right] \\
&= \alpha_{\Theta} \sum_{m=1}^{|\mathcal{M}_m|} \mathbb{E}_{Y_{0:N-2}|\pi, s_0} \left[\sum_{k=0}^{N-2} P(m|I_{k+1}) D_{\text{KL}}(p_{\Theta_m|I_{k+1}} \| p_{\Theta_m|I_k}) \right. \\
&\quad \left. - P(m|I_{N-1}) D_{\text{KL}}(p_{\Theta_m|I_{N-1}} \| p_{\Theta_m|I_0}) \right] \\
&\quad \vdots \\
&= \alpha_{\Theta} \sum_{m=1}^{|\mathcal{M}_m|} \mathbb{E}_{Y_0|\pi, s_0} \left[\sum_{k=0}^0 P(m|I_{k+1}) D_{\text{KL}}(p_{\Theta_m|I_{k+1}} \| p_{\Theta_m|I_k}) - P(m|I_1) D_{\text{KL}}(p_{\Theta_m|I_1} \| p_{\Theta_m|I_0}) \right] \\
&= 0,
\end{aligned}$$

where the sixth equality is due to

$$\begin{aligned}
& \mathbb{E}_{Y_{N-1}|Y_{0:N-2}, \pi, s_0} \left[P(m|I_N) \int p(\theta_m|I_N) \log \frac{p(\theta_m|I_0)}{p(\theta_m|I_{N-1})} d\theta_m \right] \\
&= \int P(y_{N-1}|Y_{0:N-2}, \pi, s_0) P(m|I_N) \int p(\theta_m|I_N) \log \frac{p(\theta_m|I_0)}{p(\theta_m|I_{N-1})} d\theta_m dy_{N-1} \\
&= \int P(y_{N-1}|\pi, I_{N-1}) P(m|y_{N-1}, \pi, I_{N-1}) \int p(\theta_m|m, y_{N-1}, \pi, I_{N-1}) \log \frac{p(\theta_m|I_0)}{p(\theta_m|I_{N-1})} d\theta_m dy_{N-1} \\
&= \iint P(y_{N-1}, m, \theta_m|\pi, I_{N-1}) \log \frac{p(\theta_m|I_0)}{p(\theta_m|I_{N-1})} d\theta_m dy_{N-1} \\
&= P(m|I_{N-1}) \int P(\theta_m|I_{N-1}) \log \frac{p(\theta_m|I_0)}{p(\theta_m|I_{N-1})} d\theta_m \\
&= -P(m|I_{N-1}) D_{\text{KL}}(p_{\Theta_m|I_{N-1}} || p_{\Theta_m|I_0}),
\end{aligned}$$

and the seventh equality results from repeatedly applying the steps between the second and sixth equalities $N - 1$ times.

For the part corresponding to the IG contribution from QoIs, the derivation is identical as above for the PoIs except Θ is replaced with Z , to arrive at

$$U_{I,Z}(\pi) - U_{T,Z}(\pi) = 0.$$

Combining the equivalence results from all four parts, we obtain

$$U_I(\pi) = U_T(\pi)$$

for any policy π . □

Appendix A.4. Proof of Theorem 2 (One-point equivalence)

Proof. We begin by proving the equivalence of expected utility under TIG and one-point-TIG:

$$\begin{aligned}
U_T(\pi) &= \mathbb{E}_{Y_{0:N-1}|\pi, s_0} \left[\sum_{k=0}^{N-1} r_k(S_k, \xi_k, y_k) + r_N(S_N) \right] \\
&= \mathbb{E}_{Y_{0:N-1}|\pi, s_0} \left[\alpha_M D_{\text{KL}}(P_{M|I_N} || P_M) \right. \\
&\quad \left. + \mathbb{E}_{M|I_N} \left[\alpha_\Theta D_{\text{KL}}(p_{\Theta_m|I_N} || p_{\Theta_m}) + \alpha_Z D_{\text{KL}}(p_{Z_m|I_N} || p_{Z_m}) \right] \right] \\
&= \mathbb{E}_{Y_{0:N-1}|\pi, s_0} \left[\alpha_M \mathbb{E}_{M|I_N} \log \frac{P(M|I_N)}{P(M)} \right. \\
&\quad \left. + \mathbb{E}_{M|I_N} \left[\alpha_\Theta \mathbb{E}_{\Theta_m|I_N} \log \frac{p(\Theta_m|I_N)}{p(\Theta_m)} + \alpha_Z \mathbb{E}_{Z_m|I_N} \log \frac{p(Z_m|I_N)}{p(Z_m)} \right] \right] \\
&= \mathbb{E}_{M, Y_{0:N-1}|\pi, s_0} \left[\alpha_M \log \frac{P(M|I_N)}{P(M)} \right. \\
&\quad \left. + \alpha_\Theta \mathbb{E}_{\Theta_m|I_N} \log \frac{p(\Theta_m|I_N)}{p(\Theta_m)} + \alpha_Z \mathbb{E}_{Z_m|I_N} \log \frac{p(Z_m|I_N)}{p(Z_m)} \right] \\
&= \mathbb{E}_{M, Y_{0:N-1}|\pi, s_0} \left[\alpha_M \mathbb{E}_{\Theta_m, Z_m|I_N} \log \frac{P(M|I_N)}{P(M)} \right. \\
&\quad \left. + \alpha_\Theta \mathbb{E}_{\Theta_m, Z_m|I_N} \log \frac{p(\Theta_m|I_N)}{p(\Theta_m)} + \alpha_Z \mathbb{E}_{\Theta_m, Z_m|I_N} \log \frac{p(Z_m|I_N)}{p(Z_m)} \right] \\
&= \mathbb{E}_{M, \Theta_m, Z_m, Y_{0:N-1}|\pi, s_0} \left[\alpha_M \log \frac{P(M|I_N)}{P(M)} + \alpha_\Theta \log \frac{p(\Theta_m|I_N)}{p(\Theta_m)} + \alpha_Z \log \frac{p(Z_m|I_N)}{p(Z_m)} \right] \\
&= \mathbb{E}_{M, \Theta_m, \Psi_m, Z_m, Y_{0:N-1}|\pi, s_0} \left[\alpha_M \log \frac{P(M|I_N)}{P(M)} + \alpha_\Theta \log \frac{p(\Theta_m|I_N)}{p(\Theta_m)} + \alpha_Z \log \frac{p(Z_m|I_N)}{p(Z_m)} \right] \\
&= \mathbb{E}_{M_0, \Theta_{m,0}, \Psi_{m,0}, Z_{m,0}} \mathbb{E}_{Y_{0:N-1}|\pi, s_0, M_0, \Theta_{m,0}, \Psi_{m,0}, Z_{m,0}} \left[\alpha_M \log \frac{P(M_0|I_N)}{P(M_0)} \right. \\
&\quad \left. + \alpha_\Theta \log \frac{p(\Theta_{m,0}|I_N)}{p(\Theta_{m,0})} + \alpha_Z \log \frac{p(Z_{m,0}|I_N)}{p(Z_{m,0})} \right] \\
&= \mathbb{E}_{M_0, \Theta_{m,0}, \Psi_{m,0}, Z_{m,0}} \mathbb{E}_{I_N|\pi, s_0, M_0, \Theta_{m,0}, \Psi_{m,0}} \left[\alpha_M \log \frac{P(M_0|I_N)}{P(M_0)} \right. \\
&\quad \left. + \alpha_\Theta \log \frac{p(\Theta_{m,0}|I_N)}{p(\Theta_{m,0})} + \alpha_Z \log \frac{p(Z_{m,0}|I_N)}{p(Z_{m,0})} \right] \\
&= \check{U}_T(\pi),
\end{aligned}$$

where at several occasions we use the equivalence between $\mathbb{E}_{Y_{0:k-1}|\pi, s_0, \dots}$ and $\mathbb{E}_{I_k|\pi, s_0, \dots}$, and between $\mathbb{E}_{\dots|I_k}$ and $\mathbb{E}_{\dots|Y_{0:k-1}, \pi, s_0}$, in the eighth equality the random variables M, Θ_m, Ψ_m, Z_m

are replaced with their oracle versions $M_0, \Theta_{m,0}, \Psi_{m,0}, Z_{m,0}$ which have identical distributions, and the ninth equality omits the conditioning on $Z_{m,0}$ in the inner expectation since I_N does not depend on $Z_{m,0}$.

Next, we have $U_T(\pi) = U_I(\pi)$ through Theorem 1 and its proof in Appendix A.3. Finally, we show the equivalence between $\check{U}_I(\pi)$ and $\check{U}_T(\pi)$ by cancelling out all intermediate posteriors:

$$\begin{aligned}
& \check{U}_I(\pi) \\
&= \mathbb{E}_{M_0, \Theta_{m,0}, \Psi_{m,0}, Z_{m,0}} \mathbb{E}_{I_N | \pi, s_0, M_0, \Theta_{m,0}, \Psi_{m,0}} \sum_{k=0}^{N-1} \left[\alpha_M \log \frac{P(M_0 | I_{k+1})}{P(M_0 | I_k)} + \alpha_\Theta \log \frac{p(\Theta_{m,0} | I_{k+1})}{p(\Theta_{m,0} | I_k)} \right. \\
&\quad \left. + \alpha_Z \log \frac{p(Z_{m,0} | I_{k+1})}{p(Z_{m,0} | I_k)} \right] \\
&= \mathbb{E}_{M_0, \Theta_{m,0}, \Psi_{m,0}, Z_{m,0}} \mathbb{E}_{I_N | \pi, s_0, M_0, \Theta_{m,0}, \Psi_{m,0}} \left[\alpha_M \log \frac{P(M_0 | I_N)}{P(M_0)} + \alpha_\Theta \log \frac{p(\Theta_{m,0} | I_N)}{p(\Theta_{m,0})} \right. \\
&\quad \left. + \alpha_Z \log \frac{p(Z_{m,0} | I_N)}{p(Z_{m,0})} \right] \\
&= \check{U}_T(\pi).
\end{aligned}$$

Combining the above equivalence results together, we arrive at

$$U_T(\pi) = \check{U}_T(\pi) = \check{U}_I(\pi) = U_I(\pi)$$

for any policy π . □

Appendix A.5. Omitting prior terms in the expected utility

When the prior terms $p(\cdot)$ are omitted, the expected utility is shifted by the amount:

$$\begin{aligned}
& \mathbb{E}_{M_0, \Theta_{m,0}, \Psi_{m,0}, Z_{m,0}} \mathbb{E}_{I_N | \pi, s_0, M_0, \Theta_{m,0}, \Psi_{m,0}} [\alpha_M \log P(M_0) + \alpha_\Theta \log p(\Theta_{m,0}) + \alpha_Z \log p(Z_{m,0})] \\
&= \mathbb{E}_{M_0, \Theta_{m,0}, \Psi_{m,0}, Z_{m,0}} [\alpha_M \log P(M_0) + \alpha_\Theta \log p(\Theta_{m,0}) + \alpha_Z \log p(Z_{m,0})],
\end{aligned}$$

which does not depend on the policy π . In other words, the expected utility is shifted by a constant. Hence, whether including or omitting the prior terms will not affect the optimized policy. The same result holds for both TIG and IIG rewards, and their one-point versions and variational one-point versions.

Appendix A.6. Proof of Theorem 3 (Variational lower bound)

Proof. First, we prove the equivalence between the expected utility under variational-one-point-TIG and variational-one-point-IIG:

$$\begin{aligned}
& \tilde{U}_I(\pi; \phi) \\
&= \mathbb{E}_{M_0, \Theta_{m,0}, \Psi_{m,0}, Z_{m,0}} \mathbb{E}_{I_N | \pi, s_0, M_0, \Theta_{m,0}, \Psi_{m,0}} \sum_{k=0}^{N-1} \left[\alpha_M \log \frac{q(M_0 | I_{k+1}; \phi_M)}{q(M_0 | I_k; \phi_M)} \right. \\
&\quad \left. + \alpha_\Theta \log \frac{q(\Theta_{m,0} | I_{k+1}; \phi_{\Theta_m})}{q(\Theta_{m,0} | I_k; \phi_{\Theta_m})} + \alpha_Z \log \frac{q(Z_{m,0} | I_{k+1}; \phi_{Z_m})}{q(Z_{m,0} | I_k; \phi_{Z_m})} \right] \\
&= \mathbb{E}_{M_0, \Theta_{m,0}, \Psi_{m,0}, Z_{m,0}} \mathbb{E}_{I_N | \pi, s_0, M_0, \Theta_{m,0}, \Psi_{m,0}} \left[\right. \\
&\quad \alpha_M \left(\log \frac{q(M_0 | I_1; \phi_M)}{P(M_0)} + \log \frac{q(M_0 | I_2; \phi_M)}{q(M_0 | I_1; \phi_M)} + \dots + \log \frac{q(M_0 | I_N; \phi_M)}{q(M_0 | I_{N-1}; \phi_M)} \right) \\
&\quad + \alpha_\Theta \left(\log \frac{q(\Theta_{m,0} | I_1; \phi_{\Theta_m})}{p(\Theta_{m,0})} + \log \frac{q(\Theta_{m,0} | I_2; \phi_{\Theta_m})}{q(\Theta_{m,0} | I_1; \phi_{\Theta_m})} + \dots + \log \frac{q(\Theta_{m,0} | I_N; \phi_{\Theta_m})}{q(\Theta_{m,0} | I_{N-1}; \phi_{\Theta_m})} \right) \\
&\quad \left. + \alpha_Z \left(\log \frac{q(Z_{m,0} | I_1; \phi_{Z_m})}{p(Z_{m,0})} + \log \frac{q(Z_{m,0} | I_2; \phi_{Z_m})}{q(Z_{m,0} | I_1; \phi_{Z_m})} + \dots + \log \frac{q(Z_{m,0} | I_N; \phi_{Z_m})}{q(Z_{m,0} | I_{N-1}; \phi_{Z_m})} \right) \right] \\
&= \mathbb{E}_{M_0, \Theta_{m,0}, \Psi_{m,0}, Z_{m,0}} \mathbb{E}_{I_N | \pi, s_0, M_0, \Theta_{m,0}, \Psi_{m,0}} \left[\alpha_M \log \frac{q(M_0 | I_N; \phi_M)}{P(M_0)} \right. \\
&\quad \left. + \alpha_\Theta \log \frac{q(\Theta_{m,0} | I_N; \phi_{\Theta_m})}{p(\Theta_{m,0})} + \alpha_Z \log \frac{q(Z_{m,0} | I_N; \phi_{Z_m})}{p(Z_{m,0})} \right] \\
&= \tilde{U}_T(\pi; \phi).
\end{aligned}$$

Due to the cancellation of all intermediate variational posteriors, only the prior and final variational posterior terms survive. Since the prior density is usually accessible analytically or omitted per [Appendix A.5](#), the accuracy of the variational expected utility only depends on the quality of the final variational posterior approximations, $q(\cdot | I_N; \phi_{(\cdot)})$.

Next, we prove the lower bound for variational-one-point-TIG:

$$\begin{aligned}
& U_T(\pi) - \tilde{U}_T(\pi; \phi) \\
&= \check{U}_T(\pi) - \tilde{U}_T(\pi; \phi) \\
&= \mathbb{E}_{M_0, \Theta_{m,0}, \Psi_{m,0}, Z_{m,0}} \mathbb{E}_{I_N | \pi, s_0, M_0, \Theta_{m,0}, \Psi_{m,0}} \left[\alpha_M \log \frac{P(M_0 | I_N)}{q(M_0 | I_N; \phi_M)} + \alpha_\Theta \log \frac{p(\Theta_{m,0} | I_N)}{q(\Theta_{m,0} | I_N; \phi_{\Theta_m})} \right. \\
&\quad \left. + \alpha_Z \log \frac{p(Z_{m,0} | I_N)}{q(Z_{m,0} | I_N; \phi_{Z_m})} \right] \\
&= \alpha_M \mathbb{E}_{M_0, \Theta_{m,0}, \Psi_{m,0}, Z_{m,0}} \mathbb{E}_{I_N | \pi, s_0, M_0, \Theta_{m,0}, \Psi_{m,0}} \left[\log \frac{P(M_0 | I_N)}{q(M_0 | I_N; \phi_M)} \right] \\
&\quad + \alpha_\Theta \mathbb{E}_{M_0, \Theta_{m,0}, \Psi_{m,0}, Z_{m,0}} \mathbb{E}_{I_N | \pi, s_0, M_0, \Theta_{m,0}, \Psi_{m,0}} \left[\log \frac{p(\Theta_{m,0} | I_N)}{q(\Theta_{m,0} | I_N; \phi_{\Theta_m})} \right] \\
&\quad + \alpha_Z \mathbb{E}_{M_0, \Theta_{m,0}, \Psi_{m,0}, Z_{m,0}} \mathbb{E}_{I_N | \pi, s_0, M_0, \Theta_{m,0}, \Psi_{m,0}} \left[\log \frac{p(Z_{m,0} | I_N)}{q(Z_{m,0} | I_N; \phi_{Z_m})} \right] \\
&= \alpha_M \mathbb{E}_{M_0, I_N | \pi, s_0} \left[\log \frac{P(M_0 | I_N)}{q(M_0 | I_N; \phi_M)} \right] \\
&\quad + \alpha_\Theta \mathbb{E}_{M_0, \Theta_{m,0}, I_N | \pi, s_0} \left[\log \frac{p(\Theta_{m,0} | I_N)}{q(\Theta_{m,0} | I_N; \phi_{\Theta_m})} \right] \\
&\quad + \alpha_Z \mathbb{E}_{M_0, Z_{m,0}, I_N | \pi, s_0} \left[\log \frac{p(Z_{m,0} | I_N)}{q(Z_{m,0} | I_N; \phi_{Z_m})} \right] \\
&= \alpha_M \mathbb{E}_{I_N | \pi, s_0} \mathbb{E}_{M_0 | I_N} \left[\log \frac{P(M_0 | I_N)}{q(M_0 | I_N; \phi_M)} \right] \\
&\quad + \alpha_\Theta \mathbb{E}_{M_0, I_N | \pi, s_0} \mathbb{E}_{\Theta_{m,0} | M_0, I_N} \left[\log \frac{p(\Theta_{m,0} | I_N)}{q(\Theta_{m,0} | I_N; \phi_{\Theta_m})} \right] \\
&\quad + \alpha_Z \mathbb{E}_{M_0, I_N | \pi, s_0} \mathbb{E}_{Z_{m,0} | M_0, I_N} \left[\log \frac{p(Z_{m,0} | I_N)}{q(Z_{m,0} | I_N; \phi_{Z_m})} \right] \\
&= \alpha_M \mathbb{E}_{I_N | \pi, s_0} \left[D_{\text{KL}} (P_{M_0 | I_N} \parallel q_{M_0 | I_N; \phi_M}) \right] \\
&\quad + \alpha_\Theta \mathbb{E}_{M_0, I_N | \pi, s_0} \left[D_{\text{KL}} (p_{\Theta_{m,0} | I_N} \parallel q_{\Theta_{m,0} | I_N; \phi_{\Theta_m}}) \right] \\
&\quad + \alpha_Z \mathbb{E}_{M_0, I_N | \pi, s_0} \left[D_{\text{KL}} (p_{Z_{m,0} | I_N} \parallel q_{Z_{m,0} | I_N; \phi_{Z_m}}) \right] \\
&\geq 0,
\end{aligned}$$

where the first equality invokes Theorem 2, the sixth equality is due to $p(\Theta_{m,0} | I_N)$ being equivalent to $p(\Theta_{m,0} | M_0, I_N)$ and $p(Z_{m,0} | I_N)$ being equivalent to $p(Z_{m,0} | M_0, I_N)$, and the

final inequality is due to the non-negativity of KL divergence terms and that we require $\alpha_M, \alpha_\Theta, \alpha_Z \in [0, 1]$. The bound is tight if and only if $q(\cdot|I_N; \phi_{(\cdot)}) = p(\cdot|I_N)$ and so all the KL divergence terms become zero; (except the trivial case when $\alpha_M = \alpha_\Theta = \alpha_Z = 0$, under which U, \check{U} , and \tilde{U} will always be identically zero).

Putting everything together, we arrive at

$$\tilde{U}_I(\pi; \phi) = \tilde{U}_T(\pi; \phi) \leq \check{U}_T(\pi) = \check{U}_I(\pi) = U_T(\pi) = U_I(\pi),$$

for any π and ϕ , where the last three equalities result from Theorem 2. \square

Appendix B. Algorithm details

Appendix B.1. Neural network architecture for approximate posteriors of model indicator

The overall architecture for a NN-based approximate posterior of model indicator, $q(m|i_k; \phi_M)$, is shown in Table B.4; the same architecture is used for all numerical cases in this paper. The NN takes i_k as input, and outputs the log-probabilities of each candidate model, $\log q(m|i_k; \phi_M)$. Separate NNs are trained for each stage k when the IIG formulation is used. As shown in the first part of Appendix A.6, the quality of the intermediate approximate posteriors does not directly contribute to the accuracy of the overall variational expected utility, and thus one may train these intermediate approximate posteriors more ‘roughly’, for example, by using simpler NN architectures and with shared weights among the NNs.

Table B.4: Architecture for the NN-based approximate posteriors of model indicator.

Layer	Description	Dimension	Activation
Input	i_k	$k(N_\xi + N_y)$	-
Hidden 1	Dense	256	ReLU
Hidden 2	Dense	256	ReLU
Hidden 3	Dense	256	ReLU
Output	Dense	$ \mathcal{M}_m $	LogSoftmax

Appendix B.2. Neural network architectures for approximate posteriors of PoIs and QoIs

We use GMMs and NFs as approximate posteriors for PoIs, $q(\theta_m|i_k; \phi_{\Theta_m})$, and for QoIs, $q(z_m|i_k; \phi_{Z_m})$ ¹. The same architecture is used for both PoI and QoI cases, and we introduce below only in the context of PoIs for simplicity. Separate GMMs/NFs are trained for each stage k when the IIG formulation is used.

Appendix B.2.1. Independent Gaussian mixture models

An independent GMM approximates a complex distribution through a weighted sum of multiple independent Gaussians:

$$q(\theta_m|i_k; \phi_{\Theta_m}) = \sum_{i=1}^{n_{\text{mix}}} w_i(i_k; \phi_{\Theta_m}) \mathcal{N}(\theta_m; \mu_i(i_k; \phi_{\Theta_m}), \Sigma_i(i_k; \phi_{\Theta_m})), \quad (\text{B.1})$$

¹In this section, we have dropped the oracle subscript 0 (from $\theta_{m,0}$ and $z_{m,0}$) to simplify notation.

where for the i th Gaussian, $w_i(\mathbf{i}_k; \phi_{\Theta_m})$ is its mixture weight, $\mu_i(\mathbf{i}_k; \phi_{\Theta_m}) \in \mathbb{R}^{N_{\theta_m}}$ is its mean, and $\Sigma_i(\mathbf{i}_k; \phi_{\Theta_m}) \in \mathbb{R}^{N_{\theta_m} \times N_{\theta_m}}$ is its diagonal covariance matrix with square root of the diagonal terms being the standard deviations. The weights, means, and standard deviations of the GMM are predicted using NNs, together referred to as the GMM net. These NNs share a common backend network that learns shared features. The architectures for the feature net, weight net, mean net and standard deviation net are provided in Tables B.5 to B.7. The ‘Linear mapping’ in Table B.7 refers to the process of mapping the output to a specific range that is problem dependent. This mapping ensures that the predicted means and standard deviations fall within the desired range. Additionally, a ‘nugget’ of 10^{-27} is added to Eq. (B.1) to prevent numerical underflow. When certain PoIs have compact support, independent truncated normal distributions [71] are used for the dimensions corresponding to those PoIs. The specific ranges of the linear mapping and the usage of truncated normal will be stated in each numerical case. The same GMM net architecture is used across all numerical cases.

Table B.5: Architecture for the feature net within the GMM net.

Layer	Description	Dimension	Activation
Input	\mathbf{i}_k	$k(N_{\xi} + N_y)$	-
Hidden 1	Dense	256	ReLU
Output	Dense	256	ReLU

Table B.6: Architecture for the weight net within the GMM net.

Layer	Description	Dimension	Activation
Input	Feature(\mathbf{i}_k)	256	-
Hidden 1	Dense	256	ReLU
Hidden 2	Dense	256	ReLU
Output	Dense	n_{mix}	Softmax

Table B.7: Architecture for the mean net and standard deviation net within the GMM net.

Layer	Description	Dimension	Activation
Input	Feature(\mathbf{i}_k)	256	-
Hidden 1	Dense	256	ReLU
Hidden 2	Dense	256	ReLU
Hidden 3	Dense	$n_{\text{mix}}N_{\theta_m}$	Sigmoid
Output	Identity	$n_{\text{mix}}N_{\theta_m}$	Linear mapping

Appendix B.2.2. Normalizing flows

An NF is an invertible mapping from a target random variable $\Theta_m \sim p_{\Theta_m}(\theta_m)$ ² to a standard normal random variable, $\mathbf{Z}_m \sim p_{\mathbf{Z}_m}(\mathbf{z}_m) = \mathcal{N}(0, \mathbb{I})$ ³, of the same dimension: \mathbf{Z}_m

²While we use the prior as the target distribution here for the purpose of introducing NFs, generally we will target posteriors such as $p(\theta_m | \mathbf{i}_k)$.

³ \mathbf{Z} denotes the standard normal random variable, not to be confused with the QoIs Z .

$=f(\Theta_m)$ and $\Theta_m = g(Z_m)$ where $g := f^{-1}$. In practice, we approximate f via a mapping parameterized with ϕ_{Θ_m} , which produces an approximate transformation $\tilde{Z}_m = f(\Theta_m; \phi_{\Theta_m})$ and its inverse $g(\cdot; \phi_{\Theta_m}) := f(\cdot; \phi_{\Theta_m})^{-1}$ produces $\Theta_m = g(\tilde{Z}_m; \phi_{\Theta_m})$. If acting on the exact standard normal Z_m , then $\tilde{\Theta}_m = g(Z_m; \phi_{\Theta_m})$ and also $Z_m = f(\tilde{\Theta}_m; \phi_{\Theta_m})$.

In general, the approximate mappings used in NFs are often structured as compositions of successive simple invertible mappings: $f(\tilde{\Theta}_m; \phi_{\Theta_m}) = f_n \circ f_{n-1} \circ \dots \circ f_1(\tilde{\Theta}_m) = f_n(f_{n-1}(\dots(f_1(\tilde{\Theta}_m))\dots))$ and $g(Z_m; \phi_{\Theta_m}) = g_1 \circ \dots \circ g_{n-1} \circ g_n(Z_m) = g_1(g_2(\dots(g_n(Z_m))\dots))$ with $g_i = f_i^{-1}$ and $n \geq 1$. Note that all intermediate mappings f_i and g_i depend on ϕ_{Θ_m} , but we omit their subscripts to simplify notation. The log density of $\tilde{\Theta}_m$ can be tracked via the change-of-variable formula:

$$\log q_{\tilde{\Theta}_m}(\tilde{\Theta}_m = \theta_m; \phi_{\Theta_m}) = \log p_{Z_m}(f_n \circ f_{n-1} \circ \dots \circ f_1(\tilde{\Theta}_m = \theta_m)) + \sum_{i=1}^n \log \left| \det \frac{\partial f_i \circ f_{i-1} \circ \dots \circ f_1(\tilde{\Theta}_m)}{\partial \tilde{\Theta}_m} \right|_{\tilde{\Theta}_m = \theta_m}, \quad (\text{B.2})$$

where $\frac{\partial f_i(\tilde{\Theta}_m)}{\partial \tilde{\Theta}_m}$ is the Jacobian of f_i . By applying successive transformations on Z_m , the density of the resulting variable can be highly expressive [72, 73] and effective for multi-modal, skewed, or other non-standard distribution shapes.

Among a range of choices for the architecture of invertible mappings [44, 45], we adopt the coupling layers [74] as a special type of invertible neural network (INN) [75, 76] for its efficient density evaluations and sampling in both forward (f) and inverse (g) directions. Several papers have shown that composing coupling layers can create flexible flows [77, 78, 75], and recent work by Draxler *et al.* [79] shows that coupling layers form a distributional universal approximator. The basic form of the coupling layer that completes one full transformation starts by partitioning $Z_m = [Z_{m_1}, Z_{m_2}]^\top$ into two parts of approximately equal dimension—that is, $Z_{m_1} \in \mathbb{R}^{N_{\theta_{m,1}}}$, $Z_{m_2} \in \mathbb{R}^{N_{\theta_{m,2}}}$, and $N_{\theta_{m,1}} + N_{\theta_{m,2}} = N_{\theta_m}$ —and then composes together $n = 2$ transformations that transform one part at a time. This maps Z_m to an approximate target $\tilde{\Theta}_m$, i.e., $g(Z_m; \phi_{\Theta_m}) = g_1 \circ g_2(Z_m) = \tilde{\Theta}_m$, and is defined as:

$$g_2(Z_m) = \begin{bmatrix} \tilde{\Theta}_{m_1} = [Z_{m_1} - \mathbf{t}_2(Z_{m_2})] \odot \exp[-\mathbf{s}_2(Z_{m_2})] \\ Z_{m_2} \end{bmatrix},$$

$$g_1(g_2(Z_m)) = \begin{bmatrix} \tilde{\Theta}_{m_1} \\ \tilde{\Theta}_{m_2} = [Z_{m_2} - \mathbf{t}_1(\tilde{\Theta}_{m_1})] \odot \exp(-\mathbf{s}_1(\tilde{\Theta}_{m_1})) \end{bmatrix},$$

where \odot denotes element-wise product, and $\mathbf{s}_1, \mathbf{t}_1 : \mathbb{R}^{N_{\theta_{m,1}}} \rightarrow \mathbb{R}^{N_{\theta_{m,2}}}$ and $\mathbf{s}_2, \mathbf{t}_2 : \mathbb{R}^{N_{\theta_{m,2}}} \rightarrow \mathbb{R}^{N_{\theta_{m,1}}}$ are arbitrary functions. The parameterizations of these functions make up ϕ_{Θ_m} ; for instance, if these functions are represented by NNs, then ϕ_{Θ_m} encompasses all NNs' weight and bias parameters.

The inverse of $g(\cdot; \phi_{\Theta_m})$, which is $f(\tilde{\Theta}_m; \phi_{\Theta_m}) = f_2 \circ f_1(\tilde{\Theta}_m) = Z_m$, similarly involves partitioning $\tilde{\Theta}_m = [\tilde{\Theta}_{m_1}, \tilde{\Theta}_{m_2}]$ and can be shown to be:

$$f_1(\tilde{\Theta}_m) = \begin{bmatrix} \tilde{\Theta}_{m_1} \\ Z_{m_2} = \tilde{\Theta}_{m_2} \odot \exp(\mathbf{s}_1(\tilde{\Theta}_{m_1})) + \mathbf{t}_1(\tilde{\Theta}_{m_1}) \end{bmatrix},$$

$$f_2(f_1(\tilde{\Theta}_m)) = \begin{bmatrix} Z_{m_1} = \tilde{\Theta}_{m_1} \odot \exp(\mathbf{s}_2(Z_{m_2})) + \mathbf{t}_2(Z_{m_2}) \\ Z_{m_2} \end{bmatrix}.$$

The Jacobians of f_1 and f_2 are triangular matrices:

$$\frac{\partial f_1(\tilde{\Theta}_m)}{\partial \tilde{\Theta}_m} = \begin{bmatrix} \mathbb{I}_{N_{\theta_{m,1}}} & 0 \\ \frac{\partial \mathbf{Z}_{m_2}}{\partial \tilde{\Theta}_{m_1}} & \text{diag}(\exp(\mathbf{s}_1(\tilde{\Theta}_{m_1}))) \end{bmatrix}, \quad \frac{\partial f_2(f_1(\tilde{\Theta}_m))}{\partial (f_1(\tilde{\Theta}_m))} = \begin{bmatrix} \text{diag}(\exp(\mathbf{s}_2(\mathbf{Z}_{m_2}))) & \frac{\partial \mathbf{Z}_{m_1}}{\partial \mathbf{Z}_{m_2}} \\ 0 & \mathbb{I}_{N_{\theta_{m,2}}} \end{bmatrix},$$

and have respective determinants $\exp(\sum_{j=1}^{N_{\theta_{m,2}}} \mathbf{s}_1(\tilde{\Theta}_{m_1})_j)$ and $\exp(\sum_{j=1}^{N_{\theta_{m,1}}} \mathbf{s}_2(\mathbf{Z}_{m_2})_j)$.

Multiple such complete transformations can be composed together for greater expressiveness. For example, adopting NFs with $n_{\text{trans}} = 3$ sets of complete transformations entails $f(\tilde{\Theta}_m; \phi_{\Theta_m}) = (f_2 \circ f_1)^{T^3} \circ (f_2 \circ f_1)^{T^2} \circ (f_2 \circ f_1)^{T^1}(\tilde{\Theta}_m)$ and $g(\mathbf{Z}_m; \phi_{\Theta_m}) = (g_1 \circ g_2)^{T^3} \circ (g_1 \circ g_2)^{T^2} \circ (g_1 \circ g_2)^{T^1}(\mathbf{Z}_m)$.

To incorporate the i_k -dependence into the approximate posteriors $q(\theta_m | i_k; \phi_{\Theta_m})$, the \mathbf{s} and \mathbf{t} functions are designed to additionally take i_k as input, leading to a form of conditional INNs (cINNs) [80]. Similar to the GMM setup, i_k is first fed into a feature network whose output has the same dimension as i_k . The architectures of the feature network, and the \mathbf{s}_1 , \mathbf{t}_1 , \mathbf{s}_2 , \mathbf{t}_2 networks in NFs are provided in Tables B.8 to B.10. Mirroring the GMM net, a nugget of 10^{-27} is added to Eq. (B.2) to prevent numerical underflow.

Table B.8: Architecture for the feature net within the NFs. The first value under the ‘Dimension’ column is used for the source location problem in Section 4.2 and the CES problem in Section 4.3; the second value is used for the SIR problem in Section 4.4.

Layer	Description	Dimension	Activation
Input	i_k	$k(N_\xi + N_y)$	-
Hidden 1	Dense	256 / 128	ReLU
Hidden 2	Dense	256 / 128	ReLU
Hidden 3	Dense	256 / None	ReLU
Output	Dense	$k(N_\xi + N_y)$	-

Table B.9: Architecture for the \mathbf{s}_1 and \mathbf{t}_1 nets within the NFs. The first value under the ‘Dimension’ column is used for the source location problem in Section 4.2 and the CES problem in Section 4.3; the second value is used for the SIR problem in Section 4.4.

Layer	Description	Dimension	Activation
Input	Feature(i_k) + θ_1	$k(N_\xi + N_y) + N_{\Theta_{m,1}}$	-
Hidden 1	Dense	256 / 128	ReLU
Hidden 2	Dense	256 / 128	ReLU
Hidden 3	Dense	256 / 128	ReLU
Output	Dense	$N_{\Theta_{m,2}}$	-

Appendix B.3. Neural network architectures for actor and critic

The architectures for the actor (policy) and critic (action-value function) networks from [31] are adopted in this work. The actor $\mu_{k,w}$ is a mapping from i_k to design ξ_k . Instead of learning separate actor networks for each stage k , we combine them into a single actor. The overall input to the actor network takes the form

$$i_k^{\text{actor}} = [e_k, \tilde{i}_k],$$

Table B.10: Architecture for the s_2 and t_2 nets within the NFs. The first value under the ‘Dimension’ column is used for the source location problem in Section 4.2 and the CES problem in Section 4.3; the second value is used for the SIR problem in Section 4.4.

Layer	Description	Dimension	Activation
Input	Feature(i_k) + $\tilde{\theta}_2$	$k(N_\xi + N_y) + N_{\Theta_{m,2}}$	-
Hidden 1	Dense	256 / 128	ReLU
Hidden 2	Dense	256 / 128	ReLU
Hidden 3	Dense	256 / 128	ReLU
Output	Dense	$N_{\Theta_{m,1}}$	-

where e_k is an 0-indexed one-hot encoding vector of size N that represents the current experiment stage:

$$e_k = [0, \dots, 0, \underbrace{1}_{k\text{th}}, 0, \dots, 0],$$

and \tilde{i}_k is a vector of fixed size $(N-1)(N_\xi + N_y)$ obtained by extending i_k with zero-padding:

$$\tilde{i}_k = \left[\underbrace{\xi_0, \dots, \xi_{k-1}}_{N_\xi}, \underbrace{0, \dots, 0}_{N_\xi(N-1-k)}, \underbrace{y_0, \dots, y_{k-1}}_{N_y}, \underbrace{0, \dots, 0}_{N_y(N-1-k)} \right].$$

The total dimension of i_k^{actor} is $N + (N-1)(N_\xi + N_y)$. Similarly, the overall input to the critic network is

$$i_k^{\text{critic}} = [i_k^{\text{actor}}, \xi_k],$$

with total dimension $N + (N-1)(N_\xi + N_y) + N_\xi$. The output of the critic network is a scalar. We note that without the presence of e_k , it would not be possible for the actor or the critic to distinguish between whether the state is at stage k , or at a later stage but with ξ_k and y_k actually being zero (i.e., whether zero values are padding or actual results). The architectures for the actor and critic networks are presented in Tables B.11 and B.12, respectively, with ‘Linear mapping’ in Table B.11 indicating the mapping of the output value to be within the design bounds. The same actor and critic architectures are used across all numerical cases.

Table B.11: Architecture for the actor network.

Layer	Description	Dimension	Activation
Input	i_k^{actor}	$N + (N-1)(N_\xi + N_y)$	-
Hidden 1	Dense	256	ReLU
Hidden 2	Dense	256	ReLU
Hidden 3	Dense	256	ReLU
Hidden 4	Dense	N_ξ	Sigmoid
Output	Identity	N_ξ	Linear mapping

Table B.12: Architecture for the critic network.

Layer	Description	Dimension	Activation
Input	i_k^{critic}	$N + (N - 1)(N_\xi + N_y) + N_\xi$	-
Hidden 1	Dense	256	ReLU
Hidden 2	Dense	256	ReLU
Hidden 3	Dense	256	ReLU
Output	Dense	1	-

Appendix B.4. More about the critic

While we introduced the critic $\tilde{Q}_k^{\pi w}(i_k, \xi_k; \phi)$ in Eqs. (25) to (27) for the variational one-point reward terms \tilde{r}_k and \tilde{r}_N from Section 2.5, a corresponding critic can be formed for the one-point reward terms \check{r}_k and \check{r}_N from Section 2.4:

$$\begin{aligned}
\check{Q}_k^{\pi w}(i_k, \xi_k) &= \mathbb{E}_{M_0, \Theta_{m,0}, \Psi_{m,0}, Z_{m,0} | i_k} \left[\mathbb{E}_{Y_{k:N-1} | w, s_0, i_k, \xi_k, M_0, \Theta_{m,0}, \Psi_{m,0}} \left[\check{r}_k(i_k, \xi_k, Y_k) \right. \right. \\
&\quad \left. \left. + \sum_{t=k+1}^{N-1} \check{r}_t(I_t, \mu_{t,w}(I_t), Y_t) + \check{r}_N(I_N) \right] \right] \\
&= \mathbb{E}_{M_0, \Theta_{m,0}, \Psi_{m,0}, Z_{m,0} | i_k} \left[\mathbb{E}_{Y_k | w, s_0, i_k, \xi_k, M_0, \Theta_{m,0}, \Psi_{m,0}} \left[\check{r}_k(i_k, \xi_k, Y_k) \right. \right. \\
&\quad \left. \left. + \check{Q}_{k+1}^{\pi w}(I_{k+1}, \mu_{k+1,w}(I_{k+1})) \right] \right], \\
\check{Q}_N^{\pi w}(i_N, \cdot) &= \mathbb{E}_{M_0, \Theta_{m,0}, \Psi_{m,0}, Z_{m,0} | i_N} \left[\check{r}_N(i_N) \right],
\end{aligned}$$

for $k = 0, \dots, N - 1$ and subject to $I_{k+1} = \{I_k, \xi_k, Y_k\}$.

When using the TIG formulation, these critics become

$$\begin{aligned}
\check{Q}_{T,k}^{\pi w}(i_k, \xi_k) &= \mathbb{E}_{M_0, \Theta_{m,0}, \Psi_{m,0}, Z_{m,0} | i_k} \left[\mathbb{E}_{Y_{k:N-1} | w, s_0, i_k, \xi_k, M_0, \Theta_{m,0}, \Psi_{m,0}} \left[\right. \right. \\
&\quad \left. \left. \alpha_M \log \frac{P(M_0 | I_N)}{P(M_0)} + \alpha_\Theta \log \frac{p(\Theta_{m,0} | I_N)}{p(\Theta_{m,0})} + \alpha_Z \log \frac{p(Z_{m,0} | I_N)}{p(Z_{m,0})} \right] \right] \\
\check{Q}_{T,N}^{\pi w}(i_N, \cdot) &= \mathbb{E}_{M_0, \Theta_{m,0}, \Psi_{m,0}, Z_{m,0} | i_N} \left[\alpha_M \log \frac{P(M_0 | i_N)}{P(M_0)} \right. \\
&\quad \left. + \alpha_\Theta \log \frac{p(\Theta_{m,0} | i_N)}{p(\Theta_{m,0})} + \alpha_Z \log \frac{p(Z_{m,0} | i_N)}{p(Z_{m,0})} \right],
\end{aligned}$$

for $k = 0, \dots, N - 1$ and subject to $I_{k+1} = \{I_k, \xi_k, Y_k\}$, and

$$\begin{aligned}\tilde{Q}_{T,k}^{\pi w}(i_k, \xi_k; \phi) &= \mathbb{E}_{M_0, \Theta_{m,0}, \Psi_{m,0}, Z_{m,0} | i_k} \left[\mathbb{E}_{Y_{k:N-1} | w, s_0, i_k, \xi_k, M_0, \Theta_{m,0}, \Psi_{m,0}} \left[\right. \right. \\ &\quad \left. \left. \alpha_M \log \frac{q(M_0 | I_N; \phi_M)}{P(M_0)} + \alpha_\Theta \log \frac{q(\Theta_{m,0} | I_N; \phi_{\Theta_m})}{p(\Theta_{m,0})} + \alpha_Z \log \frac{q(Z_{m,0} | I_N; \phi_{Z_m})}{p(Z_{m,0})} \right] \right], \\ \tilde{Q}_{T,N}^{\pi w}(i_N, \cdot; \phi) &= \mathbb{E}_{M_0, \Theta_{m,0}, \Psi_{m,0}, Z_{m,0} | i_N} \left[\alpha_M \log \frac{q(M_0 | i_N; \phi_M)}{P(M_0)} \right. \\ &\quad \left. + \alpha_\Theta \log \frac{q(\Theta_{m,0} | i_N; \phi_{\Theta_m})}{p(\Theta_{m,0})} + \alpha_Z \log \frac{q(Z_{m,0} | i_N; \phi_{Z_m})}{p(Z_{m,0})} \right],\end{aligned}$$

for $k = 0, \dots, N - 1$ and subject to $I_{k+1} = \{I_k, \xi_k, Y_k\}$.

Similarly, when using the IIG formulation, these critics become

$$\begin{aligned}\check{Q}_{I,k}^{\pi w}(i_k, \xi_k) &= \mathbb{E}_{M_0, \Theta_{m,0}, \Psi_{m,0}, Z_{m,0} | i_k} \left[\mathbb{E}_{Y_{k:N-1} | w, s_0, i_k, \xi_k, M_0, \Theta_{m,0}, \Psi_{m,0}} \left[\right. \right. \\ &\quad \alpha_M \log \frac{P(M_0 | I_{k+1})}{P(M_0 | i_k)} + \alpha_\Theta \log \frac{p(\Theta_{m,0} | I_{k+1})}{p(\Theta_{m,0} | i_k)} + \alpha_Z \log \frac{p(Z_{m,0} | I_{k+1})}{p(Z_{m,0} | i_k)} \\ &\quad \left. \left. + \sum_{t=k+1}^{N-1} \alpha_M \log \frac{P(M_0 | I_{t+1})}{P(M_0 | I_t)} + \alpha_\Theta \log \frac{p(\Theta_{m,0} | I_{t+1})}{p(\Theta_{m,0} | I_t)} + \alpha_Z \log \frac{p(Z_{m,0} | I_{t+1})}{p(Z_{m,0} | I_t)} \right] \right], \\ &= \mathbb{E}_{M_0, \Theta_{m,0}, \Psi_{m,0}, Z_{m,0} | i_k} \left[\mathbb{E}_{Y_{k:N-1} | w, s_0, i_k, \xi_k, M_0, \Theta_{m,0}, \Psi_{m,0}} \left[\right. \right. \\ &\quad \left. \left. \alpha_M \log \frac{P(M_0 | I_N)}{P(M_0 | i_k)} + \alpha_\Theta \log \frac{p(\Theta_{m,0} | I_N)}{p(\Theta_{m,0} | i_k)} + \alpha_Z \log \frac{p(Z_{m,0} | I_N)}{p(Z_{m,0} | i_k)} \right] \right],\end{aligned}$$

$$\check{Q}_{I,N}^{\pi w}(i_k, \cdot) = 0,$$

for $k = 0, \dots, N - 1$ and subject to $I_{k+1} = \{I_k, \xi_k, Y_k\}$, and

$$\begin{aligned}\tilde{Q}_{I,k}^{\pi w}(i_k, \xi_k; \phi) &= \mathbb{E}_{M_0, \Theta_{m,0}, \Psi_{m,0}, Z_{m,0} | i_k} \left[\mathbb{E}_{Y_{k:N-1} | w, s_0, i_k, \xi_k, M_0, \Theta_{m,0}, \Psi_{m,0}} \left[\right. \right. \\ &\quad \alpha_M \log \frac{q(M_0 | I_{k+1}; \phi_M)}{q(M_0 | i_k; \phi_M)} + \alpha_\Theta \log \frac{q(\Theta_{m,0} | I_{k+1}; \phi_{\Theta_m})}{q(\Theta_{m,0} | i_k; \phi_{\Theta_m})} + \alpha_Z \log \frac{q(Z_{m,0} | I_{k+1}; \phi_{Z_m})}{q(Z_{m,0} | i_k; \phi_{Z_m})} \\ &\quad \left. \left. + \sum_{t=k+1}^{N-1} \alpha_M \log \frac{q(M_0 | I_{t+1}; \phi_M)}{q(M_0 | I_t; \phi_M)} + \alpha_\Theta \log \frac{q(\Theta_{m,0} | I_{t+1}; \phi_{\Theta_m})}{q(\Theta_{m,0} | I_t; \phi_{\Theta_m})} + \alpha_Z \log \frac{q(Z_{m,0} | I_{t+1}; \phi_{Z_m})}{q(Z_{m,0} | I_t; \phi_{Z_m})} \right] \right], \\ &= \mathbb{E}_{M_0, \Theta_{m,0}, \Psi_{m,0}, Z_{m,0} | i_k} \left[\mathbb{E}_{Y_{k:N-1} | w, s_0, i_k, \xi_k, M_0, \Theta_{m,0}, \Psi_{m,0}} \left[\right. \right. \\ &\quad \left. \left. \alpha_M \log \frac{q(M_0 | I_N; \phi_M)}{q(M_0 | i_k; \phi_M)} + \alpha_\Theta \log \frac{q(\Theta_{m,0} | I_N; \phi_{\Theta_m})}{q(\Theta_{m,0} | i_k; \phi_{\Theta_m})} + \alpha_Z \log \frac{q(Z_{m,0} | I_N; \phi_{Z_m})}{q(Z_{m,0} | i_k; \phi_{Z_m})} \right] \right],\end{aligned}$$

$$\tilde{Q}_{I,N}^{\pi w}(i_k, \cdot; \phi) = 0,$$

for $k = 0, \dots, N - 1$ and subject to $I_{k+1} = \{I_k, \xi_k, Y_k\}$.

Remark 6. The differences between the one-point-TIG and one-point-IIG critics are

$$\begin{aligned}
\check{Q}_{T,k}^{\pi_w}(i_k, \xi_k) - \check{Q}_{I,k}^{\pi_w}(i_k, \xi_k) &= \mathbb{E}_{M_0, \Theta_{m,0}, \Psi_{m,0}, Z_{m,0} | i_k} \left[\mathbb{E}_{Y_{k:N-1} | w, s_0, i_k, \xi_k, M_0, \Theta_{m,0}, \Psi_{m,0}} \left[\right. \right. \\
&\quad \left. \left. \alpha_M \log \frac{P(M_0 | i_k)}{P(M_0)} + \alpha_\Theta \log \frac{p(\Theta_{m,0} | i_k)}{p(\Theta_{m,0})} + \alpha_Z \log \frac{p(Z_{m,0} | i_k)}{p(Z_{m,0})} \right] \right] \\
&= \mathbb{E}_{M_0, \Theta_{m,0}, \Psi_{m,0}, Z_{m,0} | i_k} \left[\right. \\
&\quad \left. \alpha_M \log \frac{P(M_0 | i_k)}{P(M_0)} + \alpha_\Theta \log \frac{p(\Theta_{m,0} | i_k)}{p(\Theta_{m,0})} + \alpha_Z \log \frac{p(Z_{m,0} | i_k)}{p(Z_{m,0})} \right], \\
\check{Q}_{T,N}^{\pi_w}(i_N, \cdot) - \check{Q}_{I,N}^{\pi_w}(i_N, \cdot) &= \mathbb{E}_{M_0, \Theta_{m,0}, \Psi_{m,0}, Z_{m,0} | i_N} \left[\right. \\
&\quad \left. \alpha_M \log \frac{P(M_0 | i_N)}{P(M_0)} + \alpha_\Theta \log \frac{p(\Theta_{m,0} | i_N)}{p(\Theta_{m,0})} + \alpha_Z \log \frac{p(Z_{m,0} | i_N)}{p(Z_{m,0})} \right],
\end{aligned}$$

for $k = 0, \dots, N - 1$ and subject to $I_{k+1} = \{I_k, \xi_k, Y_k\}$. Notably, all difference expressions are independent of ξ_k . When using the one-point reward formulations, the same policy gradient expression as Eq. (24) will emerge but with $\nabla_{\xi_k} \check{Q}_k^{\pi_w}(i_k, \xi_k)$. Since the difference of the above critics do not depend on ξ_k , $\nabla_{\xi_k} \check{Q}_k^{\pi_w}(i_k, \xi_k)$ will be identical for one-point-TIG and one-point-IIG, and hence their policy gradients will also be identical.

Remark 7. The differences between the one-point-TIG and variational one-point-TIG critics

are

$$\begin{aligned}
& \check{Q}_{T,k}^{\pi_w}(i_k, \xi_k) - \tilde{Q}_{T,k}^{\pi_w}(i_k, \xi_k; \phi) \\
&= \mathbb{E}_{M_0, \Theta_{m,0}, \Psi_{m,0}, Z_{m,0} | i_k} \left[\mathbb{E}_{Y_{k:N-1} | w, s_0, i_k, \xi_k, M_0, \Theta_{m,0}, \Psi_{m,0}} \left[\right. \right. \\
&\quad \left. \left. \alpha_M \log \frac{P(M_0 | I_N)}{q(M_0 | I_N; \phi_M)} + \alpha_\Theta \log \frac{p(\Theta_{m,0} | I_N)}{q(\Theta_{m,0} | I_N; \phi_{\Theta_m})} + \alpha_Z \log \frac{p(Z_{m,0} | I_N)}{q(Z_{m,0} | I_N; \phi_{Z_m})} \right] \right] \\
&= \mathbb{E}_{I_N | w, s_0, i_k, \xi_k} \left[\alpha_M D_{\text{KL}}(P_{M_0 | I_N} \parallel q_{M_0 | I_N; \phi_M}) \right. \\
&\quad \left. + \mathbb{E}_{M_0 | I_N} \left[\alpha_\Theta D_{\text{KL}}(p_{\Theta_{m,0} | I_N} \parallel q_{\Theta_{m,0} | I_N; \phi_{\Theta_m}}) + \alpha_Z D_{\text{KL}}(p_{Z_{m,0} | I_N} \parallel q_{Z_{m,0} | I_N; \phi_{Z_m}}) \right] \right], \\
& \check{Q}_{T,N}^{\pi_w}(i_N, \cdot) - \tilde{Q}_{T,N}^{\pi_w}(i_N, \cdot; \phi) \\
&= \mathbb{E}_{M_0, \Theta_{m,0}, \Psi_{m,0}, Z_{m,0} | i_N} \left[\right. \\
&\quad \left. \alpha_M \log \frac{P(M_0 | i_N)}{q(M_0 | i_N; \phi_M)} + \alpha_\Theta \log \frac{p(\Theta_{m,0} | i_N)}{q(\Theta_{m,0} | i_N; \phi_{\Theta_m})} + \alpha_Z \log \frac{p(Z_{m,0} | i_N)}{q(Z_{m,0} | i_N; \phi_{Z_m})} \right] \\
&= \alpha_M D_{\text{KL}}(P_{M_0 | i_N} \parallel q_{M_0 | i_N; \phi_M}) \\
&\quad + \mathbb{E}_{M_0 | i_N} \left[\alpha_\Theta D_{\text{KL}}(p_{\Theta_{m,0} | i_N} \parallel q_{\Theta_{m,0} | i_N; \phi_{\Theta_m}}) + \alpha_Z D_{\text{KL}}(p_{Z_{m,0} | i_N} \parallel q_{Z_{m,0} | i_N; \phi_{Z_m}}) \right],
\end{aligned}$$

for $k = 0, \dots, N-1$ and subject to $I_{k+1} = \{I_k, \xi_k, Y_k\}$. Notably, all difference expressions are expectations of weighted sum of KL divergence terms with non-negative weights. The difference expressions are zero if and only if the variational posterior approximations $q(\cdot | I_N; \phi_{(\cdot)})$ are equal to the true posteriors $p(\cdot | I_N)$ (except the trivial case when $\alpha_M = \alpha_\Theta = \alpha_Z = 0$). Hence, $\check{Q}_{T,k}^{\pi_w}(i_k, \xi_k; \phi)$ forms a lower bound to $\tilde{Q}_{T,k}^{\pi_w}(i_k, \xi_k)$ for all k , and learning an accurate variational posterior approximation would help reduce the error in the critic.

Remark 8. The differences between the one-point-IIG and variational one-point-IIG critics

are

$$\begin{aligned}
& \check{Q}_{I,k}^{\pi_w}(i_k, \xi_k) - \tilde{Q}_{I,k}^{\pi_w}(i_k, \xi_k; \phi) \\
&= \mathbb{E}_{M_0, \Theta_{m,0}, \Psi_{m,0}, Z_{m,0} | i_k} \left[\mathbb{E}_{Y_{k:N-1} | w, s_0, i_k, \xi_k, M_0, \Theta_{m,0}, \Psi_{m,0}} \left[\right. \right. \\
&\quad \alpha_M \log \frac{P(M_0 | I_N)}{q(M_0 | I_N; \phi_M)} + \alpha_\Theta \log \frac{p(\Theta_{m,0} | I_N)}{q(\Theta_{m,0} | I_N; \phi_{\Theta_m})} + \alpha_Z \log \frac{p(Z_{m,0} | I_N)}{q(Z_{m,0} | I_N; \phi_{Z_m})} \\
&\quad \left. \left. - \alpha_M \log \frac{P(M_0 | i_k)}{q(M_0 | i_k; \phi_M)} - \alpha_\Theta \log \frac{p(\Theta_{m,0} | i_k)}{q(\Theta_{m,0} | i_k; \phi_{\Theta_m})} - \alpha_Z \log \frac{p(Z_{m,0} | i_k)}{q(Z_{m,0} | i_k; \phi_{Z_m})} \right] \right] \\
&= \mathbb{E}_{I_N | w, s_0, i_k, \xi_k} \left[\alpha_M D_{\text{KL}}(P_{M_0 | I_N} \parallel q_{M_0 | I_N; \phi_M}) \right. \\
&\quad \left. + \mathbb{E}_{M_0 | I_N} \left[\alpha_\Theta D_{\text{KL}}(p_{\Theta_{m,0} | I_N} \parallel q_{\Theta_{m,0} | I_N; \phi_{\Theta_m}}) + \alpha_Z D_{\text{KL}}(p_{Z_{m,0} | I_N} \parallel q_{Z_{m,0} | I_N; \phi_{Z_m}}) \right] \right. \\
&\quad \left. - \alpha_M D_{\text{KL}}(P_{M_0 | i_k} \parallel q_{M_0 | i_k; \phi_M}) \right. \\
&\quad \left. - \mathbb{E}_{M_0 | i_k} \left[\alpha_\Theta D_{\text{KL}}(p_{\Theta_{m,0} | i_k} \parallel q_{\Theta_{m,0} | i_k; \phi_{\Theta_m}}) + \alpha_Z D_{\text{KL}}(p_{Z_{m,0} | i_k} \parallel q_{Z_{m,0} | i_k; \phi_{Z_m}}) \right] \right], \\
& \check{Q}_{I,N}^{\pi_w}(i_N, \cdot) - \tilde{Q}_{I,N}^{\pi_w}(i_N, \cdot; \phi) = 0,
\end{aligned}$$

for $k = 0, \dots, N-1$ and subject to $I_{k+1} = \{I_k, \xi_k, Y_k\}$. Applying triangle inequality, these difference expressions become bounded by

$$\begin{aligned}
& \left| \check{Q}_{I,k}^{\pi_w}(i_k, \xi_k) - \tilde{Q}_{I,k}^{\pi_w}(i_k, \xi_k; \phi) \right| \\
&\leq \mathbb{E}_{I_N | w, s_0, i_k, \xi_k} \left[\alpha_M D_{\text{KL}}(P_{M_0 | I_N} \parallel q_{M_0 | I_N; \phi_M}) \right. \\
&\quad \left. + \mathbb{E}_{M_0 | I_N} \left[\alpha_\Theta D_{\text{KL}}(p_{\Theta_{m,0} | I_N} \parallel q_{\Theta_{m,0} | I_N; \phi_{\Theta_m}}) + \alpha_Z D_{\text{KL}}(p_{Z_{m,0} | I_N} \parallel q_{Z_{m,0} | I_N; \phi_{Z_m}}) \right] \right] \\
&\quad + \alpha_M D_{\text{KL}}(P_{M_0 | i_k} \parallel q_{M_0 | i_k; \phi_M}) \\
&\quad + \mathbb{E}_{M_0 | i_k} \left[\alpha_\Theta D_{\text{KL}}(p_{\Theta_{m,0} | i_k} \parallel q_{\Theta_{m,0} | i_k; \phi_{\Theta_m}}) + \alpha_Z D_{\text{KL}}(p_{Z_{m,0} | i_k} \parallel q_{Z_{m,0} | i_k; \phi_{Z_m}}) \right], \\
& \left| \check{Q}_{I,N}^{\pi_w}(i_N, \cdot) - \tilde{Q}_{I,N}^{\pi_w}(i_N, \cdot; \phi) \right| = 0,
\end{aligned}$$

for $k = 0, \dots, N-1$ and subject to $I_{k+1} = \{I_k, \xi_k, Y_k\}$. Therefore, the error of the critic is contributed from both the error in the final variational posterior $q(\cdot | I_N; \phi_{(\cdot)})$ and the errors in the intermediate variational posteriors $q(\cdot | I_k; \phi_{(\cdot)})$. The critic errors become zero if all the variational posteriors equal their corresponding true posteriors (except the trivial case when $\alpha_M = \alpha_\Theta = \alpha_Z = 0$).

Appendix B.4.1. Hyperparameter tuning

Our main strategy for hyperparameter tuning is to start with a relatively large hyperparameter value and gradually decrease it.

For optimizing the GMM and NFs approximate posteriors for model indicator and PoIs, we start with the initial learning rate of 10^{-3} and an exponential learning rate decay rate 0.9999. For optimizing the critic network, we use an initial learning rate of 10^{-3} and a learning rate decay rate of 0.9999 across all numerical cases. Both posterior approximation and critic network optimizations are updated 5 steps (i.e., applying gradient ascent 5 times) within each outer iteration. Making too many update steps within each outer iteration may result in overestimation of the value function and adversely affect the policy search [81].

For optimizing the actor network, we use a learning rate decay rate of 0.9999. However, the choice of the initial learning rate is more problem-dependent. Typically, we start with an initial learning rate of 10^{-3} and gradually decrease it to 5×10^{-4} or 2×10^{-4} if divergence occurs. For the IIG formulation, an initial learning rate of 10^{-3} works well. For TIG, a smaller learning rate is generally required. This is likely due to the slower propagation of critic values from N to the earlier k stages under TIG, and a large learning rate may induce divergence in the early iterations of training.

For other hyperparameters including the number of updates n_{update} , number of sample trajectories n_{traj} , batch size n_{batch} , and replay buffer size n_{buffer} , a number of combinations are tested to identify the optimal setting. Their values are specified for each numerical case in Appendix C.

Appendix C. Numerical experiment details

Appendix C.1. Prior contrastive estimator

The PCE for batch (non-sequential) OED is introduced in [62]:

$$U^{\text{PCE}}(\xi) = \mathbb{E}_{Y_0|\Theta_0,\xi} \mathbb{E}_{\Theta_0} \mathbb{E}_{\Theta_{1:L}} \left[\log \frac{p(Y_0|\Theta_0, \xi)}{\frac{1}{L+1} \sum_{j=1}^{L+1} p(Y_0|\Theta_j, \xi)} \right],$$

where the expectation is over $\Theta_0, Y_0|\xi \sim p(\Theta, Y|\xi)$ and $\Theta_{1:L} \stackrel{\text{iid}}{\sim} p(\Theta)$, and the subscripts here in the non-sequential setting represent multi-sample indexing. One can show that $U^{\text{PCE}}(\xi)$ is a lower bound to the mutual information between Y and Θ , $\mathcal{I}(Y; \Theta|\xi)$, (i.e., the EIG of Θ)—that is, $U^{\text{PCE}}(\xi) \leq \mathcal{I}(Y; \Theta|\xi)$ —for any $L > 0$, and the bound becomes tight as $L \rightarrow \infty$ [62, Theorem 1]. However, the expectation in U^{PCE} is generally intractable to evaluate, and U^{PCE} needs to be estimated numerically, for example through MC:

$$U^{\text{PCE}}(\xi) \approx \frac{1}{n_{\text{out}}} \sum_{i=1}^{n_{\text{out}}} \log \frac{p(y_0^{(i)}|\theta_0^{(i)}, \xi)}{\frac{1}{L+1} \sum_{j=1}^{L+1} p(y_0^{(i)}|\theta_j^{(i)}, \xi)},$$

where $(y_0^{(i)}, \theta_0^{(i)}, \theta_{1:L}^{(i)})$ are n_{out} independent and identically distributed (i.i.d.) realizations of $(Y_0, \Theta_0, \Theta_{1:L})$.

For sequential OED, the PCE becomes [32]:

$$U^{\text{sPCE}}(\pi) = \mathbb{E}_{Y_{0:N-1}|\pi, \Theta_0} \mathbb{E}_{\Theta_0} \mathbb{E}_{\Theta_{1:L}} \left[\log \frac{p(Y_{0:N-1}|\Theta_0, \xi_{0:N-1})}{\frac{1}{L+1} \sum_{j=1}^{L+1} p(Y_{0:N-1}|\Theta_j, \xi_{0:N-1})} \right]$$

where Θ_0 is the data-generating parameter for $\xi_{0:N-1}, Y_{0:N-1}$ with $\xi_k = \mu_k(I_k)$ following the given policy π ; the subscripts for Y and ξ refer to the experiment (stage) index, while those

for Θ refer to the multi-sample index. One can show that $U^{\text{sPCE}}(\pi) \leq \mathcal{I}(Y_{0:N-1}; \Theta | \pi)$ for any π and $L > 0$, and the bound becomes tight as $L \rightarrow \infty$ [32, Theorem 1]. Similarly, U^{sPCE} can be estimated using MC:

$$U^{\text{sPCE}}(\pi) \approx \frac{1}{n_{\text{out}}} \sum_{i=1}^{n_{\text{out}}} \log \frac{p(y_{0:N-1}^{(i)} | \theta_0^{(i)}, \xi_{0:N-1})}{\frac{1}{L+1} \sum_{j=1}^{L+1} p(y_{0:N-1}^{(i)} | \theta_j^{(i)}, \xi_{0:N-1})},$$

where $(y_{0:N-1}^{(i)}, \theta_0^{(i)}, \theta_{1:L}^{(i)})$ are n_{out} i.i.d. realizations of $(Y_{0:N-1}, \Theta_0, \Theta_{1:L})$. We use this estimator for evaluating policies from ‘OED for PoIs’ in this paper when applicable.

From the expressions above, we can see that PCE cannot be used when nuisance parameters Ψ are present since the term $p(y_{0:N-1} | \theta_0, \xi_{0:N-1})$ would be intractable as it needs to marginalize out Ψ . Similarly, PCE cannot be used for ‘OED for QoIs’ since in that scenario, the role of Θ is replaced by Z and $p(y_{0:N-1} | \theta_0, \xi_{0:N-1})$ becomes $p(y_{0:N-1} | z_0, \xi_{0:N-1})$, which is intractable to evaluate. Lastly, PCE cannot be used for implicit likelihood cases since $p(y_{0:N-1} | \theta_0, \xi_{0:N-1})$ would not be accessible.

We can write an analogous PCE expression for model indicator by replacing Θ with M and use the exact expression for the ‘marginal-likelihood’ term in the denominator:

$$\begin{aligned} U^{\text{sPCE},M}(\pi) &= \mathbb{E}_{Y_{0:N-1} | \pi, M_0} \mathbb{E}_{M_0} \left[\log \frac{p(Y_{0:N-1} | M_0, \xi_{0:N-1})}{\frac{1}{|\mathcal{M}_m|} \sum_{j=1}^{|\mathcal{M}_m|} P(m_j) p(Y_{0:N-1} | m_j, \xi_{0:N-1})} \right] \\ &\approx \frac{1}{n_{\text{out}}} \sum_{i=1}^{n_{\text{out}}} \log \frac{p(y_{0:N-1}^{(i)} | m_0^{(i)}, \xi_{0:N-1})}{\frac{1}{|\mathcal{M}_m|} \sum_{j=1}^{|\mathcal{M}_m|} P(m_j) p(y_{0:N-1}^{(i)} | m_j, \xi_{0:N-1})}, \end{aligned}$$

where M_0 is the data-generating parameter for $\xi_{0:N-1}, Y_{0:N-1}$ with $\xi_k = \mu_k(I_k)$ following the given policy π , and $(y_{0:N-1}^{(i)}, m_0^{(i)})$ are n_{out} i.i.d. realizations of $(Y_{0:N-1}, M_0)$. The ‘likelihood’ term can be estimated, for example, via

$$\begin{aligned} p(y_{0:N-1} | m, \xi_{0:N-1}) &= \iint p(\theta_m, \psi_m | m) p(y_{0:N-1} | m, \theta_m, \psi_m, \xi_{0:N-1}) d\theta_m d\psi_m \\ &\approx \frac{1}{L} \sum_{l=1}^L p(y_{0:N-1} | m, \theta_m^{(l)}, \psi_m^{(l)}, \xi_{0:N-1}), \end{aligned}$$

where $\theta_m^{(l)}, \psi_m^{(l)} \sim p(\theta_m, \psi_m | m)$. We use this estimator for evaluating policies from ‘OED for model indicator’ in this paper.

Appendix C.2. Case 1: source location finding

Hyperparameters. Tables C.13 and C.14 present the hyperparameter settings for Case 1a and 1b, respectively. In both cases, for the ‘Linear mapping’ in the GMM net, we map the PoI GMM mean to $[-6, 6]$, PoI GMM standard deviation to $[10^{-5}, 1]$, QoI GMM mean to $[-6, 6]$, and QoI GMM standard deviation to $[10^{-5}, 2]$. The truncated normal distribution is not used.

Training stability. For Case 1b, we only illustrate training stability results for ‘OED for PoIs’ for brevity. Figures C.16 and C.17 present the training history of average \tilde{U} over four training replicates for Case 1a and 1b, respectively, for $N = 30$. The shaded regions represent the standard error. Tables C.15 and C.16 present the expected utility and standard error (\pm) for four training replicates for ‘OED for PoIs’, evaluated using PCE, for $N = 30$. The last columns display the average of the four replicates along with its standard error. The results indicate a good level of training robustness.

Table C.13: Case 1a. Hyperparameter settings. In the table, ‘lr’ stands for ‘learning rate’.

	vsOED-G-T	vsOED-G-I	vsOED-N-T	vsOED-N-I
n_{updates}	10001	10001	10001	10001
n_{traj}	1000	1000	1000	1000
n_{batch}	10000	10000	10000	10000
$a_{\phi,0}$	10^{-3}	10^{-3}	10^{-3}	10^{-3}
a_{ϕ} decay	0.9999	0.9999	0.9999	0.9999
# of ϕ updates per l -iteration	5	5	5	5
n_{mixture}	8	8	N/A	N/A
n_{trans}	N/A	N/A	4	4
$a_{w,0}$	5×10^{-4}	10^{-3}	10^{-3}	10^{-3}
a_w decay	0.9999	0.9999	0.9999	0.9999
Initial critic lr	10^{-3}	10^{-3}	10^{-3}	10^{-3}
Critic lr decay	0.9999	0.9999	0.9999	0.9999
# of ν updates per l -iteration	5	5	5	5
Max buffer size	10^6	10^6	10^6	10^6
γ	1	0.9	1	0.9
Initial $\sigma_{k,\text{explore}}$	0.5	0.5	0.5	0.5
$\sigma_{k,\text{explore}}$ decay	0.9999	0.9999	0.9999	0.9999
Target network lr	0.1	0.1	0.1	0.1

Table C.14: Case 1b. Hyperparameter settings. In the table, ‘lr’ stands for ‘learning rate’.

	vsOED-G-T	vsOED-G-I
n_{update}	10001	10001
n_{traj}	1000	1000
n_{batch}	10000	10000
$a_{\phi,0}$	10^{-3}	10^{-3}
a_{ϕ} decay	0.9999	0.9999
# of ϕ updates per l -iteration	5	5
n_{mixture}	8	8
$a_{w,0}$	2×10^{-4}	10^{-3}
a_w decay	0.9999	0.9999
Initial critic lr	10^{-3}	10^{-3}
Critic lr decay	0.9999	0.9999
# of ν updates per l -iteration	5	5
Max buffer size	10^6	10^6
γ	1	0.9
Initial $\sigma_{k,\text{explore}}$	0.5	0.5
$\sigma_{k,\text{explore}}$ decay	0.9999	0.9999
Target network lr	0.1	0.1

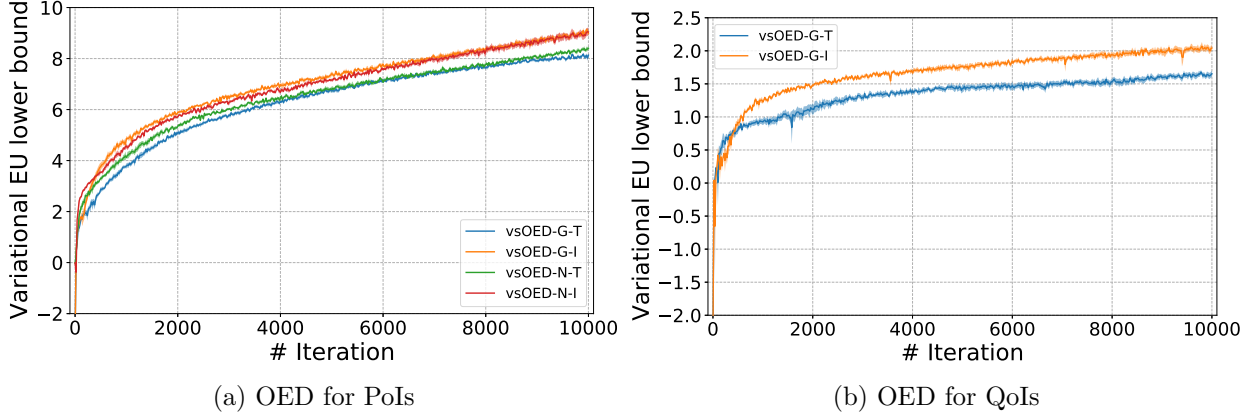


Figure C.16: Case 1a. Training history of average \tilde{U} over four training replicates for $N = 30$. The shaded regions represent standard error.

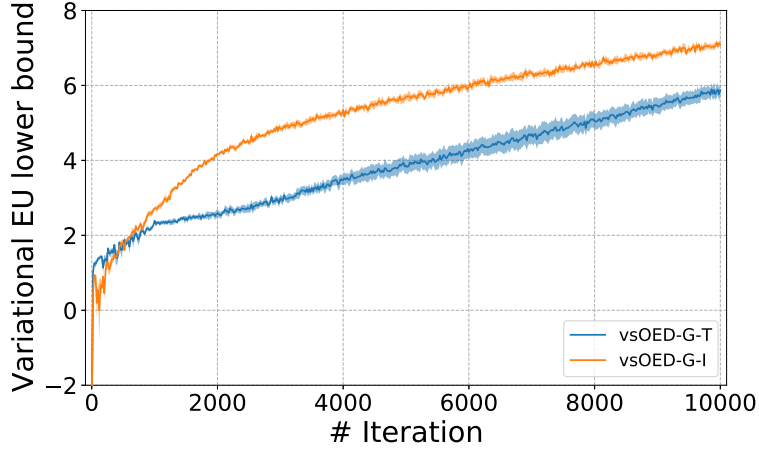


Figure C.17: Case 1b. Training history of average \tilde{U} over four training replicates for ‘OED for PoIs’ and $N = 30$. The shaded regions represent standard error.

Table C.15: Case 1a. Expected utility and standard error (\pm) for four training replicates for ‘OED for PoIs’, evaluated using PCE, for $N = 30$.

	Replicate 1	Replicate 2	Replicate 3	Replicate 4	Average
vsOED-G-T	11.26 ± 0.05	11.09 ± 0.05	11.24 ± 0.05	11.02 ± 0.04	11.15 ± 0.05
vsOED-G-I	12.50 ± 0.04	12.31 ± 0.04	12.58 ± 0.04	11.90 ± 0.04	12.32 ± 0.13
vsOED-N-T	11.24 ± 0.05	11.67 ± 0.05	11.15 ± 0.05	11.59 ± 0.05	11.42 ± 0.11
vsOED-N-I	12.39 ± 0.04	12.34 ± 0.04	12.16 ± 0.04	12.54 ± 0.04	12.36 ± 0.07

Table C.16: Case 1b. Expected utility and standard error (\pm) for four training replicates for ‘OED for PoIs’, evaluated using PCE, for $N = 30$.

	Replicate 1	Replicate 2	Replicate 3	Replicate 4	Average
vsOED-G-T	9.67 ± 0.06	9.26 ± 0.06	9.06 ± 0.06	8.83 ± 0.06	9.21 ± 0.15
vsOED-G-I	10.57 ± 0.05	10.09 ± 0.05	10.46 ± 0.05	10.43 ± 0.05	10.39 ± 0.09

Appendix C.3. Case 2: constant elasticity of substitution

Hyperparameters. Table C.17 presents the hyperparameter settings for this case. For the ‘Linear mapping’ in the GMM net, we map the PoI GMM mean to $[-1, 2]$ for ρ and β and to $[-17, 19]$ for $\log u$, and PoI GMM standard deviation to $[10^{-5}, 3]$ for all variables. The truncated normal distribution is used on ρ and β with support $[0, 1]$.

Table C.17: Case 2. Hyperparameter settings. In the table, ‘lr’ stands for ‘learning rate’.

	vsOED-G-T	vsOED-N-T
n_{update}	10001	10001
n_{traj}	1000	1000
n_{batch}	10000	10000
$a_{\phi,0}$	10^{-3}	10^{-3}
a_{ϕ} decay	0.9999	0.9999
# of ϕ updates per l -iteration	5	5
n_{mixture}	8	N/A
n_{trans}	N/A	4
$a_w,0$	10^{-3}	10^{-3}
a_w decay	0.9999	0.9999
Initial critic lr	10^{-3}	10^{-3}
Critic lr decay	0.9999	0.9999
# of ν updates per l -iteration	5	5
Max buffer size	10^6	10^6
γ	1	1
Initial $\sigma_{k,\text{explore}}$	5	5
$\sigma_{k,\text{explore}}$ decay	0.9998	0.9998
Target network lr	0.1	0.1

Training stability. Figure C.18 presents the training history of average \tilde{U} over four training replicates for $N = 10$, with the shaded regions representing the standard error. Table C.18 presents the expected utility and standard error (\pm) for four training replicates, evaluated using PCE, for $N = 10$. The last column displays the average of the four replicates along with its standard error. The results exhibits slightly more variation compared to Case 1, but overall remains robust.

Table C.18: Case 2. Expected utility and standard error (\pm) for four training replicates, evaluated using PCE, for $N = 10$.

	Replicate 1	Replicate 2	Replicate 3	Replicate 4	Average
vsOED-G-T	11.79 ± 0.07	12.34 ± 0.06	12.29 ± 0.06	11.13 ± 0.08	11.89 ± 0.25
vsOED-N-T	8.40 ± 0.10	9.51 ± 0.09	8.91 ± 0.09	10.30 ± 0.08	9.28 ± 0.35

Appendix C.4. Case 3: SIR model for disease spread

Hyperparameters. Table C.19 presents the hyperparameter settings for this case. For the ‘Linear mapping’ in the GMM net, we map the PoI GMM mean to $[-6, 4]$, and PoI GMM standard deviation to $[10^{-5}, 0.5]$. The truncated normal distribution is not used.

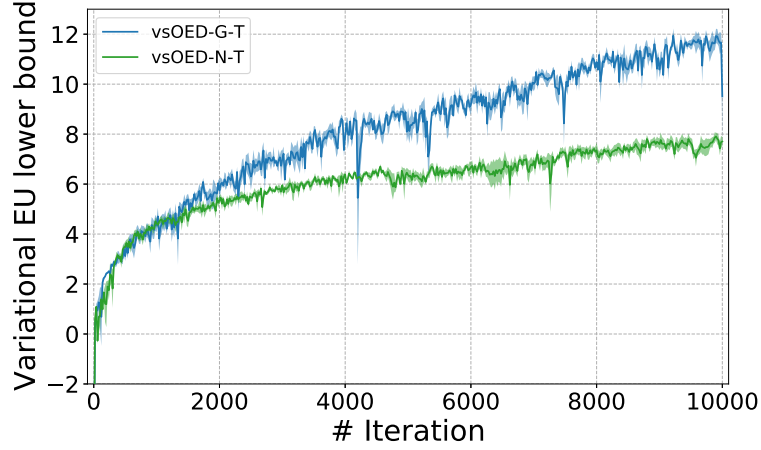


Figure C.18: Case 2. Training history of average \tilde{U} over four training replicates for $N = 10$. The shaded regions represent the standard error.

Table C.19: Case 3. Hyperparameter settings. In the table, ‘lr’ stands for ‘learning rate’.

	vsOED-G-T	vsOED-N-T
n_{update}	10001	10001
n_{traj}	1000	1000
n_{batch}	10000	10000
$a_{\phi,0}$	5×10^{-4}	10^{-3}
a_{ϕ} decay	0.9999	0.9999
# of ϕ updates per l -iteration	5	5
n_{mixture}	8	N/A
n_{trans}	N/A	4
$a_{w,0}$	5×10^{-4}	5×10^{-4}
a_w decay	0.9999	0.9999
Initial critic lr	10^{-3}	10^{-3}
Critic lr decay	0.9999	0.9999
# of ν updates per l -iteration	5	5
Max buffer size	10^6	10^6
γ	1	1
Initial $\sigma_{k,\text{explore}}$	5	5
$\sigma_{k,\text{explore}}$ decay	0.9999	0.9999
Target network lr	0.1	0.1

Training stability. Figure C.19 presents the training history of average \tilde{U} over four training replicates for $N = 10$, with the shaded regions representing the standard error. Table C.20 presents the expected utility and standard error (\pm) for four training replicates, evaluated using PCE, for $N = 10$. The last column displays the average of the four replicates along with its standard error. The training appears highly stable in this case with consistent performance across different random seeds, except for a dip in the training history for vsOED-G-T.

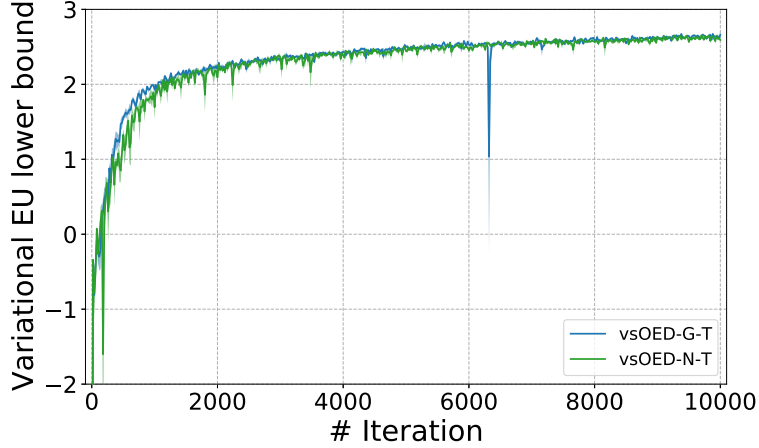


Figure C.19: Case 3. Training history of average \tilde{U} over four training replicates for $N = 10$. The shaded regions represent the standard error.

Table C.20: Case 3. Expected utility and standard error (\pm) for four training replicates, evaluated using PCE, for $N = 10$.

	Replicate 1	Replicate 2	Replicate 3	Replicate 4	Average
vsOED-G-T	4.091 ± 0.002	4.093 ± 0.002	4.090 ± 0.001	4.092 ± 0.001	4.092 ± 0.001
vsOED-N-T	4.097 ± 0.002	4.100 ± 0.002	4.091 ± 0.002	4.106 ± 0.002	4.099 ± 0.003

Appendix C.5. Case 4: convection-diffusion-reaction

Hyperparameters. Table C.21 presents the hyperparameter settings for this case. For the ‘Linear mapping’ in the GMM net, we map the PoI GMM mean to $[-1, 2]$, PoI GMM standard deviation to $[10^{-5}, 1]$, QoI GMM mean to $[-15, 3]$, and QoI standard deviation net to $[10^{-5}, 4]$. The truncated normal distribution is used on all PoIs with support $[0, 1]$.

Training stability. We only illustrate training stability results for ‘OED for PoIs’ for brevity. Figure C.20 presents the training history of average \tilde{U} (but with the prior term omitted due to the presence of nuisance parameters, per Appendix A.5) over four training replicates, with the shaded regions representing standard error. Table C.22 presents the prior-omitted \tilde{U} and standard error (\pm) for four training replicates for $N = 10$. The last column displays the average of the four replicates along with its standard error. These results indicate vsOED to have excellent training robustness.

Neural network architectures for surrogate models. The architecture for the NN-based surrogate models of G and φ are provided in Tables C.23 and C.24.

Table C.21: Case 4. Hyperparameter settings. In the table, ‘lr’ stands for ‘learning rate’.

vsOED-G-T	
n_{update}	10001
n_{traj}	1000
n_{batch}	10000
$a_{\phi,0}$	10^{-3}
a_{ϕ} decay	0.9999
# of ϕ updates per l -iteration	5
n_{mixture}	8
$a_{w,0}$	5×10^{-4}
a_w decay	0.9999
Initial critic lr	10^{-3}
Critic lr decay	0.9999
# of ν updates per l -iteration	5
Max buffer size	10^6
γ	1
Initial $\sigma_{k,\text{explore}}$	0.05
$\sigma_{k,\text{explore}}$ decay	0.9999
Target network lr	0.1

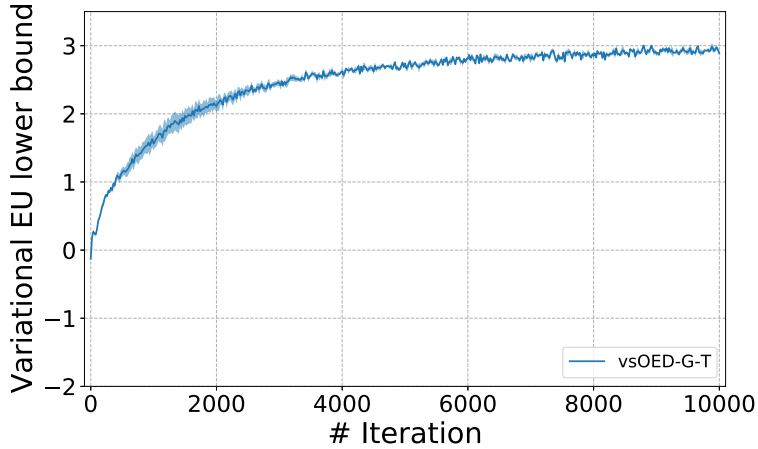


Figure C.20: Case 4. Training history of average \tilde{U} over four training replicates for $N = 10$. The shaded regions represent the standard error.

Table C.22: Case 4. Prior-omitted \tilde{U} and standard error (\pm) for four training replicates and $N = 10$.

	Replicate 1	Replicate 2	Replicate 3	Replicate 4	Average
vsOED-G-T	2.998 ± 0.002	3.057 ± 0.002	2.857 ± 0.002	3.039 ± 0.002	2.99 ± 0.04

Table C.23: Case 4. Architecture for the surrogate model of G .

Layer	Description	Dimension	Activation
Input	$[\theta_m, \psi_m, x, y]$	$2m + 4$	-
Hidden 1	Dense	256	ReLU
Hidden 2	Dense	256	ReLU
Hidden 3	Dense	256	ReLU
Hidden 4	Dense	256	ReLU
Output	Dense	1	-

Table C.24: Case 4. Architecture for the surrogate model of φ .

Layer	Description	Dimension	Activation
Input	$[\theta_m, \psi_m]$	$2m + 2$	-
Hidden 1	Dense	256	ReLU
Hidden 2	Dense	256	ReLU
Hidden 3	Dense	256	ReLU
Output	Dense	1	-